Available online at www.sciencedirect.com
SCIENCE DIRECT®
Progress in Energy and Combustion Science 32 (2006) 162–214
PROGRESS IN ENERGY AND COMBUSTION SCIENCE
www.elsevier.com/locate/pecs

Advanced models of fuel droplet heating and evaporation

Sergei S. Sazhin *

School of Engineering, Faculty of Science and Engineering, The University of Brighton, Cockroft Building, Lewes Road, Brighton BN2 4GJ, UK

Received 18 April 2005; accepted 2 November 2005
Available online 6 January 2006

Abstract

Recent developments in modelling the heating and evaporation of fuel droplets are reviewed, and unsolved problems are identified. It is noted that modelling transient droplet heating using steady-state correlations for the convective heat transfer coefficient can be misleading. At the initial stage of heating stationary droplets, the well known steady-state result $Nu=2$ leads to under prediction of the rate of heating, while at the final stage the same result leads to over prediction. The numerical analysis of droplet heating using the effective thermal conductivity model can be based on the analytical solution of the heat conduction equation inside the droplet. This approach was shown to have clear advantages compared with the approach based on the numerical solution of the same equation both from the point of view of accuracy and computer efficiency. When highly accurate calculations are not required, but CPU time economy is essential then the effect of finite thermal conductivity and re-circulation in droplets can be taken into account using the so called parabolic model. For practical applications in computation fluid dynamics (CFD) codes the simplified model for radiative heating, describing the average droplet absorption efficiency factor, appears to be the most useful both from the point of view of accuracy and CPU efficiency. Models describing the effects of multi-component droplets need to be considered when modelling realistic fuel droplet heating and evaporation. However, most of these models are still rather complicated, which limits their wide application in CFD codes. The Distillation Curve Model for multi-component droplets seems to be a reasonable compromise between accuracy and CPU efficiency. The systems of equations describing droplet heating and evaporation and autoignition of fuel vapour/air mixture in individual computational cells are stiff. Establishing hierarchy between these equations, and separate analysis of the equations for fast and slow variables may be a constructive way forward in analysing these systems.

Keywords: Droplets; Fuel; Heating; Evaporation; Convection; Radiation

Contents

* Tel.: +44 1273 642300; fax: +44 1273 642301.
E-mail address: s.sazhin@brighton.ac.uk.

0360-1285/$ - see front matter © 2005 Elsevier Ltd. All rights reserved.
doi:10.1016/j.pecs.2005.11.001

1. Introduction

The problem of modelling droplet heating and evaporation is not a new one. A discussion of the models developed prior to the early fifties is provided in [1,2]. A number of widely known monographs and review papers have been published since then, including [3–17]. Various aspects of this problem have been covered in numerous review articles, including those published in this journal [18–21]. In all these monographs and review articles, however, this problem was discussed as an integral part of a wider problem of droplet and spray dynamics. This inevitably limited the depth and the breadth of coverage of the subject. Also, most of the relevant monographs and reviews were published more than 5 years ago, and thus do not include the most recent developments in this area.

In contrast to the articles referenced above, this review will focus on the relatively narrow problem of droplet heating and evaporation. Although the application of the models will be mainly illustrated through examples referring to fuel droplets, most of them could be easily generalised to any liquid droplets if required. Only subcritical heating and evaporation will be considered. Near-critical and supercritical droplet heating and evaporation was covered in the relatively recent reviews published in this journal [22,23], and in [24]. Analysis of the interaction between droplets, collisions, coalescence, atomization, oscillations (including instabilities of evaporating droplets) and size distribution will also be beyond the scope of this review, although all these processes indirectly influence the processes considered (see [25–40]). Neither will the problem of heating and evaporation of droplets on heated surfaces be considered (see [37,41]). Although the phenomena considered in this review can be an integral part of the more general process of spray combustion, the detailed analysis of the latter will also be beyond the scope of this work (see [42–45]). Although the problem of radiative heating of droplets is closely linked with the problem of scattering of radiation, the formal modelling of the two processes can be separated. The models of the latter process were reviewed in [46] (see also [47]), and their analysis will be beyond the scope of this paper.

Soret and Dufour effects will be ignored. Soret effect describes the flow of matter caused by a temperature gradient (thermal diffusion), while Dufour effect describes the flow of heat caused by concentration gradients. The two effects occur simultaneously. Both effects are believed to be small in most cases although sometimes their contribution may be significant (see [48–52]).

In most models of droplet evaporation it is assumed that the ambient gas is ideal. This assumption becomes questionable when the pressures are high enough, as observed in internal combustion engines. The main approaches to taking into account

Nomenclature

a	coefficient introduced in Eq. (73) (m^{-b})
a_λ	liquid fuel absorption coefficient (1/m)
a_w, b_w, c_w	constants introduced in Eq. (34)
A	pre-exponential factor (1/s)
A_v, B_v	functions introduced in Eqs. (40) and (41)
$a_{0,1,2}$	coefficients introduced in Eq. (74) (m^{-b}, 1/(K m^b), 1/(K^2 m^b))
b	coefficient introduced in Eq. (73)
$b_{0,1,2}$	coefficients introduced in Eq. (74) (1, 1/K, 1/K^2)
B	branching agent
B_f	parameter introduced in Eq. (87)
B_M	Spalding mass number
B_T	Spalding heat transfer number
B_λ	Planck function (W/(m^2 μm))
c	specific heat capacity (J/(kg K))
c_k, d_k	functions introduced in Eqs. (62)–(64)
C_f	fuel vapour molar concentration (kmol/m^3)
$C_{1,2}$	coefficients in the Planck function (W μm^3/m^2, μm K)
$C_{g1,g2}$	coefficients introduced in Eq. (79)
d_f	diameter of fuel molecules (m)
D	binary diffusion coefficient (m^2/s)
E	activation energy (J)
$E_{r,\theta,\phi}$	components of wave electric field (N/C)
f	molecular distribution function
f_c	function introduced in Eq. (35)
f_m	relative contribution of components (see Eq. (137))
F	force (N)
$F_{T,M}$	correction factors: δ_T/δ_{T0}; δ_M/δ_{M0}
Fo	Fourier number: $t\kappa_g/R_d^2$
$g_0(R)$	function defined by Eq. (78) (W/(m^2 μm))
h	convection heat transfer coefficient (W/(m^2 K))
h_m	mass transfer coefficient (m/s)
h_0	$(hR_d/k_l)-1$
H_e	enthalpy (J)
I	property of the component (see Eq. (137))
I_λ	spectral intensity of thermal radiation in a given direction (W/(m^2 μm))
I_λ^0	spectral intensity of thermal radiation integrated over all angles (W/(m^2 μm))
I_λ^{ext}	spectral intensity of external radiation in a given direction (W/(m^2 μm))
$I_\lambda^{0(ext)}$	spectral intensity of external radiation integrated over all angles (W/(m^2 μm))
j	mass flux (kg/(m^2))
k	thermal conductivity (W/(m K))
k_B	Boltzmann constant (J/K)
Kn	Knudsen number
l_{coll}	characteristic mean free path of molecules (m)
l_K	thickness of the Knudsen layer (m)
L	specific heat of evaporation (J/kg)
Le	Lewis number: $k_g/(c_{pg}\rho_{total})$
m	mass (kg)
m_i	mass of individual molecules (kg)
m_λ	complex index of refraction: $n_\lambda - i\kappa_\lambda$
M	molar mass (kg/kmol)
n	index of refraction (does not depend on λ)
n_λ	index of refraction (depends on λ)
n_0	1.46
N_A	Avogadro number (1/kmol)
Nu	Nusselt number
$\dot{q}$	heat flux (W/m^2)
Q	intermediate agent
Q_a	efficiency factor of absorption
Q_f	specific combustion energy (J/kg)
$p(R)$	radiative power density (see Eq. (77)) (W/m^3)
p_n	coefficients introduced in formula (58) (K/s)
$p_\lambda(R)$	spectral distribution of radiative power density (W/(m^3 μm))
$\tilde{p}_v$	p_v/p_{amb}
$P(R)$	radiative term in Eq. (57) (K/s)
P_{ch}	chemical power per unit volume released in the gas phase (W/m^3)
P_{total}	total amount of radiation absorbed in a droplet (K/s)
P_k^1	associated Legendre polynomials
Pe	Peclet number
Pr	Prandtl number
R	distance from the droplet centre (m)
R_{cut}	parameter introduced in Eq. (151) (m)
R_g	gas constant (J/(kg K))
R_i	positions of individual molecules (m)
R_{ij}	distance between molecules (m)
R_m	the value of R_{ij} when $V=-\varepsilon_{ij}$ (m)
R_{ref}	reflection coefficient
R_u	universal gas constant (J/(kmol K))
R^*	radical
R_*	R_d/n (m)
RH	hydrocarbon fuel
Re	Reynolds number
S	function introduced in Eq. (65)
Sc	Schmidt number
Sh	Sherwood number

t	time (s)
T	temperature (K)
$\tilde{T}_0(R)$	parameter introduced in Eq. (21) (K)
$\mathbf{u}$	fluid velocity (m/s)
U	value of the net velocity of the mixture (m/s)
$\mathbf{v}$	molecular velocities (m/s)
$\|\|v_n(r)\|\|$	parameter introduced in Eq. (21)
V	Lenard–Jones 12-6 potential (J)
V_{shift}	parameter introduced in Eq. (151) (J)
w_λ	normalised absorbed spectral power density of radiation
We	Weber number
$\mathbf{x}$	position in space (m)
x_λ	size parameter: $2\pi R_d/\lambda$
$\mathbf{X}$, $\mathbf{Y}$	n- and m-dimensional vectors
Y	relative concentration
z	parameter introduced in Eq. (104)

Greek symbols

α, β, γ	parameters introduced in Eq. (138)
$\alpha_v(Re)$	parameters introduced in Eq. (49)
β_c	coefficients introduced in Eq. (33)
β_m	evaporation or condensation coefficient
β_v	parameter introduced in Eq. (53)
γ_c	parameter introduced in Eq. (6)
$\bar{\gamma}$	parameter introduced in Eq. (85)
$\delta_{T,M}$	film thickness (m)
δt	time step used for calculation of droplet parameters (s)
Δt	global time step (s)
ϵ	emissivity
ε	small positive parameter
ε_i, ε_j	parameters introduced in Eq. (149) (J)
ε_{ij}	minimal energy of interaction between molecules (J)
ε_m	species evaporation rate
ζ	parameter introduced in Eq. (24)
ζ_k	Riccati–Bessel functions
θ	angle relative to the velocity of unperturbed flow or the angle of wave propagation
θ_R	radiative temperature (K)
Θ	Heaviside unit step function
κ	thermal diffusivity (m^2/s)
κ_R	$k_l/(c_l\rho_l R_d^2)$ (1/s)
κ_λ	index of absorption
λ	wavelength (m or μm)
λ_m	3.4 μm
λ_n	eigen values obtained from the solution of Eq. (22)
λ_v	μ_l/μ_g
$\lambda_{1,2}$	spectral range of absorbed radiation (μm)
Λ_0	function introduced in Eq. (73)
μ	dynamic viscosity (kg/(m s))
μ_c	$\sqrt{1-(1/n^2)}$
$\mu_0(t)$	$(hT_g(t)R_d/k_l)$ (K)
μ_θ	$\cos\theta$
μ'_θ	parameter introduced in Eq. (76)
μ_*	$\sqrt{1-(R_*/R)^2}$
ν	kinematic viscosity (m^2/s)
ξ	parameter introduced in formula (86)
π_k	function introduced in Eqs. (62)–(63)
ρ	density (kg/m^3)
ρ_β	modified density defined by Eq. (147) (kg/m^3)
ρ_λ	$2\pi R/\lambda$
$(\rho c)_{12}$	$\rho_g c_{pg}/(\rho_l c_l)$
σ	Stefan–Boltzmann constant ($W/(m^2K^4)$)
σ_i, σ_j	parameters introduced in Eq. (150) (m)
σ_{ij}	zero energy separation between molecules (m)
σ_s	interfacial surface tension (N/m)
τ_{del}	time delay before the start of autoignition (s)
τ_k	function introduced in Eqs. (62)–(64)
τ_λ	$a_\lambda R$
τ_0	$a_\lambda R_d$
ϕ	asymuthal angle measured from the plane of electric field oscillations
$\Phi(u)$	function introduced in Eqs. (5) and (6)
χ	k_{eff}/k_l (see Eq. (54))
$\chi_{l,m}$	molar fraction of the mth species in the liquid
χ_t	parameter defined by Eq. (17)
ψ_k	Riccati–Bessel functions
Ω_Y	parameter introduced in Eq. (118)

Subscripts

b	boiling
abs	absorbed
amb	ambient
c	centre or convection
coll	collision
cr	critical
d	droplet
diff	diffusive
dr	drift
eff	effective
ext	external
f	film surrounding droplets or fuel
g	gas
ins	incident

l	liquid
lg	from liquid to gas
m	type of species in the liquid phase
p	constant pressure
r	radial component
R	radiation
R_d	outside the Knudsen layer
s	surface
sv	saturated fuel vapour
t	time dependent
v	fuel vapour
θ	component in θ direction
ϕ	component in ϕ direction
-0	inner side of the droplet surface
$+0$	outer side of the droplet surface
∞	infinitely far from the droplet surface

Superscripts

—	average
//	absolute value per unit area of the droplet surface

'real gas' effects have been discussed in [53–57]. The analysis of these effects, however, will be beyond the scope of this review.

This review is intended to be both an introduction to the problem and a comprehensive description of its current status. Most of the review is planned to be a self-sufficient text. On some occasions, however, the reader will be referred to the original papers, without detailed description of the models. Experimental results will be discussed only when they are essential for understanding or validation of the models.

The focus will be on the models suitable or potentially suitable for implementation in computational fluid dynamics (CFD) codes. These are the public domain (e.g. KIVA) or commercial (e.g. PHOENICS, FLUENT, VECTIS, STAR CD) codes. The structures of these codes can vary substantially. However, basic approaches to droplet and spray modelling used in them are rather similar. This will allow us to link the models, described in this review, with any of these codes, without making any specific references.

Following [13] the models of droplet heating can be subdivided into the following groups in order of ascending complexity:

(1) models based on the assumption that the droplet surface temperature is uniform and does not change with time;
(2) models based on the assumption that there is no temperature gradient inside droplets (infinite thermal conductivity of liquid);
(3) models taking into account finite liquid thermal conductivity, but not the re-circulation inside droplets (conduction limit);
(4) models taking into account both finite liquid thermal conductivity and the re-circulation inside droplets via the introduction of a correction factor to the liquid thermal conductivity (effective conductivity models);
(5) models describing the re-circulation inside droplets in terms of vortex dynamics (vortex models);
(6) models based on the full solution of the Navier–Stokes equation.

The first group allows the reduction of the dimension of the system via the complete elimination of the equation for droplet temperature. This appears to be particularly attractive for the analytical studies of droplet evaporation and thermal ignition of fuel vapour/air mixture (see e.g. [58–62]). This group of models, however, appears to be too simplistic for application in most CFD codes. The groups (5) and (6) have not been used and are not expected to be used in these codes in the foreseeable future due to their complexity. These models are widely used for validation of more basic models of droplet heating, or for in-depth understanding of the underlying physical processes (see, e.g. [13,63–66]). The main focus of this review will be on models (2)–(4), as these are the ones which are actually used in CFD codes, or their incorporation in them is feasible.

The review consists of two main parts. First, models of non-evaporating droplets will be reviewed (Section 2). Then evaporation models will be discussed (Section 3). The main results of the review will be summarised in Section 4.

2. Heating of non-evaporating droplets

Someone wishing to model heating of non-evaporating droplets would be required to take into account a number of important processes. These include the deformation of droplets in the air stream and the inhomogeneity of the temperature distribution at the droplet surface. Rigorous solution of this general problem, however, would have been not only difficult, but also would have rather limited practical applications. Indeed, in realistic engineering applications

modelling of simultaneous heating of a large number of droplets would be required. Moreover, this modelling would have to be performed alongside gas dynamics, turbulence and chemical modelling. This leads to the situation where the parameters of gas around droplets may be estimated with substantial errors, which are often difficult to control. This is why the focus has to be on finding a reasonable compromise between accuracy and computer efficiency of the models, rather than on the accuracy of the models alone.

The most commonly used assumption is that the droplet retains its spherical form even in the process of its movement. This assumption will be made in this review as well. The generalisations of the models to droplets of arbitrary shapes were discussed in a number of books and articles (see [2,65,67]). These generalisations could be applied to simple models of droplet heating, but it is not obvious how they can be applied to the more sophisticated models discussed below.

Another simplification widely used in droplet heating models is the assumption that the temperature over the whole droplet surface is the same (although it can vary with time). This assumption effectively allows the separation of the analysis of heat transfer in gaseous and liquid phases. It is expected to be a good approximation in the case of a stationary or very fast moving droplet, when the isotherms almost coincide with streamlines [63]. The errors introduced by this assumption in intermediate conditions are generally assumed to be acceptable.

In what follows the models for convective and radiative heating of droplets will be considered separately (Sections 2.1 and 2.2).

2.1. Convective heating

2.1.1. Stagnant droplets

In the case of stagnant droplets, there is no bulk motion of gas relative to the droplets, and the problem of their heating by the ambient gas reduces to a conduction problem. The heat conduction equation can be solved separately in the droplet and the gas, and the solutions are matched at the droplet surface. Assuming the spherical symmetry of the problem, its mathematical formulation is based on the solution of the equation

$$\frac{\partial T}{\partial t} = \kappa\left(\frac{\partial^2 T}{\partial R^2} + \frac{2}{R}\frac{\partial T}{\partial R}\right), \tag{1}$$

where

$$\kappa = \begin{cases} \kappa_l = k_l/(c_l\rho_l) & \text{when } R \le R_d \\ \kappa_g = k_g/(c_{pg}\rho_g) & \text{when } R_d < R \le \infty, \end{cases} \tag{2}$$

$\kappa_{l(g)}$, $k_{l(g)}$, $c_{l(pg)}$, and $\rho_{l(g)}$ are the liquid (gas) thermal diffusivity, thermal conductivity, specific heat capacity, and density, respectively, R is the distance from the centre of the sphere, t is time, subscripts l and g refer to liquid and gas, respectively.

This equation needs to be solved subject to the following initial and boundary conditions:

$$T|_{t=0} = \begin{cases} T_{d0}(R) & \text{when } R \le R_d \\ T_{g0}(R) & \text{when } R_d < R \le \infty, \end{cases} \tag{3}$$

$$T|_{R=R_d-0} = T|_{R=R_d+0}; \quad k_l\frac{\partial T}{\partial R}\bigg|_{R=R_d-0} = k_g\frac{\partial T}{\partial R}\bigg|_{R=R_d+0}; \quad T|_{R=\infty} = T_{g\infty}. \tag{4}$$

Assuming that $T_{d0}(R) = T_{d0} = \text{const}_1$, and $T_{g0}(R) = T_{g\infty} = \text{const}_2$, Cooper [68] has solved this problem analytically, using the Laplace transform method. His solution can be presented as

$$T(R \le R_d) = T_{g\infty} + \frac{2k_l}{\pi k_g}\sqrt{\frac{\kappa_g}{\kappa_l}}(T_{g\infty} - T_{d0})\frac{R_d}{R} \times \int_0^\infty du\Phi(u)\exp\left(-u^2 Fo\frac{\kappa_l}{\kappa_g}\right)\sin\left(u\frac{R}{R_d}\right), \tag{5}$$

$$T(R \ge R_d) = T_{g\infty} + \frac{2k_l}{\pi k_g}\sqrt{\frac{\kappa_g}{\kappa_l}}(T_{g\infty} - T_{d0})\frac{R_d}{R} \times \int_0^\infty \frac{du}{u}\Phi(u)\exp\left(-u^2 Fo\frac{\kappa_l}{\kappa_g}\right) \times \left\{\cos(\gamma_c u)\sin u + \sqrt{\frac{\kappa_g}{\kappa_l}}\sin\gamma_c \times \left[\frac{k_l}{k_g}(u\cos u - \sin u) + \sin u\right]\right\}, \tag{6}$$

where

$$\Phi(u) = \frac{(u\cos u - \sin u)}{u^2\sin^2 u + \frac{\kappa_g}{\kappa_l}\left[\frac{k_l}{k_g}(u\cos u - \sin u) + \sin u\right]^2},$$

$$Fo = t\kappa_g/R_d^2 \quad \text{(Fourier number)}$$

$$\gamma_c = \sqrt{\frac{\kappa_l}{\kappa_g}}\left[\frac{R-R_d}{R}\right]u.$$

As expected, this solution predicts diffusion of heat from gas to droplets, if $T_{g\infty} > T_{d0}$. As a result, droplet and gas temperatures approach each other in any finite domain. Initially, the heat flux from gas to droplets predicted by the equation

$$\dot{q} = -k_g \frac{\partial T}{\partial R}\Big|_{R=R_d+0} \tag{7}$$

is infinitely large. It approaches zero at $t \to \infty$.

This solution was originally applied to the problem of heating a stationary liquid sodium sphere in UO_2 atmosphere [68]. However, the applicability of this solution to more general problems, involving the time variations of gas temperature due to external factors and evaporation effects, is questionable. The only practical approach to solve this general problem is currently based on the application of computational fluid dynamics (CFD) codes. In this case one would need to take into account the distribution of temperature inside droplets at the beginning of each time step and the finite size of computational cells. These effects were taken into account in the solution suggested in [69,70]. However, these papers did not discuss how practical it is to implement the solution into a CFD code. Practically all the available and, known to me, CFD codes are based on separate solutions for gas and liquid phases, followed by their coupling [19,28,44,71]. Hence, some kind of separation of the solutions for gas and liquid phases would be essential to make them compatible with these codes.

The required separation between the solutions could be achieved based on the comparison between the thermal diffusivities of gas and liquid. Let us consider typical values of parameters for diesel fuel spray droplets and assume that these droplets have initial temperature 300 K and are injected into a gas at temperature 800 K and pressure 30 atm [61]:

$$\rho_l = 600\ \text{kg/m}^3, \qquad k_l = 0.145\ \text{W/(m K)},$$

$$c_l = 2830\ \text{J/(kg K)}, \qquad \rho_g = 23.8\ \text{kg/m}^3,$$

$$k_g = 0.061\ \text{W/(m K)}, \qquad c_{pg} = 1120\ \text{J/(kg K)}.$$

A more detailed discussion of fuel properties is given in Appendix A. For these values of parameters we obtain $\kappa_l = 8.53\times10^{-8}\ \text{m}^2/\text{s}$ and $\kappa_g = 2.28\times10^{-6}\ \text{m}^2/\text{s}$. This allows us to assume:

$$\kappa_l \ll \kappa_g. \tag{8}$$

This condition tells us that gas responds much more quickly to changes in the thermal environment than liquid. As a zeroth approximation we can ignore the changes in liquid temperature altogether, and assume that the droplet surface temperature remains constant in time. This immediately allows us to decouple the solution of Eq. (1) from the trivial solution of this equation for the liquid phase ($T(R \le R_d) = \text{const}$). The former solution can be presented as

$$T(R > R_d) = T_{g\infty} + \frac{R_d}{R}(T_{d0} - T_{g\infty})\left[1 - \text{erf}\left(\frac{R-R_d}{2\sqrt{\kappa_g t}}\right)\right], \tag{9}$$

where

$$\text{erf}(x) = \frac{2}{\sqrt{\pi}}\int_0^x \exp(-t^2)\text{d}t.$$

In the limit $R = R_d$, Eq. (9) gives $T = T_{d0}$. In the limit $t \to 0$, but $R \neq R_d$, this equation gives $T = T_{g\infty}$.

Having substituted (9) into (7) we obtain the following equation for the heat flux from gas to droplets [72]:

$$\dot{q} = \frac{k_g(T_{d0} - T_{g\infty})}{R_d}\left(1 + \frac{R_d}{\sqrt{\pi\kappa_g t}}\right). \tag{10}$$

The same expression follows from the analysis reported later in [73,74], who were apparently not aware of the original paper [72]. Moreover, this expression might have been derived even earlier, as in 1971 it was referred to in [75] as the 'well known conduction solution' without giving any references.

For $t \gg t_d \equiv R_d^2/(\pi\kappa_g)$ Eq. (10) can be further simplified and rewritten as:

$$|\dot{q}| = h(T_{g\infty} - T_{d0}), \tag{11}$$

where h is the convection heat transfer coefficient defined as

$$h = \frac{k_g}{R_d}. \tag{12}$$

Remembering that the convection heat transfer is commonly described by the Nusselt number $Nu = 2R_d h/k_g$, Eq. (12) is equivalent to the statement that $Nu = 2$. Solution (11) could be obtained directly from Eq. (1) if the time derivative of temperature is ignored (steady-state solution). It gives us the well known Newton's law for heating of stationary droplets so long as the boundary layer around droplets has had enough time to develop. Note that for the values of parameters mentioned above $t_d = 3.5\ \mu\text{s}$. That means that except at

the very start of droplet heating, this process can be based on Eqs. (11) and (12). These equations are widely used in CFD codes.

Comparing Eqs. (10)–(12), it can be seen that Newton's law (Eqs. (11) and (12)) can be used to describe the transient process discussed above, if the gas thermal conductivity k_g is replaced by the 'time dependent' gas thermal conductivity $k_{g(t)}$ defined as [72,74]

$$k_{g(t)} = k_g(1 + \zeta_t), \tag{13}$$

where

$$\zeta_t = R_d\sqrt{\frac{c_{pg}\rho_g}{\pi k_g t}}. \tag{14}$$

This is applicable only at the very start of droplet heating (at the start of calculations when a droplet is injected into the gas). Unless abrupt changes in gas temperature occur, one may assume that the boundary layer around the droplet has had enough time to adjust to varying gas temperature. This would justify the application of Newton's law in its original formulation (Eqs. (11) and (12)).

Note that in the limit $t \to \infty$ solution (9) is simplified to

$$\Delta T \equiv T - T_{g\infty} = \frac{R_d}{R}(T_{d0} - T_{g\infty}), \tag{15}$$

where ΔT indicates the local changes in gas temperature after the boundary layer around the droplet has been formed. The change of gas enthalpy, due to the presence of the droplet, in this case can be obtained as:

$$\Delta H_e = \int_{R_d}^{\infty} \rho_g c_{pg} \Delta T 4\pi R^2 \, dR$$

$$= 4\pi R_d (T_{d0} - T_{g\infty}) \rho_g c_{pg} \int_{R_d}^{\infty} R \, dR = \infty. \tag{16}$$

Thus the establishment of the required boundary layer of a single droplet leads to an infinitely large change in the enthalpy of the gas. It seems that Todes [72] was the first to draw attention to this fact. One can see, however, that if the value of ΔT was calculated for any $t \neq \infty$ from Eq. (9) then ΔH_e would have remained finite. This appears to be due to the fact that at any $t < \infty$ the second term in the square brackets in Eq. (9) cannot be ignored at $R - R_d > 2\sqrt{\kappa_g t}$. This means that Eq. (15) is not valid at these radii, and ΔH_e cannot be calculated using Eq. (16). In practice ΔH_e has never been calculated from Eq. (16), to the best of my knowledge. Instead, the amount of heat gained or lost by the droplet during a certain period of time Δt has been calculated based on the values of Nu. This gives reasonable results provided that the assumption that the droplet surface temperature remains constant in time is valid.

Cooper's [68] solution also allows us to present the heat flux in the form (11), by replacing h with $h_t = \chi_t h = \chi_t k_g / R_d$, where

$$\chi_t = \frac{-\frac{k_l}{k_g}\int_0^{\infty}(u\cos u - \sin u)\Phi(u)\exp\left(-u^2 Fo \frac{\kappa_l}{\kappa_g}\right)du}{\int_0^{\infty}\sin u \Phi(u)\exp\left(-u^2 Fo \frac{\kappa_l}{\kappa_g}\right)du}, \tag{17}$$

$\Phi(u)$ is the same as in Eqs. (5) and (6).

The plot of χ_t versus Fo for the same values of parameters as used earlier is presented in Fig. 1. As follows from this figure, χ_t is large for small Fo, as in the case of the solution with constant droplet surface temperature. In contrast to the latter solution, however, this correction to h approaches not 1, but 0 at $t \to \infty$ (or $Fo \to \infty$). These small values of χ_t are observed at the final stage of droplet heating when the difference between the ambient gas temperature and droplet surface temperature becomes close to zero. As mentioned earlier, at this stage the applicability of Eqs. (5) and (6) becomes questionable.

To summarise this part of the review, we may say that simple Eqs. (11) and (12) seem to be the most

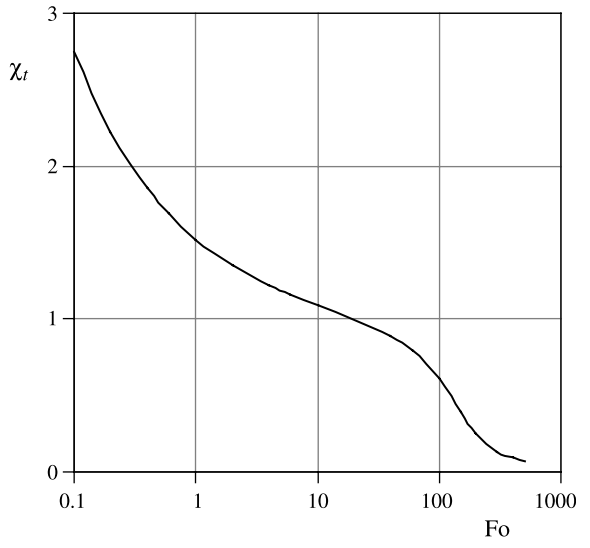

Fig. 1. Plot of χ_t, defined by Eq. (17), versus Fo.

useful for practical application in CFD codes. At the initial stage of heating, the corrections described by Eq. (13) can be introduced if required. The range of applicability of these equations for transient heating, however, has not been rigorously justified (cf. Eq. (17)).

The next stage of the analysis will be focused on the processes in the liquid phase. When the first group of models discussed in Section 1 ($T_d(R \le R_d) = \text{const}$) is used, then the problem of liquid droplet heating does not occur. For the second group of models (no temperature gradient inside droplets) the droplet temperature can be found from the energy balance equation:

$$\frac{4}{3}\pi R_d^3 \rho_l c_l \frac{dT_d}{dt} = 4\pi R_d^2 h(T_{g\infty} - T_d). \tag{18}$$

This equation merely indicates that all the heat supplied from gas to droplet is spent on raising the temperature of the droplet. It has a straightforward solution

$$T_d = T_{g\infty} + (T_{d0} - T_{g\infty})\exp\left(-\frac{3ht}{c_l \rho_l R_0}\right), \tag{19}$$

where $T_d(t=0) = T_{d0}$.

Eq. (18) and its solution (19) are widely used in various applications. In conjunction with the mass transfer Eq. (described in Section 3) Eq. (18) was used to determine experimentally the heat transferred by convection to droplets [71]. Solution (19) is widely used in most CFD codes. Sometimes this is justified by the fact that liquid thermal conductivity is much higher than that of gas. However, the main parameter which controls droplet transient heating is not its conductivity, but its diffusivity. As shown earlier, in the case of diesel engine sprays the diffusivity for liquid is more than an order of magnitude less than that for gas. This raises the question of whether the second group of models is applicable to modelling fuel droplets in these engines. The only reasonable way to answer this question is to consider the third group of models, which take into account the effect of finite liquid thermal conductivity.

The application of the third group of models can be based on the solution of Eq. (1) inside the droplet with the following boundary conditions

$$h(T_g - T_s) = k_l \frac{\partial T}{\partial R}\Big|_{R=R_d-0}, \tag{20}$$

$((T/(R)|_{R=0} = 0$, and the initial condition $T(t=0) = T_{d0}(R)$, where $T_s = T_s(t)$ is the droplet's surface temperature, $T_g = T_g(t)$ is the ambient gas temperature, the subscript ∞ has been omitted.

Assuming that $h = \text{const}$, this solution can be presented as [76,77]

$$\begin{aligned} T(R,t) = \frac{R_d}{R}\sum_{n=1}^{\infty}\Bigg\{ & q_n \exp[-\kappa_R \lambda_n^2 t] \\ & - \frac{\sin\lambda_n}{||v_n||^2 \lambda_n^2}\mu_0(0)\exp[-\kappa_R\lambda_n^2 t] \\ & - \frac{\sin\lambda_n}{||v_n||^2\lambda_n^2}\int_0^t \frac{d\mu_0(\tau)}{d\tau}\exp[-\kappa_R\lambda_n^2(t-\tau)]d\tau \Bigg\} \\ & \times \sin\left[\lambda_n\left(\frac{R}{R_d}\right)\right] + T_g(t), \end{aligned} \tag{21}$$

where λ_n are solutions of the equation

$$\lambda\cos\lambda + h_0\sin\lambda = 0, \tag{22}$$

$$||v_n||^2 = \frac{1}{2}\left(1 - \frac{\sin 2\lambda_n}{2\lambda_n}\right) = \frac{1}{2}\left(1 + \frac{h_0}{h_0^2 + \lambda_n^2}\right),$$

$$q_n = \frac{1}{R_d||v_n||^2}\int_0^{R_d} \tilde{T}_0(R)\sin\left[\lambda_n\left(\frac{R}{R_d}\right)\right]dR,$$

$$\kappa_R = \frac{k_l}{c_l\rho_l R_d^2}, \qquad \mu_0(t) = \frac{hT_g(t)R_d}{k_l}.$$

$h_0 = (hR_d/k_l) - 1$, $\tilde{T}_0(R) = RT_{d0}(R)/R_d$. The solution of Eq. (22) gives a set of positive eigenvalues λ_n numbered in ascending order ($n = 1,2,\ldots$). Proof of the convergence of the series in (21) is given in [77]. In the limit $k_l \to \infty$ solution (21) reduces to solution (19) as expected [78].

Solution (21) was generalised to the case of almost constant convection heat transfer coefficients [77]. In the case of the general time-dependent convection heat transfer coefficient, the solution of the differential equation is reduced to the solution of the Volterra integral equation of the second kind [77]. However, the practical applicability of these solutions to CFD codes has turned out to be limited [79].

The benefits of taking into account the finite thermal conductivity of fuel droplets in the CFD modelling of combustion processes in diesel engines was first demonstrated in [80]. These authors performed the calculations using KIVA II CFD code with the conventional model for droplet heating based on Eq. (19) (called the Spalding model), and with the models taking into account the finite thermal conductivity of droplets. Note that the latter effect in this paper was taken into account based on the direct numerical solution of Eq. (1), rather than on the

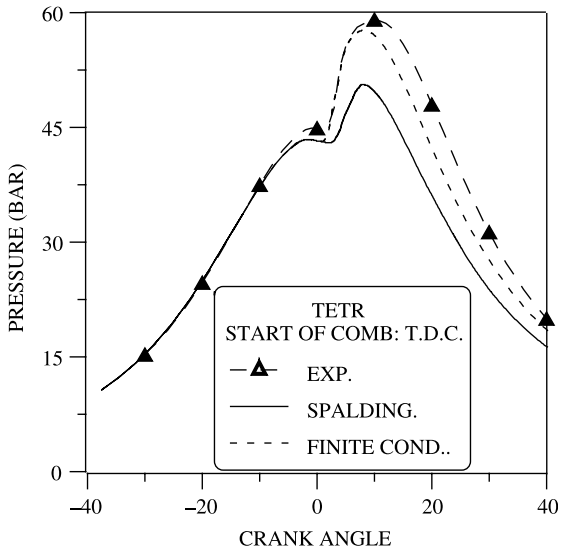

Fig. 2. In-cylinder pressure versus crank angle. Reproduced from [80] with permission of the authors and Elsevier.

analytical solution of this Eq. (see solution (21)). The results of their calculations are shown in Fig. 2 as in-cylinder pressure versus crank angle (proportional to time). The results of measurements of this pressure are shown in the same figure. It follows that taking into account the effects of finite thermal conductivity of droplets leads to better agreement with experimental data, compared with the conventional model.

Although nobody seems to contest the benefits of taking into account the finite thermal conductivity of fuel droplets in CFD modelling, the developers of CFD codes do not embrace this modelling opportunity too eagerly. The main reason for this is the additional cost of CPU time involved. This has stimulated efforts to develop a model taking into account the effect of finite thermal conductivity of droplets, but with minimal extra demands on CPU time. The idea of this new model may have been prompted by looking at the character of the plots $T(R)$ predicted by Eq. (21) . Assuming that initially $T(R)$ is constant, one can see that, except at the very start of heating, the shape of the curve $T(R)$ looks very close to a parabola. This allows us to approximate $T(R)$ as [81]

$$T(R,t) = T_c(t) + [T_s(t) - T_c(t)]\left(\frac{R}{R_d}\right)^2, \tag{23}$$

where T_c and T_s are the temperatures at the centre ($R=0$) and on the surface ($R=R_d$) of the droplet, respectively. Approximation (23) is obviously not valid at the very beginning of the heating process when $T=T_c$ in most of the droplet.

Substitution of Eq. (23) into the boundary condition at $R=R_d$ (Eq. (20)) gives [81]

$$T_s - T_c = \frac{\zeta}{2}(T_g - T_s), \tag{24}$$

where $\zeta = (Nu/2)(k_g/k_l)$, Nu is the Nusselt number introduced earlier. Eq. (23) does not satisfy Eq. (1) but it should satisfy the equation of thermal balance, which can be obtained from integrating Eq. (1) along the radius

$$\rho_l c_l \frac{R_d}{3}\frac{d\bar{T}}{dt} = h(T_g - T_s), \tag{25}$$

where

$$\bar{T} = \frac{3}{R_d^3}\int_0^{R_d} R^2 T(R)\,dR \tag{26}$$

is the average temperature of the droplet. Note that Eq. (25) is identical to Eq. (18) describing droplet heating in isothermal (infinite liquid conductivity) approximation, if h is replaced by h^* found from the modified Nusselt number:

$$Nu^* = Nu\frac{T_g - T_s}{T_g - \bar{T}}. \tag{27}$$

Having substituted Eq. (23) into Eq. (26) and remembering Eq. (24) we obtain:

$$\bar{T} = \frac{2T_c + 3T_s}{5} = T_s - 0.2\zeta(T_g - T_s). \tag{28}$$

Substitution of Eq. (28) into Eq. (27) gives:

$$Nu^* = \frac{Nu}{1 + 0.2\zeta}. \tag{29}$$

On the other hand, the combination of Eqs. (24) and (28) gives [81]:

$$T_s = \frac{\bar{T} + 0.2\zeta T_g}{1 + 0.2\zeta}, \tag{30}$$

$$T_c = \frac{(1 + 0.5\zeta)\bar{T} - 0.3\zeta T_g}{1 + 0.2\zeta}. \tag{31}$$

The combination of Eqs. (29)–(31) gives the full solution of the problem of convective droplet heating as predicted by Eq. (23). At first, Eq. (18) is solved with h replaced by h^* from Eq. (29). Then the values of T_s and T_c are obtained from Eqs. (30) and (31). These two parameters are then substituted into Eq. (23) to give the radial distribution of temperature

inside droplets. For practical engineering applications we are primarily interested in the values of T_s, which determine the rate of evaporation and break-up of droplets. The model based on Eq. (23) was called the parabolic temperature profile model [81].

As follows from the comparison of this model with the numerical solution of Eq. (1), the predictions of this model show good accuracy at large times, but can differ considerably from the numerical results for small times. The period of time when the latter happens is usually reasonably short and can be ignored in practical calculations. Actual implementation of this model into a customised version of the CFD code VECTIS is described in [82]. The predictions of the model were reasonably close to those predicted by Eq. (21), and its additional CPU requirements are very small and could be acceptable in most practical applications. The parabolic temperature profile model was generalised to take into account the initial heating of droplets in [81], but the implementation of this generalised model into CFD codes has not yet been investigated.

Note that a model similar to the parabolic temperature profile model can be developed more rigorously based on Eq. (21) if only the first term in this series is taken into account and the initial temperature inside droplets is assumed to be constant. This approach was suggested in [83]. In the limit $t \to \infty$ Eq. (18) of [83] is identical with Eq. (28) in this paper. For $t \to 0$ the accuracy of Eq. (18) of [83] becomes questionable since in this case all terms in Eq. (21) become comparable.

The analysis of Eq. (1) presented in this section was essentially based on the assumption that thermal conductivities, specific heat capacities and densities of gas and liquid are constant. This assumption is reasonable for CFD applications, where the calculations are performed over small time steps when the variations of these parameters can be ignored. They can be updated from one step to another. Attempts to take into account the temperature dependence of these parameters (i.e. to solve a non-linear heat conduction equation) started more than 50 years ago and are still continuing (e.g. [84–90].

2.1.2. Moving droplets

The analysis of heat exchange between gas and stationary droplets was simplified by the fact that this problem is essentially one-dimensional in space. The complexity of the problem of heat transfer between gas and moving droplets lies in the fact that this problem is at least two-dimensional in space. This leads to the need to replace Eq. (1) by a more general equation for the temperatures of both liquid and gas and present it in the form [16]

$$\frac{\partial T}{\partial t} + \nabla \cdot (\mathbf{u}(t, \mathbf{x})T) = \kappa \nabla^2 T, \tag{32}$$

where $\mathbf{u}(t,\mathbf{x})$ is the fluid velocity, which depends on time t and position in space $\mathbf{x}$ in the general case. The Laplacian ∇^2 is three-dimensional in the general case; its two-dimensional approximation is almost universally used. In most practical applications, the time-dependence of $\mathbf{u}$ is ignored, even if the problem of transient heat transfer is considered. In the general case, this equation is solved both in droplets and in the surrounding gas. Eq. (32) does not contain the so-called history terms. These will be briefly discussed later.

Application of Eq. (32) instead of Eq. (1) leads to qualitative differences between the mechanisms of heat transfer in the cases of stationary and moving droplets. In the case of stationary droplets, the heat transfer takes place via conduction, and is described by the heat conduction equation in both liquid and gas. In the case of moving droplets, however, convection heat transfer takes place, which incorporates effects of bulk fluid motion (advection) and diffusion effects (conduction). The modelling of heat transfer in this case needs to be based on the Navier–Stokes equations for enthalpy and momentum. For stationary droplets the thickness of the boundary layer around droplets can be infinitely large. In the case of moving droplets, however, this thickness is always finite. All these differences between the heat transfer processes in the case of stationary and moving droplets require the development of different methods of analysis. While in the case of stationary droplets we started with the general transient solution and ended up with the analysis of the limiting steady-state case, in the case of moving droplets, the starting point will be the simplest steady-state case.

2.1.2.1. Steady-state heating. In the case of steady-state droplet heating the first term in Eq. (32) can be assumed equal to zero, and this leads to considerable simplification of the solution of this equation. In some practically important cases, however, this solution can be avoided altogether, and the analysis can be performed at a semi-qualitative level, backed by experimental observations.

As mentioned in Section 1, the first simplification of the problem is based on the assumption that there is no spatial gradient along a droplet's surface. This

allows us to separate the analysis of the gas and liquid phases. If the surface temperature of the droplet is fixed, then using the dimensional analysis one can show that Nusselt number (Nu) can depend only on Reynolds and Prandtl numbers (Re and Pr). If $Re=0$ (stagnant droplet) then $Nu=2$. The qualitative analysis of the problem for large Re, but in the laminar boundary layer region, shows that Nu is expected to be proportional to $Re^{1/2}Pr^{1/3}$ [2]. Thus the general formula for Nu can be written as

$$Nu = 2 + \beta_c Re^{1/2} Pr^{1/3}, \tag{33}$$

where the coefficient β_c cannot be derived from this simplified analysis. It should be obtained either from experimental observations or from more rigorous numerical analysis of the basic equations. The most widely used value of this coefficient, supported by experimental observations, is $\beta_c=0.6$ (see e.g. [15]). In a number of papers (see e.g. [13,63]) the value $\beta_c=0.552$ is used. Sometimes the power 1/3 of the Prandtl number is replaced by 0.4 [16].

Whitaker [91] drew attention to the fact that in the wake region, for large Re, Nu is expected to be proportional to $Re^{2/3}Pr^{1/3}$. Also, the difference in gas dynamic viscosities in the vicinity of the droplet surface (μ_{gs}) and in the bulk flow ($\mu_{g\infty}$) had to be taken into account. Hence, he looked for the correlation for Nu in the form

$$Nu = 2 + \left(a_w Re^{1/2} + b_w Re^{2/3}\right) Pr^{1/3} \left(\frac{\mu_{g\infty}}{\mu_{gs}}\right)^{c_w}, \tag{34}$$

where the constants a_w, b_w and c_w had to be calculated based on available experimental data. The analysis of these data led to the following result: $a_w=0.4$, $b_w=0.06$ and $c_w=0.25$. Eq. (34) might be expected to be more accurate than Eq. (33) (at least due to the larger number of fitting constants), but it has rarely been used in practical applications. Note that the ratio $\mu_{g\infty}/\mu_{gs}$ is expected to be very close to unity.

As noticed in [6,63], Eq. (33) over-estimates the heat transfer rate at low Reynolds numbers ($Re\leq 10$). Also, this equation and Eq. (34) predict the physically incorrect super-sensitivity of the heat transfer rate to the small velocity fluctuations near $Re=0$, since $\partial Nu/\partial Re\to\infty$ when $Re\to 0$ [63].

As an alternative to Eq. (33), the following correlation was recommended [6,63]

$$Nu = 1 + (1 + RePr)^{1/3} f_c(Re), \tag{35}$$

where $f_c(Re)=1$ at $Re\leq 1$ and $f_c(Re)=Re^{0.077}$ at $1<Re\leq 400$. Eq. (35) approximated the numerical results obtained by a number of authors for $0.25<Pr<100$ with an error less than 3% [63].

Analyses of the process of heating of a spherical body in a flow of fluid were often restricted to the case of small Re when the flow can be considered as Stokesian. In this case, the radial and asymuthal components of flow velocity around a spherical solid body can be found from the following formulae [75,92]:

$$\begin{aligned} u_r =& u_0\left\{\frac{1}{2}\left(1+\frac{3Re}{16}\right)\left[2-\frac{3R_d}{R}+\left(\frac{R_d}{R}\right)^3\right]\cos\theta \right.\\ &-\frac{3Re}{64}\left[2-\frac{3R_d}{R}+\left(\frac{R_d}{R}\right)^2-\left(\frac{R_d}{R}\right)^3+\left(\frac{R_d}{R}\right)^4\right]\\ &\left.\times(3\cos^2\theta-1)+O(Re^2\log Re)\right\}, \end{aligned} \tag{36}$$

$$\begin{aligned} u_\theta =& u_0\left\{-\frac{1}{4}\left(1+\frac{3Re}{16}\right)\left[4-\frac{3R_d}{R}-\left(\frac{R_d}{R}\right)^3\right]\sin\theta \right.\\ &+\frac{3Re}{64}\left[4-\frac{3R_d}{R}+\left(\frac{R_d}{R}\right)^3-2\left(\frac{R_d}{R}\right)^4\right]\cos\theta\sin\theta\\ &\left.+O(Re^2\log Re)\right\}, \end{aligned} \tag{37}$$

where u_0 is the flow velocity unperturbed by the sphere, u_r and u_θ are the radial (away from the centre of the sphere) and circumferential (angle θ is estimated relative to the direction of the velocity in the unperturbed flow) flow velocity components.

As follows from Eqs. (36) and (37) both components of flow velocity are zero at $R=R_d$ as expected (no slip condition).

In the limit $Re\to 0$ Eqs. (36) and (37) can be simplified to:

$$u_r = u_0\left[1-\frac{3R_d}{2R}+\frac{1}{2}\left(\frac{R_d}{R}\right)^3\right]\cos\theta, \tag{38}$$

$$u_\theta = -u_0\left[1-\frac{3R_d}{4R}-\frac{1}{4}\left(\frac{R_d}{R}\right)^3\right]\sin\theta. \tag{39}$$

Note that the main advantages of Eqs. (36) and (37) compared with Eqs. (38) and (39) can be observed at R comparable with R_d. In the limit $R\to\infty$, Eqs. (38) and (39) predict the unperturbed flow velocity.

In the case of droplets in which re-circulation is allowed, Eqs. (38) and (39) can be generalised to [93] (p. 697), [73]:

$$u_r = u_0\left[1-\frac{A_v R_d}{R}+2B_v\left(\frac{R_d}{R}\right)^3\right]\cos\theta, \tag{40}$$

$$u_\theta = -u_0\left[1-\frac{A_v R_d}{2R}-B_v\left(\frac{R_d}{R}\right)^3\right]\sin\theta, \tag{41}$$

where

$$A_v = \frac{3\lambda_v+1}{2(\lambda_v+1)}, \qquad B_v = \frac{\lambda_v}{4(\lambda_v+1)},$$

$\lambda_v = \mu_l/\mu_g$ is the ratio of dynamic viscosities (note that this definition of λ_v is different from the one used in [73,93] but consistent with the definition of the parameter used later in this review). In the case when $\lambda_v = \infty$ (solid body) Eqs. (40) and (41) refer to the case when $R \geq R_d$, and they reduce to Eqs. (38) and (39). Similar equations for the volume inside the droplets could be derived from Eq. (21.14.5b) of [93]. These describe the well known Hill's spherical vortex [93]. A more in-depth analysis of re-circulation within a fluid sphere is given in [94].

If the effects of viscosity are ignored then for both solid and liquid moving spheres, the components of velocity can be presented in particularly simple forms valid for $R \geq R_d$ (see [93], p. 562):

$$u_r = u_0\left[1-\left(\frac{R_d}{R}\right)^3\right]\cos\theta, \tag{42}$$

$$u_\theta = -u_0\left[1+\frac{1}{2}\left(\frac{R_d}{R}\right)^3\right]\sin\theta. \tag{43}$$

The values of the components of fluid velocity predicted by the above-mentioned systems of equations are substituted into Eq. (32). All these systems of equations have actually been used in the analyses of steady-state and transient heating of droplets or, more generally, spherical bodies. These will be reviewed below.

Eqs. (38) and (39) were used by [95] for the asymptotic analysis of the process of heating of a spherical body in a flow of fluid. They assumed that both Reynolds number and Peclet number ($Pe \equiv Re \cdot Pr$) are small, and used the technique originally developed in [92], which led to the derivation of Eqs. (36) and (37). Their final formula was presented in the form:

$$Nu = 2\left(1+\frac{1}{4}Pe+\frac{1}{8}Pe^2\ln Pe+0.01702\,Pe^2 + \frac{1}{32}Pe^3\ln Pe+O(Pe^3)\right). \tag{44}$$

As follows from this equation, $Nu \to 2$ when $Pe \to 0$. Although this equation was derived under the assumption that $Re \ll 1$ and $Pe < 1$, it can still be applied for Re and Pe in the range from 0 to 0.7 [16]. Sometimes Re is defined based on R_d and not $2R_d$ (as in our case). This led to a different form of Eq. (44) [96].

Using Eqs. (36) and (37) but assuming that $Pe \to \infty$, an alternative expression for Nu was derived [95]:

$$Nu = 0.991Pe^{1/3}\left(1+\frac{1}{16}Re+\frac{3}{160}Re^2\ln Re+O\left(Re^2\right)\right). \tag{45}$$

The generalisation of the analysis by [95] for the case when $Re < 1$ and $Pe < 1$ by taking extra terms in the velocity field (that is replacing Eqs. (38) and (39) with Eqs. (36) and (37)), was reported in [96]. The generalisations of this equation to the case of bodies of arbitrary shape were reported in [97–99].

Based on the numerical study of the transient heat transfer from a sphere at high Reynolds and Peclet numbers, the following steady-state correlation was suggested [100]:

$$Nu = 0.922 + Pe^{1/3} + 0.1Re^{1/3}Pe^{1/3}. \tag{46}$$

If $Re = 0$ then Eq. (46) reduces to the solution by Acrivos [99]. Also the prediction of this equation is close to that of Eq. (45) at large Pe, but relatively small Re.

In [101] a mathematical model was developed to describe the heat transfer process when a melting sphere is immersed in a moving fluid. Based on this model, the following correlation for Nu was obtained

$$Nu = 2 + 0.47Re^{0.5}Pr^{0.36}, \tag{47}$$

where

$$0.003 \leq Pr \leq 10, \qquad 10^2 \leq Re \leq 5\times 10^4.$$

This model was validated with various experimental results involving metals and water. Nu predicted by Eq. (47) is reasonably close to Nu predicted by Eq. (33).

None of Eqs. (44)–(47) take into account re-circulation inside the droplets. The latter could be accounted for based on asymptotic or rigorous numerical analysis of coupled fluid dynamics and heat transfer equations. Levich [3] (see p. 408) was perhaps the first to provide an asymptotic solution for small Re, but large Pe in the form (see also [16]):

$$Nu = \sqrt{\frac{4}{3\pi}\frac{1}{1+\lambda_v}Pe}. \tag{48}$$

As this formula is valid for very large Pr, its practical applicability to the analysis of droplet heating in a gas is expected to be limited.

The earlier studies in this direction were reviewed by Feng and Michaelides [102]. Also, in this paper a comprehensive numerical analysis of heat and mass transfer coefficients of viscous moving spheres (droplets) was reported. Their analysis was based on the conventional assumptions mentioned in Section 1. Namely, it was assumed that droplets retain their spherical forms and there are no temperature gradients along the droplet surfaces. In what follows their main results will be summarised.

One of the aims of [102] was to investigate the dependence of Nu on Re, $Pe \equiv Re \cdot Pr$, $\lambda_v = \mu_l/\mu_g$ and ρ_l/ρ_g, where $\mu_{l(g)}$ and $\rho_{l(g)}$ are dynamic viscosities and densities of liquid (gas). As follows from their analysis, the dependence of Nu on ρ_l/ρ_g was negligibly small for ρ_l/ρ_g in the range 0.1–10 (bubbles and droplets), and the range of Pe from 1 to 500, $Re = 10$ and $\lambda_v = 1$. It was not expected to be important for other ranges and values of parameters. Hence, the analysis was focused on the study of the dependence of Nu on Re, Pe and λ_v. The results are presented in a table, covering the range of Re from $Re \to 0$ to 500, the range of Pe from 1 to 1000, and of λ_v from 0 to ∞ (solid). Based on the information presented in this table the following working correlations were developed [102].

At small but finite Re $(0 < Re < 1)$ and $10 \le Pe \le 1000$, the following expression for Nu was derived [102]

$$Nu(\lambda_v, Pe, Re) = \left[\frac{0.651}{1 + 0.95\lambda_v} Pe^{1/2} + \frac{0.991\lambda_v}{1 + \lambda_v} Pe^{1/3}\right][1 + \alpha_v(Re)] + \left[\frac{1.65(1 - \alpha_v(Re))}{1 + 0.95\lambda_v} + \frac{\lambda_v}{1 + \lambda_v}\right], \quad (49)$$

where

$$\alpha_v(Re) = \frac{0.61Re}{Re + 21} + 0.032.$$

Note that in the limit $Re \to 0$ and $\lambda_v \to \infty$, Nu given by expression (49) is not reduced to 2, as predicted for stationary droplets. In this limit $Pr \to \infty$ to satisfy the condition that $Pe > 10$.

At $1 \le Re \le 500$ and $10 \le Pe \le 1000$, the following expressions for Nu were suggested [102]

$$Nu(\lambda_v, Pe, Re) = \frac{2 - \lambda_v}{2} Nu(0, Pe, Re) + \frac{4\lambda_v}{6 + \lambda_v} Nu(2, Pe, Re) \quad (50)$$

for $0 \le \lambda_v \le 2$, and

$$Nu(\lambda_v, Pe, Re) = \frac{4}{2 + \lambda_v} Nu(2, Pe, Re) + \frac{\lambda_v - 2}{\lambda_v + 2} Nu(\infty, Pe, Re) \quad (51)$$

for $2 \le \lambda_v \le \infty$, where

$$Nu(0, Pe, Re) = 0.651 Pe^{1/2}\left[1.032 + \frac{0.61Re}{Re + 21}\right] + \left[1.60 + \frac{0.61Re}{Re + 21}\right],$$

$$Nu(2, Pe, Re) = 0.64 Pe^{0.43}[1 + 0.233 Re^{0.287}] + 1.41 - 0.15 Re^{0.287},$$

$$Nu(\infty, Pe, Re) = 0.852 Pe^{1/3}[1 + 0.233 Re^{0.287}] + 1.3 - 0.182 Re^{0.355}.$$

These equations could be potentially incorporated into any CFD code and used in engineering applications.

2.1.2.2. Transient heating. The complexity of the problem of transient heating of moving droplets lies in the fact that both variations in temperature and flow velocity need to be accounted for in the general case. This is something that is performed in most commercial CFD codes. This analysis, however, is usually case dependent and the results might have limited general practical applications. At the same time, in many applications the characteristic times of variation of flow parameters are much longer than the characteristic times of droplet heating. This allows us to consider the problem of droplet heating assuming that the flow is fixed. This assumption is almost universally used in the analysis of this problem. In the case of small Re, we can further assume that flow is Stokesian, with the velocities described by Eqs. (36) and (37), or their simplified versions (Eqs. (38) and (39)).

Any effects of droplet oscillations on the heating process are generally ignored. This could be justified when the droplet Weber number $We = 2u_0 R_d \rho_l/\sigma_s$ (where σ_s is the interfacial surface tension) is less than 4 [103]. This result was obtained in [103] based on experimental studies of falling droplets at Re in the range 138–971.

Most approaches to investigation of the problem of transient heating of moving droplets performed so far can be presented in two groups. The first approach is based on the assumption that the temperature of the droplet surface remains constant throughout the whole heating process. The second approach allows for

changes of droplet temperature with time. In what follows these two approaches will be considered separately.

Fixed surface temperature. Choudhoury and Drake [75] and Konopliv and Sparrow [104] were perhaps the first to solve the problem of transient heating of a solid sphere at small Reynolds and Peclet numbers, assuming that the surface temperature of the sphere is fixed. In the first paper, the steady-state velocity distribution in fluid described by Eqs. (36) and (37) was used and it was assumed that initially the temperatures of the sphere and surrounding fluid were equal. Then at $t=0$ the temperature of the sphere abruptly changed to another constant value. The solution obtained for small t in the limit of very small Re reduced to the one predicted by Eq. (10). In the limit of large t the solution predicts values of Nu close to 2. This is as expected since this solution was based on the assumption of small Re and Pe.

Konopliv and Sparrow [105] generalised the analysis of their earlier paper [104] to the case of large Pe. As in [104], the analysis was based on Eqs. (38) and (39). They drew attention to the fact that for high Pe the temperature field is confined to a boundary layer which is very thin compared with the velocity field boundary layer. This allowed these authors to simplify both the temperature equation (32) (assuming that heat conduction takes place in the radial direction only) and Eqs. (38) and (39) (assuming that R is close to R_d). Two methods were employed to obtain the solution of the simplified temperature equation. One method involved numerical inversion of an integral transform, while the second was based on an asymptotic expansion in the Laplace transform s plane. For small t both methods predicted similar results, while for larger t, the first method was recommended. In the limit of large times the results of [105] reduced to those predicted by Eq. (45) with $Re=0$.

A similar problem, but for the heating of a liquid droplet, was considered in [73]. These authors assumed that both Re and Pe are small, based their analysis on Eqs. (40) and (41) and obtained analytical expressions for Nu, valid in short and long time limits. In a short time limit, their expression reduced to Eq. (10). In a long time limit ($Fo=O(Pe^{-2})$), they obtained the following expression

$$Nu = 2\left\{1 + \frac{Pe}{2}\left[\frac{1}{2}\operatorname{erf}\left(Pe\frac{\sqrt{Fo}}{4}\right) + \frac{2}{Pe\sqrt{\pi Fo}}\exp\left(-\frac{Pe^2 Fo}{16}\right)\right] + \frac{3+2\lambda_v}{24(1+\lambda_v)}Pe^2\ln\left(\frac{Pe}{2}\right)\right\} + O(Pe^{1+}), \quad (52)$$

where Fo is the Fourier number introduced in Eqs. (5) and (6).

In [100] it was shown that the results predicted by Eq. (52) for a solid sphere, $Pe=0.5$ and long times, differ by less than 3% from the results, predicted by the numerical analyses for the Stokesian flow.

In the same paper [100] it was shown that at sufficiently small times the predicted values of Nu practically do not depend on Re. This dependence was shown to be rather weak for relatively small Pe ($Pe=2$) at all times, but significant for $Pe=200$ at large times.

Several papers have considered the problem of transient heat transfer between non-spherical bodies and ambient fluid. In [106] a model for the heat transfer processes from an oblate and a prolate spheroid at the limit of very small Pe was developed. In [107] a more general problem of heat transfer from a particle with an arbitrary shape suspended in a fluid was considered.

Variable surface temperature. Chao [108] was perhaps the first to solve the problem of conjugate heat transfer between a translating droplet and ambient gas. He took into account the re-circulation inside a droplet, but ignored the effects of viscosity. This allowed him to approximate the velocity profile outside droplets by Eqs. (42) and (43). A similar set of equations for the internal flow (Hill vortex) was used. This approximation is expected to lead to substantial errors at small Re (Stokesian flow), but could be justified for $Re>200$. Also, the assumption concerning a thin thermal boundary layer was made, which could be justified for large Pe. This allowed further simplification of Eqs. (42) and (43), assuming that $|R-R_d| \ll R_d$ and using Eq. (32) (assuming that heat conduction takes place in the radial direction only (cf. [105])). The simplified temperature equation was solved outside and inside the droplet, assuming that the temperature and heat fluxes on both sides of the interface are equal. The solution for the average value of the Nusselt number was presented in an explicit analytical form. As in the case of stationary droplets, this solution predicted large Nu for small t. For large times it asymptotically approached a steady-state solution in the form

$$Nu = \frac{2Pe^{1/2}}{\sqrt{\pi}(1+\beta_v)}, \quad (53)$$

where $\beta_v = \sqrt{k_g\rho_g c_{pg}/(k_l\rho_l c_l)}$. In the case of fuel droplets moving in gas β_v is expected to be small.

Chao and Chen [109] solved the same problem as [108] using a different analytical technique originally developed in [110]. The results were almost identical to the ones predicted by the analytical solution [108]. The previously mentioned results obtained in [105] for a sphere with fixed temperature were generalised in the same paper to the case when sphere heating is taken into account provided that the thermal conductivity of this sphere is infinitely large.

Abramzon and Borde [111] presented the results of numerical analysis of transient heat transfer to slowly moving droplets (Stokesian approximation) in a wide range of Peclet numbers $0 \leq Pe \leq 1000$. They studied the conjugate problem so that the heat transfer processes in gas and droplets were taken into account. They used the flow velocity distribution predicted by Eqs. (40) and (41) (note a printing mistake in their Eq. (2)). It was shown that the droplet heating process can be divided into two stages. In the first stage, the heat is transferred primarily by conduction, and the isotherms have almost spherical shape. In the second stage, convective heat transfer predominates. During this stage, the internal isotherms were shown to be close to streamlines. At high *Pe*, *Nu* was shown to oscillate in time about its asymptotic value. The fact that initially the droplet is heated predominantly by conduction agrees with the result reported in [100], where it was shown that *Nu* practically does not depend on *Re* at the initial stage of heating (see the discussion of [75]). It was shown that for large *Pe* ($100 \leq Pe \leq 1000$) the heating can be regarded as quasi-stationary after a short initial time lapse. During this initial time period, the analytical solution of [108] was shown to give satisfactory results. A detailed comparison of the asymptotic values of *Nu*, predicted by the numerical analysis, and previously reported results of asymptotic analyses were presented for $\lambda_v = 1$ (fluids with similar hydrodynamic properties) and $\lambda_v = \infty$ (solids).

Results of further analysis of transient heat transfer between an ambient fluid and a single sphere were reported in [112]. This analysis was restricted to solid spheres, but a wide range of *Pe* ($1 \leq Pe \leq 10{,}000$) and the ratios of volume heat capacities of the fluid to that of a sphere in the range ($0 \leq (\rho c)_{12} \equiv \rho_g c_{pg}/(\rho_l c_l) \leq 2$) were considered. The droplet thermal conductivity was assumed to be large, so that the temperature gradients inside the sphere could be ignored. The flow field was assumed to be Stokesian and the velocity distribution outside the sphere was taken in the form given by Eqs. (38) and (39). It was pointed out that for $(\rho c)_{12} = 0$ and *Pe* close to zero, the values of *Nu* asymptotically approach 2, as predicted by Eq. (10). However, for $(\rho c)_{12} \geq 0.2$ and the same *Pe*, the asymptotic values of *Nu* were shown to be close to zero. This is consistent with the prediction of Fig. 1. Note that this figure is presented for $(\rho c)_{12} = 0.0156$, for which the calculations were not performed in [112]. I anticipate that one of the main conclusions made in this paper that "at $(\rho c)_{12} \geq 0.2$ the asymptotic values of the Nusselt number appears to be considerably less than the corresponding steady-state value for the case of constant sphere temperatures" could be generalised to any $(\rho c)_{12} > 0$. In [113] the analysis presented in [112] was generalised to take into account the flow recirculation in droplets, although the range of *Pe* was reduced to $10 \leq Pe \leq 1000$. Whenever the results of [112] and [113] have been compared, the difference between them has been less than 1%.

The energy equation of a rigid sphere of infinitely large thermal conductivity in a viscous fluid subject to an unsteady flow and temperature field under the assumption of small *Pe* was developed in [114]. The values of the sphere's temperature were shown to depend on instantaneous values of fluid temperature and the 'histories' of both fluid and sphere temperature. These histories were accounted for via the so-called history integral, which, in the energy equation is analogous to the history force (Basset force) in the equation for the motion of a sphere. The presence of the history integral effectively turns the differential equation for the sphere temperature into an integro-differential equation, the analysis of which can be computer intensive. The authors of [115] presented a more detailed analysis of the effect of the history term on the transient energy equation of a sphere. More specifically, they attempted to clarify when this term can be ignored if a predetermined calculation error can be tolerated. They considered the transient heat transfer cases related to three different fluid temperature processes: step temperature change, ramp temperature change and sinusoidal temperature change. It was shown that the importance of the history term is mainly controlled by the above-mentioned parameter $(\rho c)_{12}$. In the case when $0.002 \leq (\rho c)_{12} \leq 0.2$ (the range of typical values for fuel droplets in air) this term is important and needs to be retained. More detailed analysis of the history term is given in [16].

Talley and Yao [116] drew attention to the fact that heat transfer to a moving droplet can still be correctly predicted by Eq. (1), with appropriate boundary conditions, if the liquid thermal conductivity k_l is replaced by the so-called effective thermal

conductivity k_{eff}. This approach was further developed by Abramzon and Sirignano [63] who defined k_{eff} by the following equation

$$k_{\text{eff}} = \chi k_{\text{l}}, \tag{54}$$

where the coefficient χ varies from about 1 (at droplet Peclet number $Pe_{\text{d(l)}} = Re_{\text{d(l)}} Pr_{\text{l}} < 10$) to 2.72 (at $Pe_{\text{d(l)}} > 500$) and can be approximated as:

$$\chi = 1.86 + 0.86 \tanh[2.225 \log_{10}(Pe_{\text{d(l)}}/30)]. \tag{55}$$

Liquid fuel transport properties were used for calculating $Pe_{\text{d(l)}}$. This model can predict reasonably accurately (especially at small and large $Re_{\text{d(l)}}$) the droplet average surface temperature, but not the distribution of temperature inside droplets. In our case, however, we are primarily interested in the prediction of the surface temperature, which controls droplet evaporation. Hence, the applicability of this model can be justified. It is widely known as 'the effective thermal conductivity model'. The simplicity of this model makes it particularly attractive for application in CFD codes. For example, it allows the application of solution (21) to the case of moving droplets by replacing k_{l} by k_{eff}, assuming that $h =$ const.

More recent studies of the problem of transient heating of moving droplets were more case specific, and in most cases they were linked with evaporation processes. They will be reviewed later in Section 3.

2.2. Radiative heating

2.2.1. Basic equations and approximations

Since thermal radiation propagates with a velocity close to the velocity of light, droplet motion does not influence the process of radiative heating. Hence, the analysis in this section is equally applicable to stationary and moving droplets.

The simplest model for radiative heating of droplets could be based on the assumption that droplets are opaque grey spheres, characterised by emissivity ϵ. In this case, the effect of radiative heating of droplets could be described via replacing the heat flux given by Eq. (11), with the following equation

$$|\dot{q}| = h(T_{\text{g}\infty} - T_{\text{s}}) + \sigma\epsilon(\theta_{\text{R}}^4 - T_{\text{s}}^4), \tag{56}$$

where θ_{R} is the so called radiative temperature, σ is the Stefan–Boltzmann constant. For optically thick gas θ_{R} can be identified with the ambient gas temperature $T_{\text{g}\infty}$, while for optically thin gas it can be identified with the external temperature T_{ext} (e.g. temperature of remote flame) [117,118]. The simplicity of this model makes it particularly attractive for applications, including application in CFD codes (see, e.g. [119–125]). The value of ϵ in this equation could be considered as a free parameter, which could be specified based on more rigorous calculations or obtained from the analysis of experimental data.

Assuming that there are no temperature gradients inside droplets and $\theta_{\text{R}} = T_{\text{ext}}$, Eq. (56) allows us to generalise Eq. (18) and its solution (19) to account for the effect of thermal radiation by replacing $T_{\text{g}\infty}$ with

$$T_{\text{g}\infty} + \frac{\sigma\varepsilon(T_{\text{ext}}^4 - T_{\text{e}}^4)}{h}.$$

In a similar way, radiative heating could be accounted for in solution (21). In both cases it is implicitly assumed that the external radiation is that of a black body.

In most practically important cases of fuel droplet heating, $T_{\text{s}} \ll T_{\text{ext}}$ and the contribution of the terms proportional to T_{s}^4 can be safely ignored. If this is not the case (T_{ext} is of the order of less than T_{s}) then T_{s} is still below the boiling temperature of fuel (about 600 K), and the contribution of radiative heating can almost always be ignored altogether. In the following analysis, the contribution of radiation from droplets will be ignored.

The approach based on the assumption that droplets are opaque grey spheres, however, overlooks the fact that droplet radiative heating takes place not at their surface (as in the case of convective heating) but via the absorption of thermal radiation penetrating inside the droplets. Thus, the droplets should be considered as semi-transparent rather than grey opaque bodies [126–140]. The focus of this section will be on analysis of the models of thermal radiation absorption in these semi-transparent droplets, without taking into account the contribution of radiation from droplets (see [126–128] for the analysis of the latter effect).

In the case of models (3) and (4) (conduction limit and effective conductivity), Eq. (1) for semi-transparent droplets in the presence of thermal radiation can be generalised to

$$\frac{\partial T}{\partial t} = \kappa\left(\frac{\partial^2 T}{\partial R^2} + \frac{2}{R}\frac{\partial T}{\partial R}\right) + P(R), \tag{57}$$

where $P(R)$ accounts for the radiative heating of droplets. This equation is to be solved subject to the same boundary conditions (20) as before. Spherical symmetry of the problem is assumed. Note that the units of $P(R)$ are K/s.

The solution of Eq. (57) is a straightforward generalisation of solution (21) and can be written as [77]

$$T(R,t) = \frac{R_d}{R}\sum_{n=1}^{\infty}\left\{\frac{p_n}{\kappa_R\lambda_n^2} + \exp[-\kappa_R\lambda_n^2 t]\left(q_n - \frac{p_n}{\kappa\lambda_n^2}\right)\right.$$
$$-\frac{\sin\lambda_n}{||v_n||^2\lambda_n^2}\mu_0(0)\exp[-\kappa_R\lambda_n^2 t]$$
$$\left.-\frac{\sin\lambda_n}{||v_n||^2\lambda_n^2}\int_0^t\frac{d\mu_0(\tau)}{d\tau}\exp[-\kappa_R\lambda_n^2(t-\tau)]d\tau\right\}$$
$$\times\sin\left[\lambda_n\left(\frac{R}{R_d}\right)\right] + T_g(t), \quad (58)$$

where

$$p_n = \frac{1}{R_d^2||v_n||^2}\int_0^{R_d}(RP(R))\sin(\lambda_n R/R_d)dR,$$

other notation is the same as in (21).

In the case of models (2) (no temperature gradient inside droplets) Eq. (18) for semi-transparent droplets in the presence of thermal radiation can be generalised to:

$$\frac{4}{3}\pi R_d^3\rho_l c_l\frac{dT_d}{dt} = 4\pi R_d^2 h(T_{g\infty} - T_d) + \rho_l c_l P_{total}, \quad (59)$$

where

$$P_{total} = 4\pi\int_0^{R_d} P(R)R^2\,dR \quad (60)$$

is the total amount of radiation absorbed in a droplet.

Note that in the recent paper [138] the effect of thermal radiation was accounted for not only by the term $P(R)$ in Eq. (57) but also via the modification of the boundary condition (20). I believe that this cannot be done in the case of semi-transparent droplets.

The practical application of Eqs. (58) and (60) is complicated by the fact that we do not know the value of $P(R)$. Estimates of this function, using various approximations, will be one of the main focuses of the rest of this section.

2.2.2. Mie theory

The most rigorous approach to the calculation of $P(R)$ is based on the solution of the Maxwell equations, with boundary conditions at the droplet's surface. These boundary conditions are: continuity of the normal component of the wave electric field and the jump in its tangential components controlled by the complex index of refraction of the liquid [141,142]. This is the well known Mie theory. In the case of interaction between a plane linearly polarized electromagnetic wave and a semi-transparent sphere (droplet) this theory gives the following relations for the complex amplitudes of the components of the wave electric field inside the droplet [131–144]

$$E_r = \frac{E_0\cos\varphi}{m_\lambda^2\rho_\lambda^2}\sum_{k=1}^{\infty} i^k(2k+1)d_k\psi_k(m_\lambda\rho_\lambda)P_k^1(\mu_\theta), \quad (61)$$

$$E_\theta = \frac{E_0\cos\varphi}{m_\lambda\rho_\lambda}\sum_{k=1}^{\infty}\frac{i^k(2k+1)}{k(k+1)}[c_k\psi_k(m_\lambda\rho_\lambda)\pi_k(\mu_\theta)$$
$$-id_k\psi_k'(m_\lambda\rho_\lambda)\tau_k(\mu_\theta)], \quad (62)$$

$$E_\varphi = \frac{E_0\sin\varphi}{m_\lambda\rho_\lambda}\sum_{k=1}^{\infty}\frac{i^{k+1}(2k+1)}{k(k+1)}[ic_k\psi_k(m_\lambda\rho_\lambda)\tau_k(\mu_\theta)$$
$$+d_k\psi_k'(m_\lambda\rho_\lambda)\pi_k(\mu_\theta)], \quad (63)$$

where

$$c_k = \frac{m_\lambda i}{m_\lambda\zeta_k(x_\lambda)\psi_k'(m_\lambda x_\lambda) - \zeta_k'(x_\lambda)\psi_k(m_\lambda x_\lambda)},$$

$$d_k = \frac{m_\lambda i}{\zeta_k(x_\lambda)\psi_k'(m_\lambda x_\lambda) - m_\lambda\zeta_k'(x_\lambda)\psi_k(m_\lambda x_\lambda)},$$

$$\pi_k(\mu_\theta) = \frac{P_k^1(\mu_\theta)}{\sqrt{1-\mu_\theta^2}}, \qquad \tau_k(\mu_\theta) = -\sqrt{1-\mu_\theta^2}\frac{dP_k^1(\mu_\theta)}{d\mu_\theta},$$

$m_\lambda = n_\lambda - i\kappa_\lambda$ is the complex index of refraction, $\rho_\lambda = 2\pi R/\lambda = Rx_\lambda/R_d$, $\mu_\theta = \cos\theta$, the prime denotes differentiation with respect to the argument, $\theta = 0$ is the direction of wave propagation, ϕ is the asymuthal angle measured from the plane of electric field oscillations of the incident wave (as viewed along the direction of wave propagation), E_0 is the amplitude of the electric field in the incident wave, ψ_k and ζ_k are the Riccati–Bessel functions defined as [143]

$$\psi_k(z) = \left(\frac{\pi z}{2}\right)^{1/2}J_{k+(1/2)}(z),$$

$$\zeta_k(z) = \left(\frac{\pi z}{2}\right)^{1/2}H_{k+(1/2)}^{(2)}(z),$$

$$\zeta_k(z) = (\pi z/2)^{(1/2)}H_{k+(1/2)}^{(2)}(z)$$

$J_{k+(1/2)}$ are the Bessel functions, $H_{k+(1/2)}^{(2)}$ are the Hankel functions of the second kind, $P_k^1(\mu_\theta)$ are the associated Legendre polynomials. Note that there is a printing mistake in the expression for E_ϕ given in [129] (cf. his Eq. (5)). Expressions for E_r, E_θ and E_ϕ given in [132] differ from those given above by the signs and the powers of i and signs of κ_λ. This difference is related to

the fact that we follow the definitions of complex amplitudes and the asymuthal angle given in [141,145], while Lage and Rangel [132] followed the definitions given in [142,146]. This obviously does not influence the values of $|E_r|$, $|E_\theta|$ and $|E_\phi|$ used in the following analysis. Equations similar to (61)–(63) could be obtained for the components of the wave magnetic field [146], but these will not be needed for our analysis. The distribution of thermal radiation power density absorbed inside the droplet for a given wavelength of incident radiation can be found from the equation [146]

$$p_\lambda(R,\mu_\theta,\varphi)=\frac{4\pi n_\lambda\kappa_\lambda}{\lambda}I_\lambda^{\text{ext}}\frac{|E_r|^2+|E_\theta|^2+|E_\varphi|^2}{|E_0|^2}, \tag{64}$$

where I_λ^{ext} is the intensity of external thermal radiation in a given direction. This equation was derived under the assumption that magnetic permeability of liquid is equal to 1 (this is a natural assumption for fuel droplets).

In the case of unpolarized external thermal radiation, coming from one direction $\theta=0$, we should set $\phi=\pi/4$ in the right hand side of Eq. (64) [146]. If the illumination of the droplet by unpolarized thermal radiation is spherically symmetric then the radial profile of the absorbed power can be found via integration of (64) over all angles ϕ and θ, i.e. from the equation [130,145,147,148]

$$p_\lambda(R)=2\pi\int_{-1}^{1}p_\lambda(R,\mu_\theta,\varphi)\mathrm{d}\mu_\theta=\frac{16\pi^2 n_\lambda\kappa_\lambda}{\lambda}I_\lambda^{\text{ext}}S(R), \tag{65}$$

where

$$S(R)=\frac{1}{2|m_\lambda|^4\rho_\lambda^4}\sum_{k=1}^{\infty}(2k+1)\big[k(k+1)|d_k\psi_k(m_\lambda\rho_\lambda)|^2+|m_\lambda|^2\rho_\lambda^2(|c_k\psi_k(m_\lambda\rho_\lambda)|^2+|d_k\psi_k'(m_\lambda\rho_\lambda)|^2)\big]. \tag{66}$$

The required value of $P(R)$ can be obtained from Eq. (65) via integration of the whole spectrum of thermal radiation

$$P(R)=\frac{1}{\rho_l c_l}\int_0^\infty p_\lambda(R)\mathrm{d}\lambda, \tag{67}$$

where the division of the integral by $\rho_l c_l$ converts the units of the radiation power absorbed in droplets from $\mathrm{W/m^3}$ to K/s. The total power absorbed inside droplets ($\rho_l c_l P_{\text{total}}$) is calculated from Eq. (60).

The calculations of $P(R)$ from Eq. (67) and P_{total} from Eq. (60) require the knowledge of I_λ^0, the spectral index of absorption and the index of refraction. If we assume that the external radiation is that of a black body (as was done when deriving Eq. (56)) then we can write [117,118]

$$I_\lambda^{\text{ext}}=B_\lambda(T_{\text{ext}})\equiv\frac{C_1}{\pi\lambda^5[\exp(C_2/(\lambda T_{\text{ext}}))-1]}, \tag{68}$$

$$C_1=3.742\times10^8\,\frac{\mathrm{W\,\mu m^4}}{\mathrm{m^2}},$$

$$C_2=1.439\times10^4\ \mu\mathrm{m\,K},$$

λ is the wave length in μm in this equation. The function $B_\lambda(T_{\text{ext}})$ is known as the Planck function. T_{ext} is the external temperature responsible for radiative heating (in the case of optically thick gas this should be replaced by ambient gas temperature).

Practically, the index of absorption κ_λ can only be measured experimentally (see e.g. [149]), or calculated on the basis of measured values of spectral reflectance at near normal incidence [150]. An example of such measurements is presented in Fig. 3 [133]. The plots are shown for low sulphur ESSO AF1313 diesel fuel used in cars (yellow fuel) and BP Ford reference diesel fuel used in off-road equipment (pink fuel). Also the plots referring to these diesel fuels after they have undergone a simulation of the ageing process by prolonged (6 h) boiling are shown in the same figure. As can be seen in this figure, the dependence of κ_λ on the type of diesel fuel

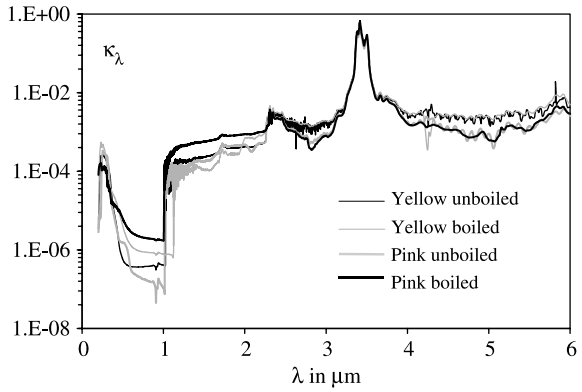

Fig. 3. Indices of absorption of four types of diesel fuel versus wavelength λ. Yellow fuel corresponds to low sulphur ESSO AF1313 diesel fuel used in cars; pink fuel corresponds to BP Ford reference diesel fuel used in off-road equipment. Reproduced from [133] with permission of ASME.

is noticeable, especially in the ranges of semi-transparency $\lambda<3$ μm and 4 μm $<\lambda<6$ μm. Peaks of absorption for all types of diesel fuel practically coincide.

The results of measurements of κ_λ could allow us to calculate the spectral distribution of the index of refraction n_λ, using Kramers–Krönig equations [118]. This, however, is expected to lead to substantial errors due to the limited range of wavelengths for which the measurements of κ_λ are usually performed (cf. Fig. 3). A more practical approach is based on subtractive Kramers–Krönig analysis, based on the measurements of n_λ at one particular wavelength, and its calculation for other wavelengths [134,151]. It was shown that for all types of fuel presented in Fig. 3, the results of these measurements and calculations can be accurately approximated by the following relationship [135]

$$n_\lambda = n_0 + 0.02\frac{\lambda-\lambda_m}{(\lambda-\lambda_m)^2+0.001}, \tag{69}$$

where $n_0=1.46$, $\lambda_m=3.4$ μm, λ is the wavelength in μm. For practical calculations of κ_λ, the dependence of n_λ on λ can be ignored and n_λ can be made equal to 1.46 [134].

Formally, Eq. (67), combined with the measured values of κ_λ and measured or calculated values of n, gives the required input parameters for Eqs. (58) and (59) describing droplet heating in the presence of thermal radiation. Direct application of Eqs. (67) and (60) is limited by the complexity of relevant calculations, and their incorporation into CFD codes is not feasible. Simpler, but practically important models will be considered in the following sections.

2.2.3. Integral absorption of radiation in droplets

A convenient and widely used approach to characterise the integral absorption of thermal radiation in droplets is based on the application of the efficiency factor of absorption Q_a. This is defined as the ratio of radiation power absorbed in a droplet to the power of thermal radiation illuminating this droplet. In view of Eq. (65) the explicit expression for Q_a can be presented as [130]

$$Q_a = \frac{P_{\lambda(abs)}}{P_{\lambda(ins)}} = \frac{\int_0^{R_d} 4\pi R^2 p_\lambda(R)\,dR}{4\pi^2 R_d^2 I_\lambda^0} = \frac{8n_\lambda\kappa_\lambda}{x_\lambda^2}\int_0^{x_\lambda} S(\rho_\lambda)\rho_\lambda^2\,d\rho_\lambda, \tag{70}$$

where S is defined by Eq. (66).

As follows from Eqs. (70) and (66), for a given value of λ, Q_a depends on n_λ, κ_λ and R_d. Remembering that n_λ remains almost constant over the whole range of λ under consideration $n\equiv n_\lambda\approx 1.46$, it was shown that Q_a is most sensitive towards the optical thickness of droplets $\tau_0=2\kappa_\lambda x_\lambda=a_\lambda R_d$, where a_λ is the absorption coefficient [136]. The results of calculations based on Eq. (70) were approximated by a particularly simple formula [152]

$$Q_a = \frac{4n}{(n+1)^2}[1-\exp(-2\tau_0)], \tag{71}$$

where $\tau_0=a_\lambda R_d$ (hereafter, the subscript λ at n is omitted). This is a slight improvement of the formula used in [136] ($Q_a=1-\exp(-2\tau_0)$). Eq. (71) is much simpler than Eq. (70), and this is expected to be particularly useful for application in CFD codes. The additional errors introduced by this equation are generally less than the errors introduced by other approximations used in the model (say, the assumption about the sphericity of droplets).

Assuming that the thermal radiation illuminating the droplet is that of a black body and n is constant, the average efficiency factor of absorption of thermal radiation in the range of λ from λ_1 to λ_2 was found as [136,133]:

$$\overline{Q_a} = \frac{4n}{(n+1)^2}\left\{1-\left[\int_{\lambda_1}^{\lambda_2}\frac{\exp(-(8\pi\kappa_\lambda R_d/\lambda)}{\lambda^5[\exp(C_2/(\lambda T_{ext}))-1]} \times d\lambda \Big/ \int_{\lambda_1}^{\lambda_2}\frac{d\lambda}{\lambda^5[\exp(C_2/(\lambda T_{ext}))-1]}\right]\right\}. \tag{72}$$

Taking into account the experimentally measured values of κ_λ (see Fig. 3) it was found that the best approximation for $\overline{Q_a}$ in the ranges $5\le R_d\le 50$ μm and $1000\le T_{ext}\le 3000$ K is provided by the function [133,136]

$$\Lambda_0 = aR_d^b \tag{73}$$

where a and b are quadratic functions of T_{ext} approximated as:

$$\left.\begin{aligned} a &= a_0 + a_1(T_{ext}/1000) + a_2(T_{ext}/1000)^2 \\ b &= b_0 + b_1(T_{ext}/1000) + b_2(T_{ext}/1000)^2 \end{aligned}\right\}. \tag{74}$$

The values of the coefficients in these expressions for a and b depend on the type of diesel fuel under consideration. If unboiled yellow diesel fuel is taken (see Fig. 3) and R_d is measured in μm, then Eq. (74) can be presented in a more explicit form [133]:

$$a = 0.10400 - 0.054320T_{ext}/1000 + 0.008(T_{ext}/1000)^2,$$
$$b = 0.49162 + 0.098369T_{ext}/1000 - 0.007857(T_{ext}/1000)^2.$$

The plots of $\overline{Q_a}$ and Λ_0 versus R_d for a range of external temperatures are shown in Fig. 4. As follows from this figure, the values of $\overline{Q_a}$ and Λ_0 are surprisingly close to each other in the whole range of temperatures under consideration. This justifies the application of approximation (73) for practical applications in CFD codes. In the case when the range of temperatures is extended to $500 \le T_{ext} \le 3000$ K then the values of a and b should be approximated by more complicated polynomials of the fourth power [133]. These, however, seem to be of limited practical importance, as the contribution of radiation at external temperatures less than 1000 K is generally small.

2.2.4. Geometric optics analysis

So far, two extreme cases have been considered: the distribution of thermal radiation absorption in droplets as predicted by the Mie theory (Section 2.2.2) and a simplified model predicting the overall absorption of thermal radiation in droplets (Section 2.2.3). In this section, we return to the problem of finding the distribution of thermal radiation absorption in droplets, but this problem will be solved using a much more simple model than the one used in Section 2.2.2.

Firstly, we assume that the size parameter $x_\lambda = 2\pi R_d/\lambda$ is much greater than unity. This enables us to replace analysis based on the Mie theory by analysis based on the geometric optics approximation. As in the previous sections, we assume that the illumination of the droplet by external radiation is spherically symmetrical, the angular distribution of this radiation is known and the droplet's shape can be approximated by that of a sphere. In this case the radiation transfer equation in the droplet can be presented as [153]

$$\mu_\theta \frac{\partial I_\lambda}{\partial R} + \frac{1-\mu_\theta^2}{R}\frac{\partial I_\lambda}{\partial \mu_\theta} + a_\lambda I_{a\lambda} = 0, \tag{75}$$

where $I_\lambda(r,\mu_\theta)$ is the spectral radiation intensity at a given point integrated along the asymuthal angle, θ is measured from the R-direction. This equation does not take into account the effects of scattering and the contribution of the internal source of thermal radiation (see [154]).

The boundary conditions for $I_\lambda(R,\mu_\theta)$ can be presented as [153]

$$\left.\begin{aligned} I_\lambda(0,-\mu_\theta) &= I_\lambda(0,\mu_\theta), \\ I_\lambda(R_d,-\mu_\theta) &= R_{ref}(n,\mu_\theta)I_\lambda(R_d,\mu_\theta) \\ &\quad + [1-R_{ref}(1/n,-\mu'_\theta)]n^2 I^{ext}_\lambda(-\mu'_\theta), \end{aligned}\right\} \tag{76}$$

where $\mu'_\theta = \sqrt{1-n^2(1-\mu_\theta^2)}$, R_{ref} is the reflection coefficient [155], I^{ext}_λ is the spectral intensity of external radiation. Note that $R_{ref}(1/n,-\mu'_\theta) = R_{ref}(n,\mu_\theta)$. The assumption that the illumination of the droplet by external radiation is spherically symmetrical does not imply the isotropy of the distribution of thermal radiation inside the droplet, except in its centre.

The first boundary condition in (76) is the symmetry condition at the droplet centre. The second boundary condition in (76) indicates that the value of $I_\lambda(R_d,-\mu_\theta)$ at the surface of the droplet is the sum of the intensity of the reflected radiation (the first term in the right hand side of this equation) and the intensity of the refracted radiation (the second term in the right hand side of this equation).

The radiation power absorbed per unit volume of the droplet is determined as

$$p(R) = \int_0^\infty p_\lambda(R)\mathrm{d}\lambda, \tag{77}$$

where

$$p_\lambda(R) = a_\lambda I^0_\lambda(R), \qquad I^0_\lambda(R) = \int_{-1}^{1} I_\lambda(R,\mu_\theta)\mathrm{d}\mu_\theta,$$

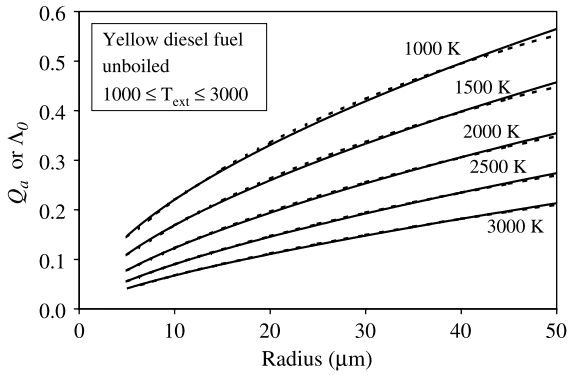

Fig. 4. Plots of $\overline{Q_a}$, defined by Eq. (72), versus R_d (solid) and Λ_0, defined by Eq. (73), versus R_d (dashed) for $T_{ext}=1000$ K, $T_{ext}=1500$ K, $T_{ext}=2000$ K, $T_{ext}=2500$ K and $T_{ext}=3000$ K (indicated near the curves) for yellow unboiled diesel fuel. Plots are based on the values of the coefficient found for external gas temperatures in the range $1000 \le T_{ext} \le 3000$ K and droplet radii in the range $5 \le R_d \le 50$ μm. Reproduced from [133] with permission of ASME.

$I^0_\lambda(R)$ is the spectral radiation power density. Note that $p(R)$ (in contrast to $P(R)$) has units of W/m^3.

Calculation of $p(R)$ based on Eqs. (75)–(77) is rather difficult. Following [129,156] this problem is simplified using the so called MDP_0 approximation. In this approximation it is assumed that in the droplet core ($R \le R_* \equiv R_d/n$)) radiation intensity is constant in the angular ranges $-1 \le \mu_\theta < 0$ and $0 < \mu_\theta \le 1$. At the droplet periphery ($R_* < R \le R_d$), however, constant values of the radiation intensity are assumed when $-1 \le \mu_\theta < -\mu_*$ and $\mu_* < \mu_\theta \le 1$, where $\mu_* = \sqrt{1-(R_*/R)^2}$. External radiation cannot penetrate into the droplet peripheral zone at $-\mu_* < \mu_\theta < \mu_*$. Numerical solutions of Eq. (75) with boundary conditions (76) have shown that the MDP_0 adequately predicts the angular dependence of the radiation intensity [129]. This approximation is based on the analysis of the following function:

$$g_0(R) = \begin{cases} I^0_\lambda(R), & R \le R_* \\ I^0_\lambda(R)/(1-\mu_*), & R_* < R \le R_d \end{cases}. \tag{78}$$

Integration of Eqs. (75) and (76) over μ_θ in the ranges $-1 \le \mu_\theta < 0$ and $0 < \mu_\theta \le 1$ (droplet core) and in the ranges $-1 \le \mu_\theta < -\mu_*$ and $\mu_* < \mu_\theta \le 1$ (droplet periphery) leads to the following boundary value problem for $g_0(R)$ [129,137,156]

$$\frac{1}{4R^2}(R^2 g_0')' + \frac{C_{g1}-1}{2R} g_0' = C_{g2} a_\lambda^2 g_0, \tag{79}$$

where

$$C_{g1} = \begin{cases} 1 & \text{when } R \le R_* \\ (1-\mu_*)/2\mu_* & \text{when } R_* < R \le R_d, \end{cases}$$

$$C_{g2} = \begin{cases} 1 & \text{when } R \le R_* \\ (1+\mu_*)^{-2} & \text{when } R_* < R \le R_d, \end{cases}$$

the differentiation is over R.

The boundary conditions for Eq. (79) are written as

$$\left.\begin{aligned} g_0' &= 0 && \text{when } R = 0 \\ \frac{1+\mu_c}{2} g_0' &= \frac{2n a_\lambda}{n^2+1}(n^2 I^{0(ext)}_\lambda - g_0) && \text{when } R = R_d, \end{aligned}\right\} \tag{80}$$

where

$$\mu_c = \sqrt{1-(1/n^2)}, \qquad I^{0(ext)}_\lambda = \int_{-1}^{1} I^{ext}_\lambda(\mu_\theta)\mathrm{d}\mu\theta.$$

When deriving Eqs. (79) and (80) it was assumed that a_λ does not depend on R and the average values of $R_{ref}(n,\mu_0)$ in the ranges $-1 \le \mu_\theta < -\mu_c$ and $\mu_c < \mu_\theta \le 1$ are equal to $R_{ref}(n,1)$.

The spectral power of the radiation absorbed per unit volume inside the droplet is determined as:

$$p_\lambda(R) = a_\lambda[1-\mu_* \Theta(R-R_*)]g_0(R), \tag{81}$$

where Θ is the Heaviside unit step function:

$$\Theta(x) = \begin{cases} 0 & \text{when } x < 0 \\ 1 & \text{when } x \ge 0. \end{cases}$$

Presentation of the results for the differential absorption of thermal radiation is simplified if the following normalised function is introduced:

$$w_\lambda(R) = p_\lambda(R) \Big/ \left[\frac{3}{R_d^3}\int_0^{R_d} p_\lambda(R) R^2\,\mathrm{d}R\right]. \tag{82}$$

Remembering (82) and the fact that the total radiation power absorbed in the droplet is given by the expression

$$\rho_l c_l P_{total} = \pi R_d^2 \int_0^\infty Q_a I^{0(ext)}_\lambda \mathrm{d}\lambda,$$

allows us to calculate the radiation power absorbed per unit volume inside the droplet as:

$$p(R) = \frac{0.75}{R_d}\int_0^\infty Q_a w_\lambda(R) I^{0(ext)}_\lambda \mathrm{d}\lambda. \tag{83}$$

If the external thermal radiation is that of a black body at temperature T_{ext} then $I^{0(ext)}_\lambda = 4\pi B_\lambda(T_{ext})$ and Eq. (83) is rewritten as:

$$P(R) = \frac{3\pi}{c_l \rho_l R_d}\int_0^\infty Q_a w_\lambda(R) B_\lambda(T_{ext})\mathrm{d}\lambda, \tag{84}$$

where B_λ is the Planck function introduced earlier. Note that $P(R)$ in Eq. (84) is in K/s.

As follows from Eq. (84), the problem of the approximate calculation of the radiation power absorbed per unit volume inside droplets reduces to the problem of finding an approximation for $w_\lambda(R)$.

Following [137] $w(R)$ can be approximated as:

$$w_\lambda(R) = \frac{[1-\mu_* \Theta((R/R_d)-1/n)]((R/R_d)^2+\bar\gamma)}{[0.6(1-\mu_c^5)-\mu_c^3/n^2]+\bar\gamma(1-\mu_c^3)}, \tag{85}$$

where $\bar{\gamma} = (1.5/\tau_0^2) - (0.6/n^2)$ and

$$w_\lambda(R) = \frac{\xi^2\tau_0^3}{3}\,\frac{\exp[-\xi(\tau_0-\tau_\lambda)]}{\tau_0(\xi\tau_0-2)+(2/\xi)\left[1-\exp(-\xi\tau_0)\right]}, \tag{86}$$

where $\xi = 2/(1+\mu_c)$.

Eq. (85) was used when $\tau_0 < n\sqrt{2.5}$, otherwise Eq. (86) was used. Eqs. (85) and (86) were used for the analysis of diesel fuel droplet heating and evaporation in the presence of thermal radiation in [139,140]. An alternative formula for $w_\lambda(R)$, valid in the whole range of τ_0, was suggested in [131].

Some authors combined the geometrical optics approximation with the Monte Carlo approach. This turned out to be particularly useful to study the anisotropic emission characteristics of a semi-transparent spherical body with spherically asymmetric temperature distribution [157].

3. Droplet evaporation

In the most general case the droplet evaporation process includes two main phases: (1) detachment of fuel molecules from the surface of the droplet into gas in the immediate vicinity of droplets (evaporation proper) and (2) diffusion of fuel vapour from the surface of the droplet into the ambient gas. The mathematical modelling of the first process is far more complicated than the modelling of the second process. Hence, in most practical applications, the researchers tried to focus just on the second process, ignoring the details of the first. The models, which they used were based on the assumption that fuel vapour in the vicinity of the droplet surface is always saturated. Hence, the rate of fuel evaporation is equal to the rate of fuel diffusion from the droplet surface to ambient gas. These are known as the hydrodynamic models of droplet evaporation. In contrast to these, models taking into account the details of detachment of fuel molecules are known as kinetic models (if they are based on the kinetic Boltzmann equation) or molecular dynamics models (if they are based on modelling of the dynamics of individual molecules).

I will start with the analysis of empirical correlations, which are not directly linked with any physical evaporation model (Section 3.1). Then hydrodynamic models of droplet evaporation will be reviewed (Section 3.2). In Section 3.3 the approaches to modelling of multi-component droplets will be briefly reviewed. Kinetic and molecular dynamics evaporation models will be reviewed in Sections 3.4 and 3.5, respectively. A brief overview of the modelling of autoignition, following droplet evaporation, will be presented in Section 3.6. Finally, in Section 3.7 a brief overview of the mathematical tools used for the coupled solution of equations describing droplet heating, evaporation and the ignition of fuel vapour/air mixture will be presented.

3.1. Empirical correlations

A brief summary of empirical correlations for the values of Nusselt numbers of non-evaporating moving droplets was given in Section 2.1.2. The most widely used of these correlations are those given by Eqs. (33) and (35). A detailed analysis of the early suggested correlations for evaporating droplets is given in [158]. Also, in this paper a detailed analysis of the experimental data on droplets suspended at the end of a tube in a wind tunnel was presented. This analysis eventually led to the following correlation [64,66,158]:

$$Nu_f = [2 + 0.57\, Re_f^{1/2} Pr_f^{1/3}]/(1+B_f)^{0.7}, \tag{87}$$

where

$$B_f = \frac{c_{pv}(T_g - T_s)}{L}\left(1 - \frac{|\dot{q}_d|}{|\dot{q}_c|} + \frac{|\dot{q}_R|}{|\dot{q}_c|}\right), \tag{88}$$

$|\dot{q}_d|$ is the heat rate spent on raising the temperature of a liquid droplet, $|\dot{q}_c|$ and $|\dot{q}_R|$ are the heat rates supplied to droplets by convection and radiation, $Re_f = 2R_d\rho_{g\infty}|\mathbf{v}_g - \mathbf{v}_d|/\mu_{gf}$, subscript f indicates that the values of parameters are taken inside the film surrounding the droplet, subscript ∞ in the term T_g is hereafter omitted. It was assumed that inside this film the temperature is equal to $(T_g + T_s)/2$ and the fuel vapour mass fraction is equal to $(Y_{v\infty} + Y_{vs})/2$, $Y_{v\infty}$ and Y_{vs} are mass fractions of fuel vapour in the vicinity of droplets and away from them. It was assumed that droplets can be treated as black bodies with emissivities equal to 0.95. This seems to be acceptable in the case of relatively large droplets used in the analysis of [158] (R_d was between about 0.5 and 3 mm), but is likely to be highly questionable in the case of smaller droplets (see Section 2.2.3). In the case of $|\dot{q}_d| = |\dot{q}_R| = 0$, B_f is identical with the Spalding heat transfer number introduced later. Eq. (87) was obtained in the following range of parameters $0.07 \le B_f \le 2.79$, and $24 \le Re_f \le 1974$. It can be extrapolated beyond this range.

Note that in the absence of evaporation $|\dot{q}_d| = |\dot{q}_c| + |\dot{q}_R|$ and $B_f = 0$. In this case Eq. (87) is identical with the corresponding equation for non-evaporating droplets (Eq. (33)). The predictions of Eq. (87) were shown to be

in agreement with the results of numerical analysis [64,159].

In a similar way as the convection heat transfer coefficient was introduced to describe droplet heating, the mass transfer coefficient h_m is used to describe their evaporation. This coefficient can be defined via the following equation:

$$m''_d = h_m(\rho_{vs} - \rho_{v\infty}), \tag{89}$$

where:

$$m''_d = \frac{|\dot{m}_d|}{4\pi R_d^2},$$

ρ_{vs} and $\rho_{v\infty}$ are densities of fuel vapour in the vicinity of droplets and away from them (ambient gas). For stationary droplets:

$$h_m = \frac{D_g}{R_d},$$

where D_g is the binary diffusion coefficient of fuel vapour in gas. In the general case, the dimensionless mass transfer coefficient was introduced via the Sherwood number defined as [160]:

$$Sh = \frac{2R_d h_m}{D_g} \tag{90}$$

(cf. the introduction of the dimensionless heat transfer coefficient via *Nu*; see the discussion following Eq. (12)).

In the case of stationary droplets $Sh = 2$. Similarly to Eq. (87), the correlation for *Sh* for moving evaporating droplets was obtained in the form [161]:

$$Sh_f = [2 + 0.87\,\mathrm{Re}_f^{1/2} Sc_f^{1/3}](1 + B_M)^{-0.7}, \tag{91}$$

where

$$B_M = \frac{\rho_{vs} - \rho_{v\infty}}{\rho_{gs}} = \frac{Y_{vs} - Y_{v\infty}}{1 - Y_{vs}} \tag{92}$$

is the Spalding mass number, $Sc_f \equiv \nu_f/D_f$ is the Schmidt number determined in the film region. Eq. (91) was obtained for $20 \le Re_f \le 2000$.

The prediction of Eq. (91) is consistent with the results of numerical analysis [64] (cf. the case of Nusselt number). Although correlations (87) and (91) were suggested about 20 years ago, they are still widely used in practical applications (e.g. [162]). A number of more recent experimental correlations were suggested [163–166]). These were mainly focused on the analysis of the effects of turbulence on droplet evaporation.

Results of the study of the dependence of *Sh* on *Re*, *Pe* and viscosity ratio λ_v based on the numerical analysis of the transient mass transfer process from a single moving droplet have been reported in [167]. The influence of *Sh* on *Re* has been found to be small for $Re < 2$ in agreement with Eq. (91). A sensitivity of *Sh* to λ_v has been shown to exist only for $0.1 < \lambda_v < 100$. Below this range the interface moves with the same velocity as the surrounding fluid, while above this range the droplet behaves similar to a rigid sphere. This is consistent with the prediction of the dependence of *Nu* on λ_v as given by Eqs. (49)–(51).

3.2. Hydrodynamic models

3.2.1. Classical model

The simplest model for droplet evaporation was suggested by Maxwell back in 1877 [2]. According to this model, the rate of droplet evaporation is controlled exclusively by the diffusion process and is given by the equation:

$$\dot{m}_d = 4\pi R^2 D_v \frac{d\rho_v}{dR}, \tag{93}$$

where D_v is the diffusion coefficient of the fuel vapour and ρ_v is its density. Since $\dot{m}_d < 0$ does not depend on *R*, this equation can be integrated from $R = R_d$ to $R = \infty$ to give:

$$\dot{m}_d = -4\pi R_d D_v(\rho_{vs} - \rho_{v\infty}), \tag{94}$$

where ρ_{vs} and $\rho_{v\infty}$ are the same as in Eq. (92).

Eq. (94) is known as the Maxwell equation [2]. Its limitation lies in the fact that it takes into account only the diffusion process, but ignores the effect of convective flow of the mixture of gas and fuel vapour away from the surface of the droplet (Stefan flow). Since the net gas flux towards the droplet is equal to zero we can write:

$$U\rho_g = D_g \frac{d\rho_g}{dR}, \tag{95}$$

where D_g is the diffusion coefficient of the gas, ρ_g is its density, and *U* is the value of the net velocity of the mixture of gas and fuel vapour away from the droplet.

Remembering Eq. (95), the droplet evaporation rate in the presence of vapour diffusion and Stefan flow can be found from the equation:

$$\dot{m}_d = 4\pi R^2 \left(D_v \frac{d\rho_v}{dR} - \rho_v U \right)$$

$$= 4\pi R^2 \left(D_v \frac{d\rho_v}{dR} - D_g \frac{\rho_v}{\rho_g} \frac{d\rho_g}{dR} \right). \tag{96}$$

Further assumptions are needed to solve Eq. (96). It is generally assumed that $D_g = D_v$. Following [2] we could assume that the total pressure and overall molar concentration of the mixture of gas and fuel vapour is constant in the vicinity of the droplet surface. A more widely used approach is based on the assumption that the total density of the mixture of gas and fuel vapour in the vicinity of the droplet surface is constant (see, e.g. [5]). None of these assumptions can be rigorously justified. Following widely used practice, we base our further analysis on the second assumption and assume that $\rho_{total} = \rho_g + \rho_v = \text{const}$. In this case the rearrangement and integration of Eq. (96) from $R = R_d$ to $R = \infty$ gives the following well known expression for $\dot{m}_d$:

$$\dot{m}_d = -4\pi R_d D_g \rho_{total} \ln(1 + B_M), \tag{97}$$

where B_M is the Spalding mass number defined by Eq. (92). If $Y_{vs} \ll 1$ and $Y_{v\infty} \ll 1$ then $B_M \ll 1$ and Eq. (97) reduces to Maxwell's Eq. (94). These conditions are typically satisfied except in the case when the droplet surface temperature approaches the boiling temperature. This can justify the application of Eq. (94) in asymptotical studies of droplet evaporation and the ignition of fuel vapour/air mixture (see [58–62,168] and Sections 3.6 and 3.7).

An alternative expression for $\dot{m}_d$ can be obtained based on the analysis of the energy balance equation. Assuming that the evaporating droplet is stationary this equation can be presented in the form [169]:

$$4\pi R^2 k_g \frac{dT}{dR} = -\dot{m}_d c_{pv}(T - T_s) - \dot{m}_d L(T_s) + |\dot{q}_d|, \tag{98}$$

where $R > R_d$. As in the previous equations, $\dot{m}_d \le 0$. The left hand side of this equation shows the heat supplied from the surrounding gas to the droplet. The first term in the right hand side shows the heat required to heat fuel vapour from T_s to $T = T(R)$ (gas temperature at the distance R from the centre of the droplet). The second and third terms in the right hand side show the heat spent on droplet evaporation and raising its temperature, respectively.

Eq. (98) can be rearranged to:

$$4\pi k_g \frac{dT}{c_{pv}(T - T_s) + L(T_s) - (|\dot{q}_d|/\dot{m}_d)} = -\frac{\dot{m}_d dR}{R^2}. \tag{99}$$

Integration of the left and the right hand sides of this equation from $T = T_s$ to $T = T_g$ and from $R = R_d$ to $R = \infty$, respectively gives:

$$\dot{m}_d = -\frac{4\pi k_g R_d}{c_{pv}} \ln(1 + B_T), \tag{100}$$

where

$$B_T = \frac{c_{pv}(T_g - T_s)}{L(T_s) - (|\dot{q}_d|/\dot{m}_d)} \tag{101}$$

is the Spalding heat transfer number [63]. From Eqs. (97) and (100) follows the relation between B_T and B_M [63]:

$$B_T = (1 + B_M)^{\varphi} - 1, \tag{102}$$

where

$$\varphi = \left(\frac{c_{pv}}{c_{pg}}\right)\frac{1}{Le}, \tag{103}$$

$Le = k_g/(c_{pg}\rho_{total})$ is the Lewis number.

If $Le = 1$ and $c_{pv} = c_{pg}$ then $B_T = B_M$. This condition is widely used in the analysis of droplet evaporation (e.g. [10]). Note that in some papers Eq. (102) is used with $\phi = 1/Le$ (see, e.g. [170–172]), which cannot be justified unless $c_{pv} = c_{pg}$. This difference in the presentation of these equations can be traced to the form of energy conservation Eq. (Eqs. (98) or (99)) used in some reviews (e.g. Eq. (3.4) in [7]) where c_{pv} was replaced by c_p, and the latter was implicitly identified with the heat capacity of the ambient gas.

From Eqs. (100) and (101) follows the relation:

$$|\dot{q}_s| = |\dot{q}_{ins}| \frac{z}{e^z - 1}, \tag{104}$$

where $|\dot{q}_s| = -\dot{m}_d L + |\dot{q}_d|$ is the heat which reaches the surface of the droplet, $|\dot{q}_{ins}| = 4\pi R_d^2 (k_g/R_d)(T_g - T_s)$ is the heat transferred from gas to droplets in the absence of evaporation, $(|\dot{q}_{ins}| - |\dot{q}_s|)$ is spent on heating fuel vapour from $T = T_s$ to $T = T_g$, $z = -\dot{m}_d c_{pv}/(4\pi k_g R_d) = \dot{m}''_d R_d c_{pv}/k_g$. Eq. (104) was first obtained in [173] and is widely used in CFD applications (e.g. [174]).

Having introduced the convective heat transfer coefficients describing droplet heating in the presence and absence of evaporation as h and h_0 and the corresponding Nusselt numbers as Nu and Nu_0, we can rearrange Eq. (104) as:

$$|\dot{q}_s| = 4\pi R_d^2 \frac{Nu}{2} \frac{k_g}{R_d}(T_g - T_s)$$

$$= \frac{z}{e^z - 1} 4\pi R_d^2 \frac{Nu_0}{2} \frac{k_g}{R_d}(T_g - T_s). \tag{105}$$

It follows from this equation that:

$$Nu = \frac{z}{e^z - 1} Nu_0 = \frac{\ln(1 + B_T)}{B_T} Nu_0. \quad (106)$$

Recalling that in the case of stationary non-evaporating droplets $Nu_0 = 2$, the combination of Eqs. (106) and (100) gives:

$$\dot{m}''_d = \frac{k_g}{2c_{pv}R_d} NuB_T, \quad (107)$$

Comparing Eqs. (89) and (94) one can see that in the case when the contribution of Stefan's flow can be ignored and the droplets are stationary then $Sh = Sh_0 = 2$. In the presence of this flow the analysis needs to be based on Eq. (97). This equation can be rewritten as:

$$\dot{m}''_d = \frac{D_g \rho_{total}}{2R_d} ShB_M, \quad (108)$$

where

$$Sh = \frac{\ln(1 + B_M)}{B_M} Sh_0. \quad (109)$$

Both Nu_0 and Sh_0 take into account the movement of droplets (see Eqs. (33)–(35) for Nu_0 and similar equations for Sh_0 with Pr being replaced by Sc).

Eq. (107) can be applied to modelling of evaporating moving droplets, if the dependence of Nu on Re and Pr is taken into account. Various models for this were discussed in Section 2.1.2. Models which are most widely used in practical applications in CFD codes are usually the simplest ones, i.e. those based on Eqs. (33) or (35). All equations presented in Section 2.1.2 are equally applicable to the analysis of Sherwood number Sh for moving droplets if we replace Nu by Sh, and Prandtl number Pr by Sc. In this case the Peclet number is defined as $Pe = ReSc$. This would allow us to use Eq. (108) for the analysis of evaporating moving droplets alongside Eq. (107).

Keeping in mind these comments about the values of Sh for moving droplets, Eq. (108) is almost universally used for the analysis of droplet evaporation processes in the CFD framework. In most cases, it is linked with the equation describing droplet heating in the absence of internal temperature gradients (Eq. (19)). As mentioned earlier in Section 2.1.1, ignoring temperature gradients inside droplets cannot always be tolerated, and a more general model taking into account these gradients would have to be used. This model could be based on direct numerical solutions of Eqs. (1) (in the absence of thermal radiation), Eqs. (57) (in the presence of thermal radiation), or analytical solutions of these equations (Eqs. (21) and (58)). To take into account the effect of droplet evaporation in analytical solutions (21) and (58) gas temperature was replaced by the so-called effective temperature defined as:

$$T_{eff} = T_g + \frac{\rho_l L \dot{R}_d}{h}, \quad (110)$$

where the value of $\dot{R}_d$ can be taken from the previous time step. This approach is based on the observation that gas temperature changes more quickly than droplet radius during the evaporation process. The latter is assumed constant in the analytical solutions, but is updated at the end of the time step. Also, the modelling of droplet heating in the presence of evaporation can be based on the parabolic model discussed in Section 2.1.1, as discussed later in this chapter. An alternative version of the parabolic model specifically designed for the analysis of droplet evaporation was suggested in [175]. The latter model was based on the assumption that the droplet surface temperature is fixed. This can be justified when the heat-up period has been completed, which makes this model rather restrictive for practical engineering applications.

Results of detailed comparison between the performances of the algorithms based on the analytical solution (58), the algorithm based on the numerical solution of the discretised Eq. (57) and the parabolic model (Eqs. (23)–(31)) are presented and discussed in [79]. As shown in this paper, the algorithm based on the analytical solution is more effective (from the points of view of accuracy and CPU time requirement) than the approach based on the numerical solution of the discretised heat conduction equation inside the droplet and more accurate than the solution based on the parabolic temperature profile model. Thermal radiation makes relatively small contribution to droplet heating and evaporation. This means we can describe this radiation using a simplified model, which takes into account the semi-transparency of droplets, but does not consider the spatial variations of radiation absorption inside them (see Section 2.2). Note that a model for droplet heating and evaporation rather similar to the one developed in [77,79] (that is based on the analytical solution of the heat transfer equation inside a droplet over the time step) but without taking into account the effect of thermal radiation was suggested in [176].

In realistic CFD codes designed for modelling spray combustion (e.g. diesel engines) the above mentioned models for droplet heating and evaporation would have been complemented by the models of droplet dynamics, break-up, gas dynamics and heating and the ignition of fuel vapour. The detailed discussion of these models is beyond the scope of this review. Note that an analysis

of various droplet break-up models can be found in the reviews mentioned in the Introduction and also papers [177–183]. A brief summary of autoignition models is given in Section 3.6.

Although the classical model of droplet evaporation has been successfully applied to many practical problems, there is still much scope for its further refinement. Two possible approaches to this refinement will be considered in Sections 3.2.2 and 3.2.3.

3.2.2. Abramzon and Sirignano model

The classical model described in the previous section was substantially refined by Abramzon and Sirignano [63]. The main ideas of this model will be summarised below.

To take into account the effect of convective transport caused by the droplet motion relative to the gas, they employed the so called 'film' theory, discussed in several well known monographs (e.g. [15,184]). The key concepts of this theory are film thicknesses δ_T and δ_M, the expressions for which are derived from the requirements that the rates of a purely molecular transport by thermal conduction or diffusion through the film must be equal to the actual intensity of the convective heat or mass transfer between the droplet surface and the external flow. For the case of heat conduction at the surface of a sphere this requirement can be written as [160]:

$$q_s'' \frac{k_g \Delta T}{R_d - \frac{R_d^2}{R_d + \delta_{T0}}} = h \Delta T, \tag{111}$$

where $q_s'' = |\dot{q}_s|/(4\pi R_d^2)$ is the value of the heat flux at the surface of the droplet $\Delta T = T_g - T_s$; index $_0$ hereafter indicates that the effects of Stefan flow are not taken into account. From Eq. (111) it follows that:

$$\delta_{T0} = \frac{2R_d}{Nu_0 - 2}. \tag{112}$$

A similar analysis of the mass transfer equation at the surface of a sphere leads to the following expression for δ_{M0}:

$$\delta_{M0} = \frac{2R_d}{Sh_0 - 2}. \tag{113}$$

The effect of Stefan flow was taken into account by introducing the correction factors:

$$F_T = \delta_T/\delta_{T0}; \qquad F_M = \delta_M/\delta_{M0}, \tag{114}$$

which represented the relative change of the film thickness due to the Stefan flow. To find the correction factors F_M and F_T, a model problem of the laminar boundary layer of the flow past a vapourising wedge was considered. The range of parameters $0 \le (B_M, B_T) \le 20$; $1 \le (Sc, Pr) \le 3$ was considered with the wedge angle in the range $(0, 2\pi)$. It was shown that in the case of an isothermal surface and constant physical properties of the fluid, the problem has a self-similar solution and F_M and F_T do not depend on the local Re and are practically insensitive to Sc, Pr and wedge angle. They were approximated as:

$$F_{M(T)} = (1 + B_{M(T)})^{0.7} \frac{\ln(1 + B_{M(T)})}{B_{M(T)}}. \tag{115}$$

Note that $F_{M(T)}$ increases from 1 to 1.285 when $B_{M(T)}$ grows from 0 to 8. For $B_{M(T)}$ in the range (8, 20) $F_{M(T)}$ remains practically constant.

In [63] it was assumed that Eq. (115) may also be used in the case of the evaporating droplets. In this case, having replaced δ_{T0} in Eq. (110) with δ_T, and remembering Eq. (112) the modified value of the Nusselt number was obtained in the form:

$$Nu^* = 2 + \frac{Nu_0 - 2}{F_T}. \tag{116}$$

Similarly, the modified Sherwood number was obtained in the form:

$$Sh^* = 2 + \frac{Sh_0 - 2}{F_M}. \tag{117}$$

Nu^* and Sh^* should substitute Nu_0 and Sh_0 in Eqs. (106) and (109), respectively. Since $Nu^* \to Nu_0$ when $F_T \to 1$ and $Sh^* \to Sh_0$ when $F_M \to 1$, Nu^* and Sh^* were called 'modified' Nusselt and Sherwood numbers. These terms, however, might be misleading, as the actual Nusselt and Sherwood numbers are calculated from Eqs. (106) and (109) with Nu_0 and Sh_0 replaced by Nu^* and Sh^*, respectively. This was mentioned in [63].

Next, the predictions of the experimental correlation for Nu (Eq. (87)), classical model (Eq. (106)), and Abramzon and Sirignano [63] model (Eqs. (106), (115) and (116)) will be compared. To achieve consistency between these models we assume that the heat-up period has been completed ($|\dot{q}_d| = 0$), effects of thermal radiation can be ignored and Nu_0 is given by Eq. (33) with $\beta_c = 0.57$. We assume that $Pr = 0.7$ and $Re = 100$, and consider three values of B_T. The results of our calculations of Nu are presented in Table 1.

As follows from this table, the values of Nu predicted by the Abramzon and Sirignano model are noticeably closer to those predicted by the experimental correlations, when compared with the classical model. A more detailed comparison between the models in a

Table 1
The values of Nu predicted by various models and various B_T

Model	Equations	$B_T=0.1$	$B_T=1$	$B_T=3$
Experimental correlation	(87)	$Nu=6.605$	4.347	2.676
Classical model	(106)	$Nu=6.732$	4.894	3.263
Abramzon and Sirignano	(106,115, 116)	$Nu=6.641$	4.501	2.975

wider range of parameters would be required to further support this conclusion. Note that empirical correlation (87) was obtained in a rather limited range of parameters (droplet radii between 0.5 and 3 mm) and its application to modelling of heating of small droplets with radii less than 10 μm, as observed in diesel engines, is not at first evident.

The effect of internal circulation on heat transfer in a droplet was simulated in [63] using two models: the 'extended model' which directly solves the convective energy equation inside the droplet and the 'effective conductivity model', described earlier. In [139,140] these models were generalised to take into account the contribution of thermal radiation and the temperature dependence of liquid fuel properties. In both models the contribution of thermal radiation was taken into account based on the model for thermal radiation absorption described in Section 2.2.4. Physical properties of diesel fuel were approximated by those for *n*-dodecane (see Appendix A). It was pointed out that the radiation absorption in diesel fuel is generally stronger than in *n*-decane, and it needs to be taken into account in modelling the combustion processes in diesel engines. Weak effect of thermal radiation in *n*-decane droplets, however, may be related to the fact that due to lack of experimental data, the absorption coefficient was assumed to be zero at $\lambda<2.6$ μm. When data were available, the absorption of radiation of *n*-decane was generally less than that of diesel fuel, especially in the regions of semi-transparency (λ not close to 3.4 μm). Comparison between the calculations, performed using the 'extended model' with distributed radiation absorption heat source and those based on the 'effective-conductivity' model with the uniform distribution of the internal heat source, showed exceptionally good agreement between the results. This allowed the authors of [139,140] to recommend using the 'effective-conductivity' model with uniform radiation absorption for spray combustion calculations, including application in diesel engines.

Note that in the absence of radiation, the droplet temperature approaches an equilibrium or 'wet-bulb' temperature. At that temperature, all of the heat coming to the droplet surface from the gas is spent on evaporation (latent heat), and the net heat penetrating to the liquid phase becomes zero $\dot{q}_d=0$. In the presence of radiation, however, the droplet surface temperature continues to rise above the wet-bulb temperature [139, 140]. As the surface droplet temperature increases, the heat coming to the droplet surface through convection decreases, but the heat used for vapourisation, increases. As a result, the value of $\dot{q}_d$ becomes negative, as confirmed by calculations presented in [139,140]. At the end of the evaporation period, the total radiation absorption decreases very quickly with the droplet radius (see Section 2.2), while the heat transferred through the droplet surface, $|\dot{q}_d|$, decreases relatively slowly. At a certain moment, the total amount of heat going into the droplet interior becomes negative and $d\bar{T}/dt<0$ (see [139,140]). Therefore the temperature of the irradiated droplet reaches its maximal value, and then decreases toward the wet-bulb temperature of the droplet without radiation. Physically, this resembles the situation where a droplet suspended at room temperature is heated by internal heat sources. Since the vaporization is relatively slow, the droplet temperature will approach some steady-state value, which is higher than the regular wet-bulb temperature. If the internal heat sources are suddenly 'turned-off', the droplet temperature will decrease to the wet-bulb temperature. These results were confirmed by calculations reported in [139,140] and [185] (the analysis in the latter paper was based on the classical evaporation model). The importance of taking the radiation effect into account when modelling droplet evaporation was indicated earlier in [125].

3.2.3. Yao, Abdel-Khalik and Ghiaasiaan model

As in the case of the Abramzon and Sirignano model, thermal and mass thicknesses δ_T and δ_M were introduced in [186] in such a way that $T=T_g$ at $R=R_d+\delta_T$ and $Y_F=Y_{F_\infty}$ at $R=R_d+\delta_M$. The effect of Stephan flow was taken into account, but in a way different from that suggested in [63] (via functions $F(B_M)$ and $F(B_T)$). The boundary conditions at the droplet surface were the same as in the two previous models. Although the key equations presented in this section are the same as in [186], some details of the analysis are slightly different from those given in the original paper [186].

As in the previous models, the analysis of [186] is based on Eq. (99), but the right hand side of this equation was integrated not from $R=R_d$ to $R=\infty$, but from $R=R_d$ to $R=R_d+\delta_T$ to take into account the finite

thickness of the thermal boundary layer. As a result the following expression for B_T is obtained:

$$B_T = \exp\left[\frac{\Omega_Y \delta_T}{R_d + \delta_T}\right] - 1, \tag{118}$$

where

$$\Omega_Y = \frac{\dot{m}''_d c_{pv} R_d}{k_g}.$$

Remembering that heat reaching droplets is spent on their heating and evaporation we can write:

$$h(T_g - T_s)4\pi R_d^2 = L|\dot{m}_d| + |\dot{q}_d|, \tag{119}$$

where h is the convection heat transfer coefficient in the presence of the Stefan flow. From Eqs. (118) and (119) and remembering the definition of B_T we obtain:

$$h = \frac{\dot{m}''_d c_{pv}}{\exp\left[\frac{\Omega_Y \delta_T}{R_d + \delta_T}\right] - 1} \tag{120}$$

This expression for h is the same as derived in [186], who followed a different route. In the limit $\dot{m}''_d \to 0$ Eq. (120) can be simplified to:

$$h = \frac{k_g(R_d + \delta_T)}{R_d \delta_T}. \tag{121}$$

This equation is equivalent to Eq. (112) obtained in the limit when the contribution of the Stephan flow can be ignored. In the limit when $\delta_T \to \infty$, Eq. (121) gives a trivial result $h = k_g/R_d$. Eq. (118) can be rewritten in the form:

$$\dot{m}''_d = \frac{k_g}{c_{pv} R_d}\left(1 + \frac{R_d}{\delta_T}\right)\ln(1 + B_T)$$

$$= \frac{k_g}{2c_{pv} R_d} Nu B_T, \tag{122}$$

where

$$Nu = 2\left(1 + \frac{R_d}{\delta_T}\right)\frac{\ln(1 + B_T)}{B_T}. \tag{123}$$

Eq. (123) is a straightforward generalisation of Eq. (106) to take into account the contribution of the finite thickness of the thermal boundary layer. It reduces to Eq. (106) if δ_T is replaced by δ_{T0} defined by Eq. (112).

The effect of the mass boundary layer was taken into account when analysing Eq. (96) (similar to the effect of the thermal boundary layer). This equation was integrated not from $R = R_d$ to $R = \infty$, as in the classical model but from $R = R_d$ to $R = R_d + \delta_M$ to take into account the finite thickness of the mass boundary layer. As a result, the following equation for $\dot{m}''_d$ was obtained:

$$\dot{m}''_d = \frac{D_g \rho_{total}}{R_d}\left(1 + \frac{R_d}{\delta_M}\right)\ln(1 + B_M). \tag{124}$$

Alternatively, this equation could be presented in the form (108) with Sh defined as:

$$Sh = 2\left(1 + \frac{R_d}{\delta_M}\right)\frac{\ln(1 + B_M)}{B_M}. \tag{125}$$

Eq. (125) is a straightforward generalisation of Eq. (109) to take into account the contribution of the finite thickness of the mass boundary layer. It reduces to Eq. (109) if δ_M is replaced by δ_{M0} as defined by Eq. (113).

Eqs. (123) and (125) reduce to those predicted by the Abramzon and Sirignano [63] model if δ_T and δ_M are defined by Eqs. (114).

Note that in Eqs. (123) and (125) the dependence of Nu and Sh on Re, Pr and Sc takes place via the dependence of δ_T and δ_M on Re, Pr and Sc. The value of δ_M in [186] was determined via Eq. (125), assuming that Sh is known. The latter was taken from the empirical correlation (91). Once the mass evaporation flux has been found then the value of Ω_Y can be determined. Eq. (122) was rearranged to:

$$B_T = \frac{2\Omega_Y}{Nu}. \tag{126}$$

Thus, using the empirical correlation for Nu (Eq. (87)) one can find B_T. Finally, remembering the definition of B_T (Eq. (101)) the value of $|\dot{q}_d|$ is found. The calculation of the values of δ_T is not needed in this approach. The dependence on the separately measured or calculated values of Nu and Sh seems to constitute the main limitation of the model of [186].

To the best of my knowledge, none of the droplet evaporation models considered so far takes into account the motion of the droplet surface boundary during the evaporation process (it is assumed fixed during the time step). The effect of a moving boundary has been considered in the literature (e.g. [187–190]) but not in connection with the droplet evaporation problem. It is expected that this effect might be particularly important at the final stages of droplet evaporation when the changes in droplet radius during the time step are comparable with the value of the radius itself.

3.3. Multi-component droplets

The droplet evaporation models described so far have been based on the assumption that liquid consists

of one component only. This assumption is not valid for most practically important fuels, including diesel and gasoline. The application of the single component assumption in this case was justified not by the physical nature of the problem, but by the fact that it led to considerable simplification of the modelling of the processes involved. In the case of multi-component droplets, different components evaporate at different rates, creating concentration gradients in the liquid phase. The latter leads to the liquid phase mass diffusion described by the diffusion equation for the mass fractions of each component [8,191]:

$$\frac{\partial Y_{\mathrm{l,m}}}{\partial t} = D_{\mathrm{l}}\left(\frac{\partial^2 Y_{\mathrm{l,m}}}{\partial R^2} + \frac{2}{R}\frac{\partial Y_{\mathrm{l,m}}}{\partial R}\right), \tag{127}$$

where subscripts l and m indicate liquid phase and particular type of species, respectively. Spherical symmetry was assumed. Also, it was assumed that the diffusion coefficient D_{l} is the same for all liquid components. An analysis of the diffusion equation for $Y_{\mathrm{l,m}}$ without the spherical symmetry assumption is discussed in [192].

If we further assume that the diffusion coefficients referring to all species in the gas phase are the same (this assumption was relaxed in [52]), then the evaporation rate of the mth species can be presented as:

$$\dot{m}_{\mathrm{m}} = \varepsilon_{\mathrm{m}}\dot{m}_{\mathrm{d}} = -4\pi\varepsilon_{\mathrm{m}}R_{\mathrm{d}}D_{\mathrm{g}}\rho_{\mathrm{total}}\ln(1+B_{\mathrm{M}}), \tag{128}$$

where ε_{m} describes the species evaporation rate. When deriving Eq. (128) we took into account Eq. (97). Note that the latent heat of evaporation of multi-component droplets can be found from the expression:

$$L = \sum_{\mathrm{m}} \varepsilon_{\mathrm{m}} L_{\mathrm{m}}, \tag{129}$$

where L_{m} is the latent heat of evaporation of the mth species.

If there were no supply of the mth species to the surface from the interior of the droplet then:

$$Y_{\mathrm{l,m(s)}} = \varepsilon_{\mathrm{m}}, \tag{130}$$

where the additional subscript s indicates 'surface'. In the general case, this supply of the mth species can be described by the following mass diffusion flow rate:

$$\dot{m}_{\mathrm{m(suppl)}} = -4\pi R_{\mathrm{d}}^2 D_{\mathrm{l}} \frac{\partial Y_{\mathrm{l,m}}}{\partial R}\Big|_{R=R_{\mathrm{d}}}. \tag{131}$$

In the steady-state case, $\dot{m}_{\mathrm{m(suppl)}}$ is equal to the difference between the actual evaporation flux and the evaporation flux which would take place in the absence of supply. This allows us to write the mass balance equation at the surface of the droplet in the following form:

$$\frac{\partial Y_{\mathrm{l,m}}}{\partial R}\Big|_{R=R_{\mathrm{d}}} = \frac{D_{\mathrm{g}}\rho_{\mathrm{total}}\ln(1+B_{\mathrm{M}})}{D_{\mathrm{l}}\rho_{\mathrm{l}}R_{\mathrm{d}}}(Y_{\mathrm{l,m}} - \varepsilon_{\mathrm{m}}). \tag{132}$$

This equation was derived in [13] following a different procedure. It can be considered as a boundary condition for Eq. (127) at the droplet surface. This needs to be supplemented by the conditions at the droplet centre:

$$\frac{\partial Y_{\mathrm{l,m}}}{\partial R}|_{R=0} = 0 \tag{133}$$

and the relevant initial conditions.

In the equilibrium state, the partial pressure of the mth fuel vapour species at the surface of the droplet can be found from the Raoult law:

$$p_{\mathrm{v,m}} = \chi_{\mathrm{l,m}} p^*_{\mathrm{v,m}}, \tag{134}$$

where $\chi_{\mathrm{l,m}}$ is the molar fraction of the mth species in the liquid near the droplet surface, $p^*_{\mathrm{v,m}}$ is the partial vapour pressure of the mth species in the case when $\chi_{\mathrm{l,m}}=1$. A molecular interpretation of Eq. (134) can be found in [54] (pages 169–70). Eq. (134) is an approximate one and deviations from the Raoult law are possible [13].

Using the Clausius–Clapeyron equation for a single species we can write [9]:

$$\ln\left(\frac{p^*_{\mathrm{v,m}}}{p_{\mathrm{amb}}}\right) = \frac{L_{\mathrm{m}}}{R_{\mathrm{u}}M_{\mathrm{m}}}\left(\frac{1}{T_{\mathrm{b,m}}} - \frac{1}{T_{\mathrm{s}}}\right), \tag{135}$$

where M_{m} is the molar mass, $T_{\mathrm{b,m}}$ is the boiling temperature of the mth species, p_{amb} is the ambient pressure. When deriving Eq. (135) we took into account that $p^*_{\mathrm{v,m}}$ is equal to the ambient pressure when $T_{\mathrm{s}}=T_{\mathrm{b,m}}$. In view of Eq. (134), Eq. (135) can be rewritten as [13]:

$$\frac{\chi_{\mathrm{v,m}}}{\chi_{\mathrm{l,m}}} = \tilde{p}_{\mathrm{v}}^{-1}\exp\left[\frac{L_{\mathrm{m}}}{R_{\mathrm{u}}M_{\mathrm{m}}}\left(\frac{1}{T_{\mathrm{b,m}}} - \frac{1}{T_{\mathrm{s}}}\right)\right], \tag{136}$$

where $\tilde{p}_{\mathrm{v}} = p_{\mathrm{v}}/p_{\mathrm{amb}}$.

As in the case of one component droplets, the solution of Eq. (127) might be too CPU intensive for practical implementation into engineering CFD codes. In practice this approach has been applied mainly to the case of binary droplets [191–194].

Two limiting cases were suggested, in which the solution of this equation becomes no longer necessary. These are (a) the rapid regression or zero diffusivity limit, and (b) the uniform concentration or infinite-diffusivity limit [13,195]. In the first limit the composition of droplets remains constant during the whole evaporation process. The analysis of this case

would be similar to the analysis of one-component droplets. In the second limit, the droplet composition changes with time in such a way that the mass fraction of its less volatile components increases. Although the second limit is strictly applicable to the description of slow evaporation processes only [13], in practice it is used in a much wider range of applications (see e.g. [195]).

The analysis of this section so far has been based on the assumption that the droplets are stationary, and there is no contribution from convection processes. In the general case of moving droplets, the situation becomes much more complicated, and recirculation inside the droplets would need to be taken into account [13]. This, however, would make the whole model far too complicated for most engineering applications, as in the case of single component droplets. The analysis of moving droplets can be greatly simplified when the actual recirculation inside them is accounted for by the increase of diffusivity in them by the same factor χ (see Eq. (55)) as was used for the analysis of heat transfer (with Pr replaced by Sc) [196]. This increase of diffusivity inside droplets could provide further support to the infinite diffusivity limit discuss earlier. Analysis of Eq. (127) together with the heat transfer equation, in which the contribution of thermal radiation was taken into account, was discussed in [197]. A simplified model, based on the assumption that the absorption of thermal radiation is homogeneous, was used. The effect of a moving boundary and the finite thickness of the boundary layer on the evaporation of multi-component droplets was taken into account in the models discussed in [198,199].

In realistic situations, the analysis based on Eq. (127) is applicable only in the case when the number of components in the droplets is small (e.g. [200,201]). In realistic cases, such as diesel or gasoline fuels, when the number of components in a droplet is measured in hundreds, this approach ceases to be practical. An alternative approach is based on so called continuous thermodynamics [202–205]. This approach has been developed for the well-mixed droplet model (infinite-diffusivity limit) and is based on the introduction of the distribution function $f_m(I)$ such that:

$$\int_{I_1}^{I_2} f_m(I)\mathrm{d}I = 1, \tag{137}$$

where I is the property of the component (usually taken as the molar mass), f_m characterises relative contribution of the components having this property in the vicinity of I, I_1 and I_2 are limiting values of this property. For most practically important fuels $f_m(I)$ can be approximated by relatively simple functions. For example the following function was considered in [203–206]:

$$f_m(I) = \frac{(I-\gamma)^{\alpha-1}}{\beta^\alpha \Gamma(\alpha)} \exp\left[-\left(\frac{I-\gamma}{\beta}\right)\right], \tag{138}$$

where $\Gamma(\alpha)$ is the Gamma function, α and β are parameters that determine the shape of the distribution, γ determines the original shift. In the case of this choice of f_m, we need to take $I_1 = \gamma$ and $I_2 = \infty$. The authors of [207] considered a more general function presented as the weighted sum of the functions (138) (double-Gamma-PDF).

The main attractive feature of this approach to modelling of multi-component droplet evaporation is that the composition of fuel can be characterised by just a few key parameters (two parameters α and β for given γ in the case when function (138) is taken), instead of hundreds of values of mole fractions of individual components, required in the conventional approach (based on the solution of Eq. (127)). As in the conventional approach it is assumed that the diffusion coefficients for all the components are the same. See [203–207] for details of the implementation of this approach,

Recently, a new computationally effective model for multi-component droplet evaporation was suggested in [208]. This model was called the Distillation Curve Model (DC model) and it is capable of taking into account the distillation curve of the actual multi-component fuels. The most important feature of this model is the description of fractional boiling during the droplet evaporation process as a function of a single variable: the actual mean molar mass of fuel inside the droplet. An additional advantage is that the model is based on algebraic equations, which brings clear advantages from the point of view of CPU efficiency. The influence of diffusion resistance in droplets on evaporation is quantified by the liquid Peclet number [208]:

$$Pe_l = \frac{|\dot{m}_d|}{4\pi R_d D_l \rho_l}. \tag{139}$$

A more detailed analysis of this model is given in [208].

3.4. Kinetic models

The analysis presented so far was implicitly based on the assumption that both liquid and gas phases can be treated as a continuum. That means that the actual

velocity distribution of molecules does not affect the physical properties of these phases. The latter are controlled by the number of molecules per unit volume, their average mass and their average velocities. This assumption is generally valid for both phases, unless the ambient pressure is low enough and as long as the droplets are not too small. However, the validity of this assumption is no longer obvious when the interface between liquid droplets and the ambient gas is modelled, even in the case when the pressure is well above 1 atm. That means that although the liquid phase can always be treated as a continuum, the properties of gas in the vicinity of the liquid–gas interface can depend not only on the average velocities of molecules, but also on the distribution of molecules by velocities. The latter is generally described in terms of distribution functions.

In general, the model which needs to be used for the analysis of droplet evaporation is determined by the so called Knudsen number $Kn = l_{\text{coll}}/R_{\text{d}}$, where l_{coll} is the characteristic mean free path of molecules. It is generally believed that in the case when $Kn < 0.01$ the gas may be approximated as a continuum. In another limiting case when $Kn > 3$ the mean free path of molecules is large compared with the dimensions of the system, and a free molecular regime takes place. In the transitional regime $0.01 \leq Kn \leq 3$ the mean free path of molecules is comparable with the dimensions of the system. This is known as the slip regime. In this case gas can be regarded as a continuum at several mean paths away from the droplet surface, but kinetic effects should be taken into account in the vicinity of the droplet surface [209]. In the case of fuel droplets in internal combustion engines Kn is generally well below 0.01, and this justifies the application of the continuum medium approximation for their analysis. The validity of this approximation, however, is not at first obvious, as was shown in [210]. Hence, the analysis of kinetic models of evaporation in this review can be justified.

The most general approach to the analysis of the velocity distributions of gas molecules is based on the so-called multi-particle distribution functions, which take into account not only the positions and velocities of individual molecules, but also the correlations between them. This eventually leads to the infinite chain of Bogolubov–Born–Green–Kirkwood–Yvon (BBGKY) equations for multi-particle distribution functions [211]. In practice this chain has to be truncated. In the 0th approximation, assuming that interactions between individual molecules take place only during collision processes, this chain reduces to a single Boltzmann equation, which can be presented in the following form [211,212]:

$$\frac{\partial f}{\partial t} + \mathbf{v}\frac{\partial f}{\partial x} + \mathbf{F}\frac{\partial f}{\partial v} = \left(\frac{\partial f}{\partial t}\right)_{\text{coll}}, \tag{140}$$

where $f = f(t,\mathbf{v},\mathbf{x})$ is the molecular distribution function, $\mathbf{v}$, $\mathbf{x}$ and $\mathbf{F}$ are velocity, position and force acting on individual molecules; the right hand side of this equation is the collision integral which takes into account collisions between molecules.

The physical meaning of f can be defined via the product:

$$\Delta f = f(t,\mathbf{v},\mathbf{x})\Delta\mathbf{x}\Delta\mathbf{v},$$

where $\Delta\mathbf{x}$ is a small element of volume around $\mathbf{x}$, $\Delta\mathbf{v}$ is a small range of velocities around $\mathbf{v}$. Δf indicates the number of molecules in the element of volume $\Delta\mathbf{x}$ around $\mathbf{x}$, having velocities in the range $\mathbf{v}$ to $\mathbf{v}+\Delta\mathbf{v}$.

Integration of both parts of Eq. (140) over velocities gives the well-known continuity equation (analogous to conservation of mass). Similarly, the integration of both parts of this equation with weights (components of impulse of molecules and energy of molecules) gives the equations of conservation of momentum (Navier–Stokes equation) and energy. When deriving these equations, it is assumed that the total number of molecules, their total impulse and energy are conserved during the collision process.

The contribution of $\mathbf{F}$ in Eq. (140) is generally ignored, and this can be simplified to:

$$\frac{\partial f}{\partial t} + \mathbf{v}\frac{\partial f}{\partial x} = \left(\frac{\partial f}{\partial t}\right)_{\text{coll}}. \tag{141}$$

This could not be done in the case of ionised gases even in the absence of external fields [211–213], but in the case of non-ionised gases $\mathbf{F}$ could only come from the gravitational force, which is negligible for small molecules.

The most general expression for the collision integral can be presented as [214,215]:

$$\left(\frac{\partial f}{\partial t}\right)_{\text{coll}} = \frac{d_f^2}{2}\int_{-\infty}^{+\infty} \mathrm{d}\mathbf{v}_1 \int_0^{\pi} \sin\theta\,\mathrm{d}\theta \int_0^{2\pi} \mathrm{d}\phi (f'f_1' - ff_1)|\mathbf{v}-\mathbf{v}_1|, \tag{142}$$

where d_{f} is the diameter of colliding molecules, θ and φ are relative angular coordinates of molecules, superscript$'$ indicates the velocities and the distribution functions after collisions, $f = f(\mathbf{v})$, $f_1 = f(\mathbf{v}_1)$, $f' = f(\mathbf{v}')$,

$f_1' = f(v_1')$. The first integral in the right hand side of Eq. (142) is calculated in the three-dimensional velocity space. When deriving Eq. (142) it was assumed that molecules are rigid elastic spheres. In the case of evaporating fuel droplets, the collision integral represents the sum of two terms: the one describing collisions between molecules of fuel vapour, and the other describing collisions between molecules of fuel vapour with molecules of other gases. In most cases, including this review, the focus has been on the analysis of the first term. A more general analysis taking into account the contribution of both processes was reported in [216–220].

The general analysis of Eqs. (141) and (142) is possible using numerical methods (see [214–223]). The application of these methods to analysis of the droplet evaporation process were reported in [216–220]. The detailed analysis of these methods and their applications would require a separate paper, and is beyond the scope of this review.

The analysis of Eqs. (141) and (142) is considerably simplified when the collision integral (142) is not calculated but modelled. Several explicit analytical expressions for $(\partial f/\partial t)_{\text{coll}}$ have been suggested(see e.g. [211–226]), the analysis of which is beyond the scope of this review.

Further analysis of Eq. (141) largely depends on the relative values of the mean free path of molecules between collisions and the characteristic size of the system. In the case of droplets this is described by the Knudsen number Kn as mentioned earlier. The review of the approaches to the analysis of this equation, suggested so far, will be presented mainly following [210].

When $Kn \gg 1$ the contribution of collisions can be ignored altogether and we have a free molecular flow. In this case the right hand side of Eq. (141) can be assumed equal to zero, and the equation can allow analytical solutions. Assuming that both incoming and outgoing molecular fluxes are Maxwellian with temperatures T_∞ and T_s, respectively, one can derive from Eq. (141) the Hertz–Knudsen–Langmuir formula for mass flux of fuel vapour from the droplet surface [227–231]:

$$j_{\text{lg}} \equiv \dot{m}_{\text{d}}'' = \frac{|\dot{m}_{\text{d}}|}{4\pi R_{\text{d}}^2} = \frac{\beta_{\text{m}}}{\sqrt{2\pi R_{\text{g}}}}\left(\frac{p_{\text{vs}}}{\sqrt{T_{\text{s}}}} - \frac{p_{\text{v}\infty}}{\sqrt{T_{\text{g}}}}\right), \qquad (143)$$

where $|\dot{m}_{\text{d}}|$ is the rate of droplet mass loss, β_{m} is the evaporation coefficient (assumed to be equal to the condensation coefficient), R_{g} is gas constant, p_{vs} is the saturated fuel vapour partial pressure corresponding to T_{s}, $p_{\text{v}\infty}$ is the fuel vapour partial pressure at large distances from it, T_{s} is the droplet surface temperature and T_{g} is the gas temperature at large distances from the droplet.

The coefficient $\beta_{\text{m}} \leq 1$ shows what proportion of vapour molecules striking the liquid surface is absorbed by this surface. The remaining portion $(1-\beta_{\text{m}})$ shows the fraction of reflected molecules. The value of β_{m} depends on the contacting surfaces [1] and can be determined experimentally [232,233]. Methods of molecular dynamics and direct modelling of droplet evaporation could also be used to estimate this coefficient [234–237]. A comprehensive review of theoretical and experimental studies of this coefficient for water is presented in [238]. So far, the values of β_{m} for diesel fuel have not been measured or estimated, to the best of my knowledge.

Eq. (143) has been widely used for the analysis of evaporation and condensation processes despite the simplistic assumptions used for its derivation (e.g. [239]). A more general approach to the evaporation–condensation problem takes into account the effects of collisions. This leads to the introduction of the concept of the Knudsen layer, separating the liquid surface from the bulk of the vapour, which is described using the continuum equations. The thickness of the Knudsen layer l_{K} is typically estimated as several molecular mean free pass lengths l_{coll} for small drift vapour velocities v_{dr}, $10 l_{\text{coll}}$ for $v = 0.5 v_{\text{sound}}$, and $100–200 l_{\text{coll}}$ for v_{dr} close to v_{sound} [240]. The value of l_{coll} is estimated based on the temperature of the surface T_{s}.

For practical modelling purposes, diesel fuel can be approximated by n-dodecane $C_{12}H_{26}$($M_{C_{12}H_{26}} = 170.3$ kg/kmol) for which the gas constant is estimated as $R_{\text{g}} = 48.88$ J/(kgK). Other physical properties of n-dodecane are summarised in Appendix A. Assuming that vapour temperature is equal to surface temperature $T_{\text{s}} = 600$ K we obtain $v_{\text{sound}} = 202.6$ m/s. For this T_{s} the saturated vapour pressure of n-dodecane is equal to $p_{vs} = 6.4 \times 10^5$ N/m^2. Using Eq. (143), assuming that $p_{v\infty} = 0$ and $\beta_{\text{m}} = 0.5$, we obtain $j_{\text{lg}} = 745$ kg/(m^{2}s). From gas law we have $\rho_{\text{vs}} = 21.8$ kg/m^3. Hence, $v_{\text{dr}} = j_{1\text{g}}/\rho_{\text{sv}} = 34$ m/s. This value could be further modified if different β_{m} are used. In all cases, however, we can assume that $l_{\text{K}} < 5 l_{\text{coll}}$. Note that this result is not very sensitive to the value of T_{s}. For example for $T_{\text{s}} = 400$ K we obtain: $v_{\text{sound}} = 165$ m/s and $v_{\text{dr}} = 28$ m/s. More accurate analysis of the problem (see Eq. (145)) would predict slightly larger values of v_{dr}, but the validity of the assumption that $v_{\text{dr}} \ll v_{\text{sound}}$ would remain valid. Assuming that liquid fuel evaporates into its own vapour, l_{coll} can be estimated as [229]:

$$l_{\rm coll} = [\sqrt{2}\pi d_f^2(\rho_{\rm vs}N_{\rm A}/M_{\rm f}]^{-1},$$

where $M_{\rm f}$ is the molar mass of fuel, $N_{\rm A}$ is the Avogadro number.

Taking the diameter of *n*-dodecane molecules $d_f = 10^{-9}$ m, $\rho_{vs} = 21.8$ kg/m^3 (corresponding to $T_{\rm s} = 600$ K) and $M_{\rm f} = 170.3$ kg/kmol, we obtain: $l_{\rm coll} = 2.9\times10^{-9}$ m. This gives us an estimate of $l_{\rm k}$ for diesel engines: $l_{\rm k} < 1.5\times10^{-8}$ m $= 0.015$ μm. This is about 2 orders of magnitude less than the droplet radii. As will be shown later, following [210], despite the small thickness, the contribution of the Knudsen layer cannot be a priori ignored, even in this case.

Strictly speaking Eq. (141) can be applied only when $l_{\rm coll}$ is much greater than $d_{\rm f}$ [241]. From this point of view, the results following from this equation are expected to be reliable only for the set of parameters when the condition $l_{\rm coll} \gg d_{\rm f}$ is satisfied. In the case when $l_{\rm coll}$ is close to $d_{\rm f}$ (which is expected near the critical state) the model can show the trends of the processes, rather than give reliable quantitative estimates. Also, the solutions of the Boltzmann equation do not take into account the contribution of processes inside the fuel vapour molecules.

The above-mentioned estimates of $l_{\rm coll}$ and $l_{\rm K}$ ignore the contribution of molecules of air in the Knudsen layer. This can be justified by the small thickness of this layer at temperatures well above room temperature (when the evaporation rate is high enough). A general kinetic theory of liquid fuel evaporation taking into account the contribution of molecules of air in the Knudsen layer has not been developed, to the best of my knowledge, apart from preliminary results reported in [216–220]. Hence the assumption that the liquid fuel evaporates into its own vapour is generally held.

The velocity distribution for the molecules in the Knudsen layer is affected by collisions and can be obtained from the solution of Eq. (141). Schrage [1] drew attention to the fact that the effects of collisions lead to the formation of the shifted Maxwellian distribution of molecules near the outer boundary of the Knudsen layer. The authors of [242] assumed that this distribution function is formed in the whole Knudsen layer up to the liquid surface. Considering the case when vapour drift velocity is much less than the velocity of sound (weak evaporation; this assumption is consistent with the above mentioned estimates) and using matching boundary conditions in this layer, they derived the modified expression for $j_{\rm lg}$ at $Kn \ll 1$ and $(T_{\rm g} - T_{\rm s})/T_{\rm s} \ll 1$. This took into account the convection of vapour and collision processes and could be presented in the form:

$$j_{\rm lg} = \frac{2\beta_{\rm m}}{(2-\beta_{\rm m})\sqrt{2\pi R_{\rm g}}}\left(\frac{p_{\rm vs}}{\sqrt{T_{\rm s}}} - \frac{p_{\rm v\infty}}{\sqrt{T_{\rm g}}}\right), \tag{144}$$

For $\beta_{\rm m} = 1$ this equation predicts a value of $j_{\rm lg}$ twice as large as the one predicted by Eq. (143). A simple derivation of Eq. (144) is given [209].

Further development of the kinetic theory of evaporation and condensation was reported in [243–246]. The problem was solved using two forms of the collision term in the Boltzmann equation: the conventional one and the one suggested by Bhatnagar, Gross and Krook [225]. The latter form of the collision term secures the conservation of particles during the collision process, and has been widely used to model collisions in gases and plasma (see e.g. [226]). The results have turned out to be practically independent of the form of the collision term used.

The analysis performed in [246] allowed the authors to obtain a number of equations useful for computing the dynamics of evaporation and condensation processes, including the one describing the mass flux of vapour leaving the droplet and moving into a dense medium ($Kn \ll 1$):

$$j_{\rm lg} = \frac{\beta_{\rm m}(p_{\rm vs} - p_{\rm Rd})}{(1-0.4\beta_{\rm m})\sqrt{2\pi R_{\rm g} T_{\rm s}}}, \tag{145}$$

where $p_{\rm Rd}$ is the vapour pressure just outside the Knudsen layer. Eq. (145) has been widely used in various applications (e.g. [247]). It is valid in the case of weak evaporation and condensation which is expected to take place when $(T_{\rm Rd} - T_{\rm s})/T_{\rm s} \ll 1$. Further development of the theory of weak evaporation has been reported in [248–256]. These developments, however, do not undermine the usefulness of Eq. (145) for practical applications. This equation is more accurate than Eqs. (143) and (144) and has been widely used (see e.g. [210]).

The increase in intensity of evaporation leads to further deformation of the molecular distribution function in the Knudsen layer. At a certain stage, the linearisation of this distribution function (which was used when deriving Eq. (145)) is no longer possible. This leads to the situation when $v_{\rm dr}$ becomes comparable with the velocity of sound and the theory of weak evaporation and condensation is no longer valid. A theory of intensive evaporation has been developed in [257–278]. A review of computational and experimental results referring to intensive condensation, with particular emphasis on the problem of determining $\beta_{\rm m}$, was presented in [279].

The authors of [263] showed that the mass flux of vapour leaving the droplet can be approximated by the following expression (valid for both weak and strong evaporation):

$$j_{\rm lg} = 0.6\sqrt{2R_{\rm g}T_{\rm s}}(\rho_{\rm vs}-\rho_{\rm Rd})\sqrt{\rho_{\rm Rd}/\rho_{\rm vs}}, \quad (146)$$

where $\rho_{\rm Rd}$ is the vapour density at the outer boundary of the Knudsen layer. This equation have been derived under the assumption that $\beta_{\rm m}=1$.

For arbitrary $\beta_{\rm m}$ the value of $j_{\rm lg}$ can be obtained via the replacement of $\rho_{\rm vs}$ in Eq. (146) by [259,263]:

$$\rho_\beta = \left(1-2\sqrt{\pi}\frac{j_{\rm lg}}{\rho_{\rm vs}\sqrt{2R_{\rm g}T_{\rm s}}}\frac{1-\beta_{\rm m}}{\beta_{\rm m}}\right)\rho_{\rm vs}. \quad (147)$$

The solution of the system of Eqs. (146) and (147) with two unknowns $j_{\rm lg}$ and ρ_β would allow us to find the required value of $j_{\rm lg}$ for arbitrary $\beta_{\rm m}\le 1$. In the limit of weak evaporation $(\rho_{vs}-\rho_{\rm Rd})/\rho_{vs}\ll 1$ Eq. (146) reduces to Eq. (145) for $\beta_{\rm m}=1$ (see [210]).

One of the fundamental differences in predictions of kinetic and hydrodynamic models lies in the behaviour of temperature, velocity and species concentrations near the boundaries. It is well known that the hydrodynamic models predict continuous changes of all these parameters near the boundaries, while the kinetic models predict jumps in their values over distances of the order of several mean free paths between intermolecular collisions (jumps in the values of concentrations and temperature and velocity slips) [280–282]. The values of these jumps are usually calculated from the analysis of the Boltzmann equation [209,280,283]. Once they are calculated, then the analysis of the processes in the gas, including the processes of evaporation, can be based on the hydrodynamic theory. The boundary conditions in this case take into account jumps in the values of the above-mentioned parameters near the boundaries [284,285]. I am not aware of any detailed comparison between this approach to kinetic modelling of the evaporation processes and the approach based on calculating the mass flux from the droplet surface, as discussed earlier.

The kinetic model based on Eq. (145) and the hydrodynamic model based on Eq. (97) were applied to modelling heating and evaporation processes of typical fuel droplets in diesel engines [210]. The application of Eq. (145) to the kinetic model, describing weak evaporation, was justified by the predicted results. The values of drift vapour velocities were much less than the velocity of sound. Also, in the kinetic model it was assumed that fuel vapour leaving the Knudsen layer was removed from the outer boundary of this layer via diffusion. Thus the mass flux of fuel vapour leaving the droplets is assumed to be equal to the diffusion mass flux from the outer boundary of the Knudsen layer $j_{\rm diff}$. This approach is known as the flux matching method and is widely used in kinetic modelling of droplet evaporation and condensation (e.g. [286]).

The condition $j_{\rm lg}=j_{\rm diff}$ allowed the authors of [210] to determine the value of the mass fraction of fuel vapour at the outer boundary of the Knudsen layer ($Y_{\rm vRd}$). This equation was solved under the assumption that $T_{\rm Rd}=T_{\rm s}$. The value of $Y_{\rm vRd}$ was less or equal to the saturated value Y_{vs}. The value of $j_{\rm diff}$ was determined from the conventional hydrodynamic theory. The gas pressure and the initial droplet temperature were taken to be equal to 30 bar and 300 K, respectively. The effects of temperature gradients inside droplets were ignored. In the kinetic model two values of $\beta_{\rm m}$ were used: $\beta_{\rm m}=0.5$ and $\beta_{\rm m}=0.04$. These are the average and minimal values of $\beta_{\rm m}$ measured for water [232,233]. The value of $\beta_{\rm m}=0.04$ is close to $\beta_{\rm m}=0.06$ estimated by Shusser et al [287] for butane. As mentioned earlier, the values of $\beta_{\rm m}$ for diesel fuel have not been measured or estimated to the best of my knowledge.

Fig. 5 shows the results of calculations for an initial droplet radius equal to 5 μm and initial ambient gas temperature equal to 750 K. Droplets with this initial radius are most likely to be observed in diesel engines [288]. The chosen initial gas temperature is typical for the end of the compression stroke in diesel engines [288]. As follows from this figure, kinetic effects lead to a small increase of evaporation time and droplet temperature for $\beta_{\rm m}=0.5$. This increase becomes larger for smaller values of $\beta_{\rm m}$. The overall shapes of the diameter versus time plots, as predicted by hydrodynamic and kinetic models, appear to be rather similar. A similar analysis was performed for the initial ambient gas temperature 2000 K and for both these temperatures and the initial droplet radius equal to 20 μm. In all cases the kinetic effects were shown to be more pronounced for smaller droplets (5 μm) than for larger ones (20 μm), and for higher initial gas temperatures. As expected, the kinetic model predicted longer evaporation time and higher droplet temperature compared with the hydrodynamic model. The droplet evaporation time and droplet temperature increased with decreasing evaporation coefficient.

The kinetic effects appeared to be even more pronounced for droplets with an initial radius of 1 μm. In this case, however, the kinetic model was less reliable, as it did not take into account the effects of

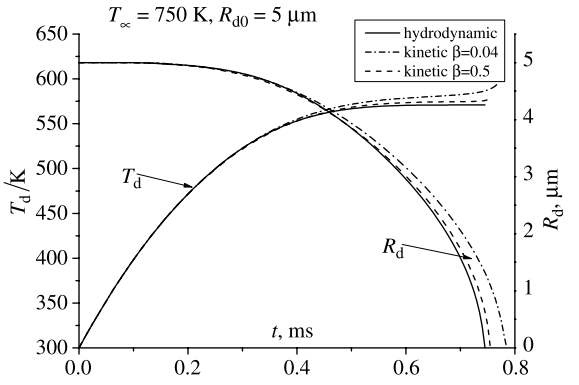

Fig. 5. Plots of droplet temperature (in K) and droplet radius (in μm) versus time for ambient gas pressure 30 bar, ambient gas temperature $T_g = 750$ K, and initial droplet radius $R_{d0} = 5$ μm, calculated based on hydrodynamic and kinetic models with the evaporation coefficients $\beta_m = 0.5$ and 0.04. Reproduced from [210] with permission of Elsevier.

surface tension. For droplets with initial radii comparable with 1 μm, these effects are expected to be noticeable [289].

The main conclusion of the analysis reported in [210] is that the kinetic effects on droplet evaporation are always noticeable, despite the fact that this evaporation takes place at rather high pressures (up to 30 atm and even more). This showed the limitation of the applicability of the hydrodynamic approach to accurate modelling of this process. The authors of [210] recommended that kinetic effects are taken into account when modelling the evaporation process of diesel fuel droplets in realistic internal combustion engines.

3.5. Molecular dynamics simulations

One of the main limitations of the kinetic model, described in Section 3.4, is that it relies on the value of the evaporation coefficient. The difficulties in obtaining this coefficient experimentally have already been mentioned. The ultimate approach to its calculation would have to be based on the analysis of molecular dynamics on the liquid–gas interface. This leads us to the new approach to modelling droplet evaporation based on molecular dynamics (MD) simulation.

The first step in a MD simulation is the choice of the model that best represents the interaction between molecules. This model has to take into account attraction between molecules when the distance between them is large enough, and the repelling forces when molecules approach close to one another. The model almost universally used in MD simulations is based on the so called Lennard–Jones 12–6 potential, whose analytical form can be presented as [15]:

$$V(R_{ij}) = 4\varepsilon_{ij}\left[\left(\frac{\sigma_{ij}}{R_{ij}}\right)^{12} - \left(\frac{\sigma_{ij}}{R_{ij}}\right)^{6}\right], \tag{148}$$

where R_{ij} is the distance between molecules i and j, ε_{ij} and σ_{ij} are the minimal energy and the zero energy separation distance relative to the pair of molecules (a different form of this potential was used in [237,290]). For cross interactions between different species mixing rules, such as the Lorenz–Berthelot, are commonly used [236,291]:

$$\varepsilon_{ij} = \sqrt{\varepsilon_i \varepsilon_j}, \tag{149}$$

$$\sigma_{ij} = (\sigma_i + \sigma_j)/2, \tag{150}$$

where the parameters ε_i and σ_i refer to specific molecules. Data about them is widely available [15,292,293]. For example, for Nitrogen molecules [236]: $\varepsilon_{N_2} = 95.9\, k_B\ J$ and $\sigma_{N_2} = 0.371$ nm, where $k_B = 1.38066 \times 10^{-23}$ J/K is the Boltzmann constant. When these constants are not known they can be estimated from the properties of fluid at the critical point, liquid at the normal boiling point and solid at the melting point [15]. At $R_{ij} > R_m$, where R_m corresponds to the value of R_{ij} when $V = -\varepsilon_{ij}$, the value of V decreases rapidly with increasing R_{ij}. At $R_{ij} = 3\sigma_{ij}$ the absolute value of V is less than $0.01\varepsilon_{ij}$ [15]. This allows us to ignore the interaction between the molecules separated by more than about $R_{ij} = 3\sigma_{ij}$. The actual threshold values were taken to be equal to $R_{ij} = 3\sigma_{ij}$ [236], $R_{ij} = 3.5\sigma_{ij}$ [294], $R_{ij} = 2.5\sigma_{ij}$, $R_{ij} = 5\sigma_{ij}$ and $R_{ij} = 10\sigma_{ij}$ [295]. In [294] this threshold value of R_{ij} was accounted for via presenting the expression for the potential in the form:

$$V(R_{ij}) = \begin{cases} 4\varepsilon_{ij}\left[\left(\frac{\sigma_{ij}}{R_{ij}}\right)^{12} - \left(\frac{\sigma_{ij}}{R_{ij}}\right)^{6}\right] + V_{shift} & \text{if } 0 < R_{ij} \le R_{cut} \\ 0 & \text{if } R_{ij} > R_{cut}, \end{cases} \tag{151}$$

where

$$V_{\text{shift}} = -4\varepsilon_{ij}\left[\left(\frac{\sigma_{ij}}{R_{\text{cut}}}\right)^{12} - \left(\frac{\sigma_{ij}}{R_{\text{cut}}}\right)^{6}\right].$$

Once the values of $V(R_{ij})$ have been calculated, the actual trajectory of the ith molecule is calculated from Newton's law [295]:

$$m_i \frac{\mathrm{d}^2 R_i}{\mathrm{d}t^2} = \sum_{j=1}^{j=N} \nabla V(R_{ij}), \tag{152}$$

where R_i and m_i are the position and mass of the ith molecule, the summation is performed for all molecules in the sphere with the radius R_{cut}.

Potentially, this approach could allow us to solve the problem of droplet evaporation in a self-consistent way without any additional assumptions. Even the formalism of the kinetic theory could be made redundant once this approach has been fully implemented. This approach, however, has a number of serious limitations, which severely limit the range of its applicability. Firstly, the number of molecules, which can be analysed, is limited by available computing power. It seems that the largest number of molecules ever simulated was reported in [296]: 24,000. Secondly, the molecules analysed by this approach should be near spherical. Ideal candidates for this would be monoatomic molecules, such as Ar or Xe [236,295,297], although the model has been applied to N_2 as well [236]. The applicability of this approach to simulating evaporation of diesel fuel becomes highly questionable. Even if we assume that the latter is n-dodecane $C_{12}H_{26}$, this large molecule does not allow a spherical shape approximation.

An alternative approach to molecular dynamics simulation of the droplet evaporation processes could be based on quantum mechanical methods (see e.g. [298,299]). The actual calculation of β_{m} for evaporating fuel droplets, using this approach, is not a trivial problem and it has not yet been performed to the best of my knowledge (V. Gunko, private communication). The development of the evaporation models is closely linked with the development of solvation models. The latter are reviewed in [300]. Paper [300] also provides a method of estimating the difference in the free energies of molecules in the liquid and gaseous states.

3.6. Evaporation and autoignition

In most practical engineering applications, heating and evaporation of fuel droplets leads to autoignition of a fuel vapour/air mixture. Temperature rise of the fuel vapour/air mixture during the autoignition process leads to the enhancement of droplet heating and evaporation processes. Hence, the analysis of fuel droplet heating and evaporation in realistic engine conditions should be coupled with the analysis of autoignition. Possible approaches to coupled solutions of the equations describing all these processes will be discussed in Section 3.7. In this section the focus will be on a brief overview of various approaches to the modelling of autoignition.

Autoignition can be defined as an onset of combustion in a reactive medium raised above a certain temperature and pressure [9,301]. Sometimes autoignition is called spontaneous ignition, self-ignition or homogeneous ignition [9]. It can be triggered by rapid compression of the fuel–oxidizer mixture, as in diesel engines, or by pressure waves due to very fast heat release, as in spark ignition engines.

In early approaches, autoignition was modelled as a one step chemical reaction [302,303]. In the simplest case, the chemical power released in the gas phase per unit volume was calculated based on the Arrhenius approximation [9]:

$$P_{\text{ch}} = M_{\text{f}} Q_{\text{f}} C_{\text{f}} A \exp\left(-\frac{E}{R_{\text{u}} T_{\text{g}}}\right), \tag{153}$$

where M_{f} is the molar mass of fuel, Q_{f} is the specific combustion energy, C_{f} is the fuel vapour molar concentration, A is the pre-exponential factor (in 1/s), E is the activation energy (in J/kmol). Eq. (153) is based on the assumption that there is no deficiency of Oxygen in the system. The simplicity of this equation and its straightforward generalisations (see [9]) makes it particularly attractive for qualitative analysis of the autoignition process and its analytical study (see [58–62,168]).

In many realistic situations, however, the autoignition chemistry is much more complicated and its modelling based on Eq. (153) leads to misleading results. An in-depth analysis of autoignition models is a vast topic, the coverage of which would require a separate review, similar to [20]. In what follows only a brief summary of autoignition models will be presented, mainly with regard to their application to modelling the autoignition process in diesel engines.

There are two main parameters, which characterise the autoignition process: the initial temperature above which autoignition can develop T_{g0} and the time delay before the start of autoignition τ_{del} [304]. Both these parameters strongly depend on pressure, fuel composition, condition of internal surface of the engine and

other factors [305–310]. The detailed kinetic mechanism (DKM) of the autoignition process includes up to about 1000 chemical reactions and over a hundred species [311–319]. Additional problems in the construction of DKMs are due to the scarcity or lack of kinetic data on many of the reactions involved. Even quantum chemistry methods cannot ensure accurate calculation of rate constants due to the fact that the decisive factor in this calculation is the small value difference between the high energy levels of reacting molecules [320]. The incorporation of this model into a CFD code for the modelling of the autoignition process would be a difficult task. This stimulated the development of a number of reduced chemical models (e.g. [308,321–330]). The one suggested in [327] was successfully used in [331] for modelling autoignition of isolated *n*-heptane droplets. The general approach to simplification of DKMs was discussed by Maas and Pope [332]. Poppe et al. [322] considered the model based on 30 reactions and 21 species. Basevich and Frolov [324] went even further and reduced the number of reactions to 21 and the number of species to 13. However, even this simplification turned out to be insufficient to model the chemical processes in combination with the flow and heat transfer calculations in realistic 3D geometries. Further simplification of this model led to a four-step model with adjusted rate coefficients as suggested by Müller et al. [333]. The practical applicability of this model was questioned by Griffiths in the accompanying discussion of this paper. He drew attention to the fact that according to this model, ignition was brought about entirely by thermal feedback, while the chain branching process was ignored. This is difficult to justify in a model intending to capture the key features of the autoignition process.

A number of authors considered turbulent autoignition models in an attempt to take into account the contribution of flow characteristics [305, 334–341]. Although these models are very important for the in-depth understanding of the process, the complexity of turbulence modelling requires considerable simplification of the chemical kinetics. For example, the model for turbulent combustion used in [339,341] is based on the four-step model suggested by Müller et al. [333].

A group of researchers from Shell Research Ltd attempted to capture the essential features of the process rather than to construct a chemically and physically rigorous model [344]. They achieved this by introducing generic species with chemical reaction constants deduced from experimental data, and developed a model based on the eight step chain branching reaction scheme incorporated into four processes:

Initiation:

$$RH + O_2 \rightarrow 2R^*$$

Propagation:

$$R^* \rightarrow R^* + P \qquad R^* \rightarrow R^* + B \qquad R^* \rightarrow R^* + Q$$

$$R^* + Q \rightarrow R^* + B$$

Branching:

$$B \rightarrow 2R^*$$

Termination:

$$R^* \rightarrow \text{out} \quad 2R^* \rightarrow \text{out}$$

RH represents hydrocarbon fuel (C_nH_{2m}), R^* is the radical, B is the branching agent, Q is the intermediate agent, and P is the product, consisting of CO, CO_2 and H_2O. Following Benson [345] the branching agent is related to hydroperoxide (RO_2H) at low temperatures and to hydrogen peroxide (H_2O_2) at high temperatures. The intermediate species can be generally related to aldehydes (RCHO).

This model has been validated and further developed by a number of researchers [342–352] and is now the most widely used in automotive applications. It is known as the Shell model.

Based on the analysis of the ignition in a monodisperse spray in conditions relevant to diesel engines, it was shown that in the case of droplets with an initial radius (R_{d0}) about or greater than 6 μm the physical ignition delay (due to droplet heating and evaporation) dominates over the chemical ignition delay (time required for chemical reactions), while for the smaller droplets with $R_{d0} \leq 2.5$ μm the opposite is true [351]. The start of the ignition process was predicted near the periphery of both monodisperse and polydisperse sprays in agreement with current understanding of this phenomenon. The ignition stage of the polydisperse diesel combustion predicted by the Shell autoignition model in combination with conventional models for droplet heating and evaporation was shown to agree with available experimental data for a medium duty truck diesel engine [351]. Since most of the droplets in diesel engines have radii about or greater than 6 μm, accurate modelling of droplet heating and evaporation seems to be more important than accurate modelling of the chemical autoignition process. This provides additional support for the application of the Shell model for modelling the latter process when

compared with more accurate, but more complicated models. Also, this provides a stimulus for the development of more accurate models for droplet heating and evaporation. Note that the chemical ignition delay is strongly influenced by the droplet surface temperature, which is largely controlled by the selected model of droplet heating and evaporation.

Analysis of the problem of turbulent combustion of fuel sprays, following the autoignition process, is beyond the scope of this review (see [353–356] and the references therein).

As mentioned earlier, taking into account finite thermal conductivity in droplets is expected to increase noticeably the accuracy of modelling of the ignition process in diesel engines (see Fig. 2). The reasons for this effect were investigated more closely in [185]. In this paper, the effect of the temperature gradient inside fuel droplets on droplet evaporation, break-up and the ignition of fuel vapour/air mixture was investigated based on a zero-dimensional code. This code takes into account the coupling between the liquid and gas phases and describes the autoignition process based on the Shell model. The effect of temperature gradient inside droplets was investigated by comparing the 'effective thermal conductivity' model and the 'infinite thermal conductivity' model, both of which have been implemented in this code. It was pointed out that in the absence of break-up, the influence of the temperature gradient in droplets on droplet evaporation in a realistic diesel engine environment is generally small (a few percent). In the presence of the break-up process, however, the temperature gradient inside the droplets can lead to a significant decrease in evaporation time. This was attributed to the fact that the effect of temperature gradient inside droplets leads to a substantial increase in droplet surface temperature at the initial stages of its heating. This is translated into a decrease in surface tension and the threshold radii of the unstable droplets. Even in the absence of break-up, the effect of the temperature gradient inside the droplets was shown to lead to a noticeable decrease in the total ignition delay. In the presence of break-up this effect is enhanced substantially, leading to more than halving of the total ignition delay. It was recommended that the effect of the temperature gradient inside droplets is taken into account in CFD codes describing droplet break-up and evaporation processes, and the ignition of the evaporated fuel/air mixture.

The results reported in [357,185] are based on the coupled solutions of ordinary differential equations for droplets and chemical reactions. A more detailed review of the mathematical aspects of these coupled solutions is presented in Section 3.7.

3.7. Coupled solutions

The general problem of simultaneous transient heat and mass transfer has been solved by coupled numerical solutions of the conservation Eqs. (see e.g. [64,66, 358–365]), their analytical solutions (see e.g. [366]) and asymptotic analyses in the limiting cases (see e.g. [367–373]). None of the results of these studies are directly applicable in multidimensional CFD codes, to the best of my knowledge.

The traditional CFD approach to modelling droplet heating, evaporation and dynamics is based on the Lagrangian approach for sprays coupled with the Eulerian representation of the gas phase. This approach is, arguably, well suited to coupled solutions for droplet heating, evaporation and dynamics, since the momentum and heat exchange terms are dominant in the process when the volume fraction of droplets is small enough. However, the droplet parameters then have to be calculated using much shorter time steps δt (typically 10^{-6} s for internal combustion engines) than the global time steps used for calculating the gas phase Δt (typically 10^{-4} s). The details of this approach are discussed in standard textbooks (see e.g. Chapter 6 in [13]).

Although this approach is widely used, its limitations are well known. These limitations are particularly important when the system of ordinary differential equations (ODEs) describing droplet dynamics is stiff, and when the time scales over which gas parameters change are less than the time scales over which spray parameters change (a typical example: autoignition in diesel engines). Stiff ODE solvers do not always solve the problem satisfactorily; even the most elaborate integration schemes for droplet ODEs produce noticeable errors, as coupling between droplets and flow is hindered by the fact that the flow equations are solved on a much larger timescale. Moreover, this approach does not take into account different time scales during which the variables change. This often leads to the application of excessively large time steps for the calculation of some variables and unnecessarily short time steps for the calculation of others. For example, during the onset of autoignition in diesel engines, gas temperature is the 'fast' variable, while droplet temperature remains almost constant. Hence, there is no need to calculate the droplet temperature at small time steps, while the global time scale for the

calculation of gas temperature needs to be considerably decreased.

Some of these difficulties can be overcome via the decomposition of complex systems into simpler subsystems. This decomposition is de facto almost universally used in engineering and physics applications. It allows the numerical simulation to focus on the subsystems, thus avoiding substantial difficulties and instabilities related to numerical simulation of the original systems. The simplest decomposition of these systems is based on the sequential solution of individual subsystems comprising these systems. In this approach, the solution of each individual subsystem for a given subset of variables is based on the assumption that all the other variables are fixed. The sequence of the solutions of individual subsystems is often chosen rather arbitrarily and the results sometimes vary substantially depending on the order in which these subsystems are solved. In the case of a multi-scale system, the reliability of this approach becomes altogether questionable [374]. Most of the following analysis in this section is based on [374]. The focus will be on the systems of ODEs.

It is believed that to overcome the above-mentioned problems, the multi-scale nature of ODEs needs to be investigated before any attempt to solve them is made. This idea could be prompted by the approaches used in [375] for the analysis of the processes in CO_2 lasers. Before solving a system of five stiff ODEs describing five temperatures in these lasers, the characteristic time-scales of these equations were analysed [375]. This allowed the authors of [375] to replace the solution of five stiff equations by the system of just three non-stiff equations without any significant loss of accuracy. The approach used in [349] was different from that used in [375], but the ultimate result—reduction of the number of ODEs to be solved, and elimination of the stiffness of the system of equations—remained the same. In mathematical terms, in both papers the dimension of the ODE systems was reduced. In other words, the system was decomposed into lower dimension subsystems.

Similar system decompositions into lower dimension subsystems have been used in constructing reduced chemical mechanisms based on Intrinsic Low-Dimensional Manifolds (ILDM) (e.g. [376–378]) and Computational Singular Perturbation (CSP) (e.g. [379–383]). There are many similarities between these methods. They are based on a rigorous scale separation such that 'fast' and 'slow' subspaces of the chemical source term are defined and mechanisms of much reduced stiffness are constructed. These approaches, however, were developed with a view to their use in modelling chemical kinetics. Their generalisation to multidimensional CFD codes has not been considered, to the best of my knowledge.

A useful analytical tool for the analysis of stiff systems of ODEs, used for modelling of spray heating, evaporation and ignition, could be based on the geometrical asymptotic approach to singularly perturbed systems (integral manifold method) as developed by Gol'dshtein and Sobolev [384,385] for combustion applications (see also [386]). This approach overcomes some of the earlier mentioned problems and is, essentially, focused on systems of ordinary differential equations of the form:

$$\frac{d\mathbf{X}}{dt} = F(\mathbf{X}, \mathbf{Y}) \qquad \varepsilon \frac{dY}{dt} = G(\mathbf{X}, \mathbf{Y}), \tag{154}$$

where $\mathbf{X}$ and $\mathbf{Y}$ are n and m-dimensional vector variables, and ε is a small positive parameter $\varepsilon \ll 1$. The first subsystem is called a slow subsystem and the second one is called a fast subsystem.

According to a standard definition [387], a manifold (surface) $M := \{(\mathbf{X},\mathbf{Y}):\mathbf{Y} = h(\mathbf{X}, \varepsilon)\}$ is an integral manifold of Eq. (154) if any phase trajectory $\gamma(\mathbf{X},\mathbf{Y})$ of these equations intersecting with M belongs to M in the domain of existence of M The general theory of integral manifolds states that integral (invariant) manifolds M belong to the ε-neighborhood of the slow (quasi-stationary) manifold $M_0 := \{(\mathbf{X},\mathbf{Y}):y = h_0(\mathbf{X})\}$, where $\boldsymbol{Y} = h_0(\mathbf{X})$ is an isolated solution of the second equation in System (154) with $\varepsilon = 0$ [61]:

$$G(\mathbf{X}, h_0(\mathbf{X})) = 0.$$

The slow variable is generally assumed to be constant during the fast processes.

These approaches to decomposing systems of ODEs were developed and investigated with a view to application to rather special problems, and were based on a number of assumptions. These include fixing of the decomposition over the whole period of the process, and not allowing its hierarchy to change with time. The underlying philosophy of these approaches, however, seems to be attractive for application to the analysis of a wide range of physical and engineering problems including spray modelling in CFD codes. The development of a new general method of decomposing the system of ODEs, which allows the nature of decomposition to change with time (dynamic decomposition), is the main objective of recent investigations reported in [374].

As in the original integral manifold method, the formal approach to decomposition of the system of

ODEs suggested in this paper is based on the division of system variables into 'fast' and 'slow'. This leads to the division of this system into 'fast' and 'slow' subsystems. In contrast to the original version of the integral manifold method, however, linearised variations of slow variables during the time evolution of the fast variables were taken into account as the first order approximation to the fast manifold. The usefulness of this division depends on whether the 'fast' subsystem has a lower dimension compared with the 'slow' subsystem. The procedure can be iterative and result in a hierarchical division of the original system. For example the 'slow' subsystem can, in its turn, be subdivided into 'slow' and 'very slow' subsystems.

The proposed procedure was initially focused on the simplest possible subdivision of the original system into two subsystems, and applied to spray combustion modelling. Note that 'fast'—'slow' decomposition in this case can be different for different phase space regions and for different time intervals. Hence, this approach was called dynamic decomposition (see also [388]). Wider ranging application of this method is anticipated.

4. Concluding remarks

Although much progress in the development of models for fuel droplet heating and evaporation has been made over recent years, a number of questions still remain unanswered. These will be briefly discussed in this section alongside the main achievements in this direction, mainly from the perspective of developers of CFD codes.

At the moment it is relatively straightforward to numerically solve the problem of transient convective heating of a moving droplet injected into gas at a certain moment of time $t=0$. However, it is much less clear how to solve the same problem within CFD codes. Traditionally, the latter calculations are based on the application of Newton's law, and steady state correlations for the convective heat transfer coefficient. As demonstrated in Section 2.1.1, for the case of stagnant droplets, these correlations can be misleading in the transient case. At the initial stage of heating the well known steady state result $Nu=2$ leads to underprediction of the rate of heating, while at the final stage of heating the same result leads to over prediction of this rate.

The importance of taking into account the effects of finite thermal conductivity of fuel droplets and recirculation within them has gradually been accepted by the engineering community. The solution of the problem with internal recirculation is greatly simplified when the so-called effective thermal conductivity model is used. In this model actual liquid thermal conductivity is replaced by effective thermal conductivity, which depends on the liquid's Peclet number. This model predicts correctly the average droplet surface temperature, which is the most important parameter for practical applications. It allows the reduction of complicated two- or three-dimensional problems of moving droplet heating to a one-dimensional problem of spherically symmetrical droplet heating. It has been shown that the numerical analysis of droplet heating using the effective thermal conductivity model can be based on the analytical solution of the heat conduction equation inside the droplet. This approach was shown to have clear advantages compared with that based on the numerical solution of the discretised equation, both from the point of view of accuracy and CPU efficiency. When highly accurate calculations are not required, but CPU time economy is essential, then the effect of finite thermal conductivity and recirculation in droplets can be taken into account using the parabolic temperature profile model.

A number of reasonably accurate models for fuel droplet radiative heating have been suggested. However, in practical applications in CFD codes, the simplified model describing the average droplet absorption efficiency factor appears to be the most useful. Even for extreme values of external temperatures, the predictions of droplet heating and evaporation based on this model turn out to be very close to those of more accurate models taking into account the distributed absorption of radiation inside droplets.

The models, which seem to be most accurate at describing droplet evaporation and heating of evaporating droplets are based on empirical correlations. The physical model describing these processes developed by Abramzon and Sirignano in 1989 [63] is still widely used in practical applications. This model combines accuracy and computer efficiency, which enables its application in practical spray combustion calculations. It takes into account many important effects, such as variable physical properties and the non-unitary Lewis number in the gas phase, influence of the Stefan flow on heat and mass transfer, hydrodynamics drag and the effect of transient liquid heating inside the droplet.

It is generally recognised that the effect of multicomponent droplets needs to be taken into account when modelling realistic fuel droplet evaporation at high pressures. However, the models describing these effects are still rather complicated, which limits their wide application in CFD codes. The development of

simplified, robust, reasonably accurate and easy to use models must be the main priority. The development of the Distillation Curve Model by Burger et al [208] seems to be an important step in this direction.

Although hydrodynamic models of droplet evaporation are almost universally used in engineering applications, their foundation has not yet been rigorously proven or justified. Kinetic and molecular dynamics models are inevitably far too complicated for practical applications for the solution of engineering problems. These models, however, can be used as benchmarks for future simpler models, which consider the processes on the droplet/gas interface.

The Shell autoignition model is still widely used for the analysis of the autoignition of fuel vapour/air mixture in internal combustion engines, although its limitations are well known. It is too complicated for asymptotical analysis of droplet heating and evaporation and ignition of fuel vapour/air mixture. At the same time, it has to rely on fitting techniques to find the values of the numerical coefficients used in this model, which limits its applicability.

The existence of the problem of stiff ordinary differential equations describing droplet heating and evaporation and autoignition of fuel vapour/air mixture in individual computational cells frequently arises and its importance is appreciated by developers of CFD codes. Establishing the hierarchy of these equations, and separate analysis of equations for fast and slow variables may be a constructive way forward in solving this problem. It seems, however, that no numerical algorithm capable of performing this operation dynamically and suitable for implementation into CFD codes has been suggested so far.

Acknowledgements

The author is grateful to European Regional Development Fund Franco-British INTERREG IIIa (Project Ref 162/025/247) for partial financial support of the work on this review, his colleagues W Abdelghaffar, B Abramzon, V Babushok, C Bai, M Bardsley, V Bykov, C Crua, L Dombrovsky, G Feng, I Goldfarb, V Gol'dshtein, M Heikal, R Johns, D Kennaird,P Krutitskii, A Kryukov, G Kuzmenko, V Levashov, C Marooney, S Martynov, S Meikle, S Mikhalovsky, E Sazhina, R Wood and A Zinoviev in collaboration with whom some results presented in this review were originally obtained and E. Michaelides and G.F. Yao for useful discussions of selected topics covered in the review.

Appendix A. Physical properties of fuels

This section essentially reproduces the Appendix of [185], where the approximations of the temperature dependence of some important fuels are summarised. These data are essential for the application of the models described in the review.

Physical properties of tetradecane

Using data presented in [389], the latent heat of evaporation in J/kg is approximated as:

$$L = 4.7999679442\times10^{5} - 447.99679239\,T + 1.0772809826\,T^{2} - 8.4415064357\times10^{-3}T^{3} + 2.907585478\times10^{-5}T^{4} - 4.3509615486\times10^{-8}T^{5} + 2.1527777826\times10^{-11}T^{6}$$

when $T<T_{cr}=693$ K (critical temperature) and zero otherwise [390].

Using data presented in [389], the specific heat capacity of liquid in J/kg K is approximated as $c_l = 1453.5010887\times\exp(0.0014122933017T)$.

The specific heat capacity of vapour at constant pressure is approximated as [390]

$$c_{pv} = -1.7787319 + 6.4564177\,T - 3.2454867\times10^{-3}\,T^{2} + 4.5752023\times10^{-7}\,T^{3} + 8.510382\times10^{-11}\,T^{4}.$$

The saturated vapour pressure is assumed to be equal to $p_{sv} = 10^{5}\times10^{4.1379-1740.88/(T-105.43)}$ N/m^2 when $T<T_{cr}$ and zero otherwise [390]. Using data presented in [389], the density of liquid is approximated as $\rho_l = 915.017 - 0.366493\,T - 4.68132\times10^{-4}\,T^{2}$ and the thermal conductivity of liquid in W/(m K) is approximated as

$$k_l = 0.16243019148 + 1.1551271437\times10^{-4}\,T - 7.6492882118\times10^{-7}\,T^{2} + 5.9731934732\times10^{-10}\,T^{3}$$

when $T<T_{cr}$ and zero otherwise.

Physical properties of *n*-heptane

Latent heat of evaporation in J/kg is approximated as [391]:

$$L = 317.8 \times 10^3 \left(\frac{T_{cr} - T}{T_{cr} - T_b} \right)^{0.38},$$

where $T_{cr} = 540.17$ K and $T_b = 371.4$ K [390], when $T < T_{cr}$ and zero otherwise. Using data presented in [389], the specific heat capacity of liquid in J/kg K is approximated as

$$c_l = 13058.45044066 - 126.5095282565\,T + 0.52796138486638\,T^2 - 0.0009457386295687\,T^3 + 6.369853422618 \times 10^{-7}\,T^4.$$

The specific heat capacity of vapour at constant pressure is approximated as [390]

$$c_{pv} = 799.3401062 + 0.3448263942\,T + 0.01285548641\,T^2 - 1664.890863 \times 10^{-8}\,T^3 + 644.6826474 \times 10^{-11}\,T^4.$$

The saturated vapour pressure is assumed to be equal to $p_{sv} = 10^5 \times 10^{4.02677 - 1258.34/(T - 53.85)}\,\mathrm{N/m^2}$ when $T < T_{cr}$ and zero otherwise [390]. Using data presented in [389], the density of liquid is approximated as:

$$\rho_l = -941.03 + 19.96181\,T - 0.08612051\,T^2 + 1.579494 \times 10^{-4}\,T^3 - 1.089345 \times 10^{-7}\,T^4$$

when $T \le 538$ K and

$$\rho_l = 4.195281 \times 10^7 - 2.360524 \times 10^5\,T + 442.7316\,T^2 - 0.2767921\,T^3$$

when $T > 538$ K. Using data presented in [389], the thermal conductivity of liquid in W/(m K) is approximated as $k_l = 0.25844890110 - 4.5549450549 \times 10^{-4}\,T$ when $T < T_{cr}$ and zero otherwise.

Physical properties of *n*-dodecane

Latent heat of evaporation in J/kg [392]:

$$L = 329037.62 + 1883.02\,T - 10.99644\,T^2 + 0.021056\,T^3 - 1.44737 \times 10^{-5}\,T^4$$

when $T < T_{cr} = 659$ K (critical temperature) [390] and zero otherwise.

Using data presented in [389], the specific heat capacity of liquid in J/kg K is approximated as:

$$c_l = 803.42 + 5.076\,T - 0.00221\,T^2 + 1.673 \times 10^{-6}\,T^3.$$

The specific heat capacity of vapour at constant pressure is approximated as [393]

$$c_{pv} = 380.63 + 4.1372\,T + 2.004 \times 10^{-4}\,T^2 - 1.8009 \times 10^{-6}\,T^3 + 7.7875 \times 10^{-10}\,T^4 - 1.0152 \times 10^{-13}\,T^5.$$

The saturated vapour pressure is assumed to be equal to

$$p_{sv} = 6894.757 \times \exp[12.12767 - 3743.84/(T - 93.022)]$$

when $T < T_{cr}$ and zero otherwise. The density of liquid is approximated as [394]:

$$\rho_l = 1104.98 - 1.9277\,T + 0.003411\,T^2 - 3.2851 \times 10^{-6} T^3.$$

The thermal conductivity of liquid *n*-dodecane and liquid diesel fuel in W/(m K) was taken from Table A1 in [390]. The surface tension is approximated as [393]: $\sigma_s = 0.0528 \left(1 - \frac{T}{T_{cr}} \right)^{0.121}$.

Physical properties of diesel fuel

In this section a compilation of physical properties of a 'typical' diesel fuel is given. These are expected to differ slightly from any particular diesel fuel.

Latent heat of evaporation in J/kg is approximated as [391]: $L = 254 \times 10^3((T_{cr} - T)/(T_{cr} - T_b))^{0.38}$, where $T_{cr} = 725.9$ and $T_b = 536.4$ K, when $T < T_{cr}$ and zero otherwise.

The specific heat capacity of liquid in J/(kg·K) is approximated as [393]: $c_l = 264 + 6.33\,T - 0.00296\,T^2$. The specific heat capacity of vapour at constant pressure is approximated as equal to that of *n*-dodecane [393]. The saturated vapour pressure is assumed to be equal to [391]:

$$p_{sv} = \begin{cases} 1000 \times \exp[8.5872101 - 2591.5232/(T-43)] & \text{when } T < 380\,\text{K} \\ 1000 \times \exp[14.060729 - 4436.099/(T-43)] & \text{when } 380 \le T < 500\,\text{K} \\ 1000 \times \exp[12.93692 - 3922.5184/(T-43)] & \text{when } 500 \le T < 620\,\text{K} \\ 1000 \times \exp[16.209535 - 5810.817/(T-43)] & \text{when } 620 \le T < T_{cr} \\ 0 & \text{when } T \ge T_{cr}. \end{cases}$$

The density of liquid is approximated as [394]: $\rho_l = 840/[1 + 0.00067(T - 288)]$. The thermal conductivity of liquid in W/(m K) is presented in Table 1 in [185]. The surface tension is approximated as [393]: $\sigma_s = 0.059(1 - (T/T_{cr}))^{0.121}$.

References

[1] Schrage RW. A theoretical study of interphase mass transfer. New York: Columbia University Press; 1953.
[2] Fuchs NA. Evaporation and droplet growth in gaseous media. London: Pergamon Press; 1959.
[3] Levich VG. Physicochemical hydrodynamics. Englewood Cliffs, NJ: Prentice-Hall; 1962.
[4] Spalding DB. Convective mass transfer; an introduction. London: Edward Arnold; 1963.
[5] Faeth GM. Current status of droplet and liquid combustion. Prog Energy Combust Sci 1977;3:191–224.
[6] Clift R, Grace JR, Weber ME. Bubbles, drops and particles. New York: Academic Press; 1978.
[7] Faeth GM. Evaporation and combustion of sprays. Prog Energy Combust Sci 1983;9:1–76.
[8] Sirignano WA. Fuel droplet vaporization and spray combustion theory. Prog Energy Combust Sci 1983;9:291–322.
[9] Kuo K-K. Principles of combustion. Chichester: Wiley; 1986.
[10] Lefebvre AH. Atomization and sprays. Bristol, PA: Taylor & Francis; 1989.
[11] Leal LG. Laminar flow and convective transport processes. Oxford: Butterworth–Heinemann; 1992.
[12] Borman GL, Ragland KW. Combustion engineering. London: McGraw-Hill; 1998.
[13] Sirignano WA. Fluid dynamics and transport of droplets and sprays. Cambridge: Cambridge University Press; 1999.
[14] Turns SR. An introduction to combustion. 2nd ed. New York: McGraw-Hill; 2000.
[15] Bird RB, Stewart WE, Lightfoot EN. Transport phenomena. Chichester: Wiley; 2002.
[16] Michaelides EE. Hydrodynamic force and heat/mass transfer from particles, bubbles, and drops—the Freeman scholar lecture. ASME J Fluid Eng 2003;125:209–38.
[17] Fritsching U. Spray simulation. Cambridge: Cambridge University Press; 2004.
[18] Chiu HH. Advances and challenges in droplet and spray combustion. 1. Towards a unified theory of droplet and spray combustion. Prog Energy Combust Sci 2000;26:381–416.
[19] Gouesbet G, Berlemont A. Eulerian and Lagrangean approaches for predicting the behaviour of discrete particles in turbulent flows. Prog Energy Combust Sci 1999;25:133–59.
[20] Aggarwal SK. A review of spray ignition phenomena: present status and future research. Prog Energy Combust Sci 1998;24:565–600.
[21] Michaelides EE, Feng Z-G. Analogies between the transient momentum and energy equations of particles. Prog Energy Combust Sci 1996;22:147–62.
[22] Bellan J. Supercritical (and subcritical) fluid behavior and modelling: drops, steams, shear and mixing layers, jets and sprays. Prog Energy Combust Sci 2000;26:329–66.
[23] Givler SD, Abraham J. Supercritical droplet vaporization and combustion studies. Prog Energy Combust Sci 1996;22:1–28.
[24] Zhu G-S, Reitz RD, Aggarwal SK. Gas-phase unsteadiness and its influence on droplet vaporization in sub- and super-critical environments. Int J Heat Mass Transfer 2001;44:3081–93.
[25] Mashayek F, Pandya RVR. Analytical description of particle laden flows. Prog Energy Combust Sci 2003;29:329–78.
[26] Babinsky E, Sojka PE. Modelling drop size distribution. Prog Energy Combust Sci 2002;28:303–29.
[27] Sovani SD, Sojka PE, Lefebvre AH. Effervescent atomization. Prog Energy Combust Sci 2001;27:483–521.
[28] Loth E. Numerical approaches for motion of dispersed particles, droplets and bubbles. Prog Energy Combust Sci 2000;26:161–223.
[29] Orme M. Experiments on droplet collisions, bounce, coalescence and disruption. Prog Energy Combust Sci 1997;23:65–79.
[30] Dwyer HA, Stapf P, Maly R. Unsteady vaporization and ignition of a three-dimensional droplet array. Combust Flame 2000;121:181–94.
[31] Harstad K, Bellan J. Evaluation of commonly used assumptions for isolated and cluster heptane drops in nitrogen at all pressures. Combust Flame 2001;127:1861–79.
[32] Mashayek F. Dynamics of evaporating drops. Part II: free oscillations. Int J Heat Mass Transfer 2001;44:1527–41.
[33] Mashayek F, Ashgriz N, Minkowycz WJ, Shotorban B. Coalescence collision of liquid drops. Int J Heat Mass Transfer 2003;46:77–89.
[34] Mihálykó Cs, Lakatos BG, Matejdesz, Blickle T. Population balance model for particle-to-particle heat transfer in gas–solid systems. Int J Heat Mass Transfer 2004;47:1325–34.
[35] Shusser M, Weihs D. Stability of rapidly evaporating droplets and liquid shells. Int J Multiphase Flow 2001;27:299–345.
[36] Kamiuto K, Yee SS. Correlated radiative transfer through a packed bed of opaque spheres. Int Commun Heat Mass Transfer 2005;32:133–9.
[37] Crafton EF, Black WZ. Heat transfer and evaporation rate of small liquid droplets on heated horisontal surfaces. Int J Heat Mass Transfer 2004;47:1187–200.
[38] Meléan Y, Sigalotti LDG. Coalescence of colliding van der Waals liquid drops. Int J Heat Mass Transfer 2005;48:4041–61.
[39] Imaoka RT, Sirignano WA. A generalized analysis for liquid-fuel vaporization and burning. Int J Heat Mass Transfer 2005;48:4342–53.
[40] Imaoka RT, Sirignano WA. Transient vaporization and burning in dense droplet arrays. Int J Heat Mass Transfer 2005;48:4354–66.
[41] Kandlikar SG, Steinke ME. Contact angles and interface behavior during rapid evaporation of liquid on a heated surface. Int J Heat Mass Transfer 2002;45:3771–80.

[42] Heywood JB. Internal combustion engines fundamentals. New York: McGraw-Hill; 1988.
[43] Li SC. Spray stagnation flames. Prog Energy Combust Sci 1997;23:303–47.
[44] Reitz RD, Rutland CJ. Development and testing of diesel engine CFD models. Prog Energy Combust Sci 1995;21: 173–96.
[45] Tsai C-H, Hou S-S, Lin T-H. Spray flames in a one-dimensional duct of varying cross-sectional area. Int J Heat Mass Transfer 2005;48:2250–9.
[46] Jones AR. Light scattering for particle characterization. Prog Energy Combust Sci 1999;25:1–53.
[47] Rysakov VM. Light scattering by 'soft' particles of arbitrary shape and size. J Quant Spectrosc Radiat Transfer 2004;87: 261–87.
[48] Soret Ch. Sur l'état d'équilibre que prend au point de vue de sa concentration une dissolution saline primitivement homogene dont deux parties sont portées a des températures différentes. Arch Sci Physiques Nat 1879;2:48–61.
[49] de Groot SR, Mazur P. Non-equilibrium thermodynamics. Amsterdam: North-Holland; 1962.
[50] Coelho RML, Silva Telles A. Extended Graetz problem accompanied by Dufour and Soret effects. Int J Heat Mass Transfer 2002;45:3101–10.
[51] Postelnicu A. Influence of a magnetic field on heat and mass transfer by natural convection from vertical surfaces in porous meadia considering Soret and Dufour effects. Int J Heat Mass Transfer 2004;47:1467–72.
[52] Gopalakrishnan V, Abraham J. Effects of multicomponent diffusion on predicted ignition characteristics of an *n*-heptane diffusion flame. Combust Flame 2004;136:557–66.
[53] Reid RC, Prausnitz JM, Sherwood TK. The properties of gases and liquids. 3rd ed. New York: McGraw-Hill; 1977.
[54] Atkins P, de Paula J. Atkins' physical chemistry. 7th ed. Oxford: Oxford University Press; 2002.
[55] Peng D-Y, Robinson DB. A new two-constant equation of state. Ind Eng Chem Fundam 1976;15:59–64.
[56] Hohmann S, Renz U. Numerical simulation of fuel sprays at high ambient pressure: the influence of real gas effects and gas solubility on droplet vaporisation. Int J Heat Mass Transfer 2003;46:3017–28.
[57] Kim H, Sung N. The effect of ambient pressure on the evaporation of a single droplet and a spray. Combust Flame 2003;135:261–70.
[58] Goldfarb I, Gol'dshtein V, Kuzmenko G, Greenberg JB. On thermal explosion of a cool spray in a hot gas. Proceedings of the 27th international symposium on combustion (Colorado, USA), vol. 2; 1998. p. 2367–74.
[59] McIntosh AC, Gol'dshtein V, Goldfarb I, Zinoviev A. Thermal explosion in a combustible gas containing fuel droplets. Combust Theory Modell 1998;2:153–65.
[60] Goldfarb I, Gol'dshtein V, Kuzmenko G, Sazhin SS. Thermal radiation effect on thermal explosion in gas containing fuel droplets. Combust Theory Modell 1999;3:769–87.
[61] Sazhin SS, Feng G, Heikal MR, Goldfarb I, Goldshtein V, Kuzmenko G. Thermal ignition analysis of a monodisperse spray with radiation. Combust Flame 2001;124:684–701.
[62] Bykov V, Goldfarb I, Gol'dshtein V, Greenberg JB. Thermal explosion in a hot gas mixture with fuel droplets: a two reactants model. Combust Theory Modell 2002;6:1–21.
[63] Abramzon B, Sirignano WA. Droplet vaporization model for spray combustion calculations. Int J Heat Mass Transfer 1989; 32:1605–18.
[64] Haywood RJ, Nafziger R, Renksizbulut M. A detailed examination of gas and liquid transient processes in convection and evaporation. ASME J Heat Transfer 1989;111:495–502.
[65] Polyanin AD, Kutepov AM, Vyazmin AV, Kazenin DA. Hydrodynamics, mass and heat transfer in chemical engineering. London: Taylor & Francis; 2002 p. 149–214.
[66] Chiang CH, Raju MS, Sirignano WA. Numerical analysis of convecting, vaporizing fuel droplet with variable properties. Int J Heat Mass Transfer 1992;35:1307–24.
[67] Wadewitz A, Specht E. Limit value of the Nusselt number for particles of different shape. Int J Heat Mass Transfer 2001;44: 967–75.
[68] Cooper F. Heat transfer from a sphere to an infinite medium. Int J Heat Mass Transfer 1977;20:991–3.
[69] Sazhin SS, Abdelghaffar WA, Martynov SB, Sazhina EM, Heikal MR, Krutitskii PA. Transient heating and evaporation of fuel droplets: recent results and unsolved problems. In: Proceedings of 5th international symposium on multiphase flow, heat mass transfer and energy conversion Xi'an, China, 3–6 July 2005; 2005 [CD-ROM].
[70] Sazhin SS, Krutitskii PA, Martynov SB, Mason D, Heikal MR, Sazhina EM. Transient heating of a semitransparent droplet. In: Proceedings of HEFAT2005 (Fourth international conference on heat transfer, fluid mechanics and thermodynamics), Cairo, Egypt; 2005. Paper number: SS1.
[71] Castanet G, Lavieille P, Lemoine F, Lebouché M, Atthasit A, Biscos Y, et al. Energetic budget on an evaporating monodisperse droplet stream using combined optical methods. Evaluation of the convective heat transfer. Int J Heat Mass Transfer 2002;45:5053–67.
[72] Todes OM. Quasi-stationary regimes of mass and heat transfer between a spherical body and ambient medium. In: Fedoseev VA, editor. Problems of evaporation, combustion and gas dynamics in disperse systems. Proceedings of the sixth conference on evaporation, combustion and gas dynamics in disperse systems (October 1966). Odessa: Odessa University Publishing House; 1968. p. 151–9 [in Russian].
[73] Feng Z-G, Michaelides EE. Unsteady heat transfer from a sphere at small Peclet numbers. ASME J Fluids Eng 1996;118: 96–102.
[74] Sazhin SS, Goldshtein V, Heikal MR. A transient formulation of Newton's cooling law for spherical bodies. ASME J Heat Transfer 2001;123:63–4.
[75] Choudhoury PN, Drake DG. Unsteady heat transfer from a sphere in a low Reynolds number flow. Quart J Mech Appl Math 1971;24:23–36.
[76] Gröber H, Erk S. Die Grudgesetze der Wärmeübertragung. 3rd ed. Berlin: Springer; 1961. p. 57–9.
[77] Sazhin SS, Krutitskii PA, Abdelghaffar WA, Mikhalovsky SV, Meikle ST, Heikal MR. Transient heating of diesel fuel droplets. Int J Heat Mass Transfer 2004;47:3327–40.
[78] Sazhin SS, Krutitskii PA. A conduction model for transient heating of fuel droplets. In: Begehre HGW, Gilbert RP, Wong MW, editors. Progress in analysis vol. II. Proceedings of the 3rd international ISAAC (International Society for Analysis, Applications and Computations) congress (August 20–25, 2001, Berlin). Singapore: World Scientific; 2003. p. 1231–9.

[79] Sazhin SS, Abdelghaffar WA, Krutitskii PA, Sazhina EM, Heikal MR. New approaches to numerical modelling of droplet transient heating and evaporation. Int J Heat Mass Transfer 2005;48:4215–28.
[80] Bertoli C, Migliaccio M. A finite conductivity model for diesel spray evaporation computations. Int J Heat Fluid Flow 1999; 20:552–61.
[81] Dombrovsky LA, Sazhin SS. A parabolic temperature profile model for heating of droplets. ASME J Heat Transfer 2003; 125:535–7.
[82] Sazhin SS, Dombrovsky LA, Krutitskii PA, Sazhina EM, Heikal MR. Analytical and numerical modelling of convective and radiative heating of fuel droplets in diesel engines. In: Taine J, editor. Proceedings of the twelfth international heat transfer conference, Grenoble, vol. 1 (August 18–23, 2002). Paris: Editions Scientifique et Medicale Elsevier SAS; 2002. p. 699–704.
[83] Zeng Y, Lee CF. A preferential vaporization model for multicomponent droplets and sprays. Atomization Sprays 2002;12:163–86.
[84] Zeldovich YaB, Kompaneets AS. On the theory of propagation of heat with temperature dependent thermal conductivity. Moscow: Academie of Science of USSR Publishing House; 1950 [in Russian].
[85] Goodman TR. Application of integral methods to transient nonlinear heat transfer. In: Irvine Jr TF, Hartnett JP, editors. Advances in heat transfer, vol. 1. New York: Academic Press; 1964. p. 51–122.
[86] Carslaw HS, Jaeger JC. Conduction of heat in solids. Oxford: Clarendon Press; 1986.
[87] Kartashov EM. Analytical methods in the heat transfer theory in solids. Moscow: Vysshaya Shkola; 2001 [in Russian].
[88] Becker M. Nonlinear transient heat conduction using similarity groups. ASME J Heat Transfer 2000;122:33–9.
[89] Dowding KJ, Blackwell BF. Sensitivity analysis for nonlinear heat conduction. ASME J Heat Transfer 2001;123:1–10.
[90] Cai R, Zhang N. Some algebraically explicit analytical solutions of unsteady non-linear conduction. ASME J Heat Transfer 2001;123:1189–91.
[91] Whitaker S. Forced convection heat transfer correlations for flow in pipes, past flat plates, single cylinders, single spheres, and for flow in packed beds and tube bundles. AIChE J 1972; 18:361–71.
[92] Proudman I, Pearson JRA. Expansion at small Reynolds numbers for a flow past a sphere and a circular cylinder. J Fluid Mech 1956;2:237–62.
[93] Panton RL. Incompressible flow. New York: Wiley; 1996.
[94] Barry DA, Parlange J-Y. Recirculation within a fluid sphere at moderate Reynolds numbers. J Fluid Mech 2002;465:293–300.
[95] Acrivos A, Taylor TE. Heat and mass transfer from single spheres in Stokes flow. Phys Fluids 1962;5:387–94.
[96] Rimmer PL. Heat transfer from a sphere in a stream of small Reynolds number. J Fluid Mech 1968;32:1–7 [Erratum 1969 35:827-8].
[97] Brenner H. Forced convection heat and mass transfer at small Peclet numbers from a particle of arbitrary shape. Chem Eng Sci 1963;18:109–22.
[98] Batchelor GK. Mass transfer from a particle suspended in a fluid with a steady linear ambient velocity distribution. J Fluid Mech 1979;95:369–400.
[99] Acrivos A. A note on the rate of heat and mass transfer from a small particle freely suspended in linear shear field. J Fluid Mech 1980;98:299–304.
[100] Feng Z-G, Michaelides EE. A numerical study of the transient heat transfer from a sphere at high Reynolds and Peclet numbers. Int J Heat Mass Transfer 2000;43:219–29.
[101] Melissari B, Argyropoulos SA. Development of a heat transfer dimensionless correlation for spheres immersed in a wide range of Prandtl number fluids. Int J Heat Mass Transfer 2005; 48:4333–41.
[102] Feng Z-G, Michaelides EE. Heat and mass transfer coefficients of viscous spheres. Int J Heat Mass Transfer 2001;44:4445–54.
[103] Winnikov S, Chao BT. Droplet motion in purified systems. Phys Fluids 1966;9:50–61.
[104] Konopliv N, Sparrow EM. Temperature and heat transfer history of a solid body in a forced convection flow. Q Appl Math 1971;29:225–35.
[105] Konopliv N, Sparrow EM. Unsteady heat transfer and temperature for Stokesian flow about a sphere. ASME J Heat Transfer 1972;94:266–72.
[106] Feng Z-G, Michaelides EE. Unsteady heat and mass transfer from a spheroid. AIChE J 1997;43:609–14.
[107] Pozrikidis C. Unsteady heat or mass transport from a suspended particle at low Peclet numbers. J Fluid Mech 1997;334:111–33.
[108] Chao BT. Transient heat and mass transfer to a translating droplet. ASME J Heat Transfer 1969;91:273–81.
[109] Chao BT, Chen LS. Series solution of unsteady heat or mass transfer to a translating fluid sphere. Int J Heat Mass Transfer 1970;13:359–67.
[110] Chao BT, Cheema LS. Unsteady heat transfer in laminar boundary layer over a flat plate. Int J Heat Mass Transfer 1968; 11:1311–24.
[111] Abramzon B, Borde I. Conjugate unsteady heat transfer from a droplet in creeping flow. AIChE J 1980;26:536–44.
[112] Abramzon B, Elata C. Heat transfer from a single sphere in Stokes flow. Int J Heat Mass Transfer 1984;27:687–95.
[113] Juncu Gh. Unsteady heat and/or mass transfer from a fluid sphere in creeping flow. Int J Heat Mass Transfer 2001;44: 2239–46.
[114] Michaelides EE, Feng Z-G. Heat transfer from a rigid sphere in a nonuniform flow and temperature field. Int J Heat Mass Transfer 1994;37:2069–76.
[115] Gay M, Michaelides EE. Effect of the history term on the transient energy equation for a sphere. Int J Heat Mass Transfer 2003;46:1575–86.
[116] Talley DG, Yao SC. A semi-empirical approach to thermal and composition transients inside vaporizing fuel droplets. Proceedings of twenty-first Symposium (International) on Combustion. The Combustion Institute; 1986, p. 609–16.
[117] Siegel R, Howell JP. Thermal radiation heat transfer. Washington: Hemisphere; 1992.
[118] Modest MF. Radiative heat transfer. 2nd ed. Amsterdam: Academic Press; 2003.
[119] Sleicher CA, Churchill SW. Radiant heating of dispersed particles. Ind Eng Chem 1956;48:1819–24.
[120] Viscanta R, Merriam RL. Heat transfer by combined conduction and radiation between concentric spheres separated by radiating medium. ASME J Heat Transfer 1968;90: 248–56.

[121] Saitoh T, Yamazaki K, Viscanta R. Effect of thermal radiation on transient combustion of a fuel droplet. J Thermophys Heat Transfer 1993;7:94–100.
[122] Marchese AJ, Dryer FL. The effect of non-luminous thermal radiation in microgravity droplet combustion. Combust Sci Technol 1997;124:371–402.
[123] Sazhin SS, Sazhina EM, Heikal MR. Modelling of the gas to fuel droplets radiative exchange. Fuel 2000;79:1843–52.
[124] Su J. Improved lumped models for transient radiative cooling of a spherical body. Int Commun Heat Mass Transfer 2004;31: 85–94.
[125] Yang J-R, Wong S-C. On the discrepancies between theoretical and experimental results for microgravity droplet evaporation. Int J Heat Mass Transfer 2001;44:4433–43.
[126] Miliauskas G. Regularities of unsteady radiative-conductive heat transfer in evaporating semitransparent liquid droplets. Int J Heat Mass Transfer 2001;44:785–98.
[127] Miliauskas G. Interaction of the transfer processes in semitransparent liquid droplets. Int J Heat Mass Transfer 2003;46:4119–38.
[128] Liu LH, Li BX, Tan HP, Yu QZ. Emissive power of semitransparent spherical particles with nonuniform temperature. Int J Heat Mass Transfer 2002;45:4907–10.
[129] Dombrovsky LA. Thermal radiation from nonisothermal spherical particles of a semitransparent material. Int J Heat Mass Transfer 2000;43:1661–72.
[130] Dombrovsky LA, Sazhin SS. Absorption of external thermal radiation in asymmetrically illuminated droplets. J Quant Spectrosc Radiat Transfer 2004;87:119–35.
[131] Dombrovsky LA. Absorption of thermal radiation in large semi-transparent particles at arbitrary illumination of a polydisperse system. Int J Heat Mass Transfer 2004;47: 5511–22.
[132] Lage PLC, Rangel RH. Total thermal radiation absorption by a single spherical droplet. J Thermophys Heat Transfer 1993;7: 101–9.
[133] Sazhin SS, Abdelghaffar WA, Sazhina EM, Mikhalovsky SV, Meikle ST, Bai C. Radiative heating of semi-transparent diesel fuel droplets. ASME J Heat Transfer 2004;126:105–9 [Erratum 2004; 126:490–1].
[134] Dombrovsky LA, Sazhin SS, Mikhalovsky SV, Wood R, Heikal MR. Spectral properties of diesel fuel droplets. Fuel 2003;82:15–22.
[135] Dombrovsky LA, Sazhin SS, Heikal MR. A model for computation of radiative characteristics of diesel fuel droplets. In: Leontiev A, Klimenko A, editors. Proceedings of third Russian national heat and mass transfer conference, vol. 6. Moscow: Moscow Power Engineering Institute Publishing House; 2002. p. 262–5 [in Russian].
[136] Dombrovsky LA, Sazhin SS, Sazhina EM, Feng G, Heikal MR, Bardsley MEA, et al. Heating and evaporation of semi-transparent diesel fuel droplets in the presence of thermal radiation. Fuel 2001;80:1535–44.
[137] Dombrovsky LA, Sazhin SS. Absorption of thermal radiation in a semi-transparent spherical droplet: a simplified model. Int J Heat Fluid Flow 2003;24:919–27.
[138] Tseng CC, Viskanta R. Effect of radiation absorption on fuel droplet evaporation. Combust Sci Technol 2005;177:1511–42.
[139] Abramzon B, Sazhin S. Droplet vaporization model in the presence of thermal radiation. Int J Heat Mass Transfer 2005; 48:1868–73.
[140] Abramzon B, Sazhin S. Convective vaporization of fuel droplets with thermal radiation absorption. Fuel 2006;85: 32–46.
[141] Van de Hulst HC. Light scattering by small particles. New York: Dover; 1957.
[142] Bohren CF, Huffman DR. Absorption and scattering of light by small particles. New York: Wiley; 1983.
[143] Dombrovsky LA. Radiation heat transfer in disperse systems. New York: Begell House; 1996.
[144] Xu H. Electromagnetic energy flow near nanoparticles—I: single spheres. J Quant Spectrosc Radiat Transfer 2004;87: 53–67.
[145] Prishivalko AP. Optical and thermal fields in light scattering particles. Minsk: Nauka; 1983 [in Russian].
[146] Dusel PW, Kerker M, Cooke DD. Distribution of absorption centres within irradiated spheres. J Opt Soc Am 1979;69:55–9.
[147] Mackowski DW, Altenkirch RA, Menguç MP. Internal absorption cross sections in a stratified sphere. Appl Opt 1990;29:1551–9.
[148] Tuntomo A, Tien CL, Park SH. Internal distribution of radiant absorption in a spherical particle. ASME J Heat Transfer 1991; 113:402–12.
[149] Aliev VA, Panfilovich KB. Radiation and conduction heat transfer in semi-transparent organic liquids. Kazan: Kazan State University Publishing House; 2003 [in Russian].
[150] Pinkley LW, Sethna PP, Williams D. Infrared band intensities of saturated hydrocarbons. J Phys Chem 1978;82:1532–7.
[151] Ahrenkiel RK. Modified Kramers–Krönig analysis of optical spectra. J Opt Soc Am 1971;61:1651–5.
[152] Dombrovsky LA. Spectral model of absorption and scattering of thermal radiation by diesel fuel droplets. High Temp 2002; 40:242–8.
[153] Özişik MN. Radiative transfer and interaction with conduction and convection. New York: Wiley; 1973.
[154] Pomraning GC, Siewert CE. On the integral form of the equation of transfer for a homogeneous sphere. J Quant Spectrosc Radiat Transfer 1982;28:503–6.
[155] Born M, Wolf E. Principles of optics. London: Pergamon Press; 1975.
[156] Dombrovsky LA. A modified differential approximation for thermal radiation of semitransparent nonisothermal particles: application to optical diagnostics of plasma spraying. J Quant Spectrosc Radiat Transfer 2002;73:433–41.
[157] Liu LH. Anisotropic emission characteristics of semi-transparent spherical particle with spherically asymmetric temperature distribution. J Quantum Spectrosc Radiat Transfer 2004;85:135–43.
[158] Renksizbulut M, Yuen MC. Experimental study of droplet evapopration in a high-temperature air stream. ASME J Heat Transfer 1983;105:384–8.
[159] Renksizbulut M, Yuen MC. Numerical modeling of droplet evapopration in a high-temperature air stream. ASME J Heat Transfer 1983;105:389–97.
[160] Incropera FP, DeWitt DP. Fundamentals of heat and mass transfer. New York: Wiley; 1996.
[161] Nafziger R. Convective droplet transport phenomena in high temperature air streams, MASc Thesis, University of Waterloo, Ontario, Canada; 1988.
[162] Yang J-R, Wong S-C. An experimental and theoretical study of the effects of heat conduction through the support fiber on the evaporation of a droplet in a weakly convective flow. Int J Heat Mass Transfer 2002;45:4589–98.

[163] Wu J-S, Liu Y-J, Sheen H-J. Effects of ambient turbulence and fuel properties on the evaporation rate of single droplets. Int J Heat Mass Transfer 2001;44:4593–603.
[164] Birouk M, Gökalp I. A new correlation for turbulent mass transfer from liquid droplets. Int J Heat Mass Transfer 2002;45: 37–45.
[165] Wu J-S, Hsu K-H, Kuo P-M, Sheen H-J. Evaporation model of a single hydrocarbon fuel droplet due to ambient turbulence at intermediate Reynolds numbers. Int J Heat Mass Transfer 2003;46:4741–5.
[166] Xu G, Ikegami M, Honma S, Ikeda K, Ma X, Nagaishi H, et al. Inverse influence of the initial diameter on droplet burning rate in cold and hot ambiences: a thermal action of flame in balance with heat loss. Int J Heat Mass Transfer 2003;46: 1155–69.
[167] Paschedag AR, Piarah WH, Kraume M. Sensitivity study for the mass transfer at a single droplet. Int J Heat Mass Transfer 2006; in press.
[168] Goldfarb I, Sazhin S, Zinoviev A. Delayed thermal explosion in flammable gas containing fuel droplets: asymptotic analysis. Int J Eng Math 2004;50:399–414.
[169] Sirignano WA, Law CK. Transient heating and liquid phase mass diffusion in droplet vaporization. In: Zung JT, editor. Evaporation–combustion of fuels. Advances in chemistry series, vol. 166. Washington, DC: American Chemical Society; 1978. p. 1–26.
[170] Mao C-P, Szekely GA, Faeth GM. Evaluation of a locally homogeneous flow model of spray combustion. J Energy 1980; 4:78–87.
[171] Aggarwal SK, Chitre S. Computations of turbulent evaporating sprays. J Propul 1991;7:213–20.
[172] Park TW, Aggarwal SK, Katta VR. Gravity effects on the dynamics of evaporating droplets in a heated jet. J Propul Power 1995;11:519–28.
[173] El Wakil MM, Uyehara OA, Myers PS. A theoretical investigation of the heating-up period of injected fuel droplets vaporizing in air. NACA Technical Note 3179; 1954.
[174] Klingsporn M, Renz U. Vaporization of a binary unsteady spray at high temperature and high pressure. Int J Heat Mass Transfer 1994;37(Suppl. 1):265–72.
[175] Dombrovsky LA, Sazhin SS. A simplified non-isothermal model for droplet heating and evaporation. Int Commun Heat Mass Transfer 2003;30:787–96.
[176] Mukhopadhyay A, Sanyal D. A semi-analytical model for evaporating fuel droplets. ASME J Heat Transfer 2005;127: 199–203.
[177] Liu AB, Reitz RD. Mechanisms of air-assisted liquid atomization. Atomization Sprays 1993;3:55–75.
[178] Tanner FX. Development and validation of a cascade atomization and droplet break-up model for high-velocity dense sprays. Atomization Sprays 2004;14:211–42.
[179] Reitz RD, Diwakar R. Effect of drop breakup on fuel sprays. SAE report 860469; 1986.
[180] Reitz RD, Diwakar R. Structure of high-pressure fuel sprays. SAE report 870598; 1987.
[181] Sazhin SS, Crua C, Kennaird D, Heikal MR. The initial stage of fuel spray penetration. Fuel 2003;82:875–85.
[182] Gorokhovski M. The stochastic Lagrangean model of drop breakup in the computation of fuel sprays. Atomization Sprays 2001;11:505–19.
[183] Gorokhovski M, Saveliev VL. Analyses of Kolmogorov's model of breakup and its application into Lagrangean computation of liquid sprays under air-blast atomization. Phys Fluids 2003;15:184–92.
[184] Frank-Kamenetskii DA. Diffusion and heat transfer in chemical kinetics. New York: Plenum Press; 1969.
[185] Sazhin SS, Abdelghaffar WA, Sazhina EM, Heikal MR. Models for droplet transient heating: effects on droplet evaporation, ignition, and break-up. Int J Therm Sci 2005;44: 610–22.
[186] Yao GF, Abdel-Khalik SI, Ghiaasiaan SM. An investigation of simple evaporation models used in spray simulations. ASME J Heat Transfer 2003;125:179–82.
[187] Caldwell J, Kwan YY. On the perturbation method for the Stephan problem with time-dependent boundary conditions. Int J Heat Mass Transfer 2003;46:1497–501.
[188] Caldwell J, Savović S, Kwan YY. Nodal integral and finite difference solution of one-dimensional Stefan problem. ASME J Heat Transfer 2003;125:523–7.
[189] Savović S, Caldwell J. Finite difference solution of one-dimensional Stefan problem with periodic boundary conditions. Int J Heat Mass Transfer 2003;46:2911–6.
[190] Gupta SC. The classical Stefan problem: basic concepts, modelling and analysis. Amsterdam: Elsevier; 2003.
[191] Landis RB, Mills AF. Effect of internal diffusional resistance on the evaporation of binary droplets. Proceedings of the fifth international heat transfer conference, Tokyo, Japan; 1974. Paper B7.9.
[192] Brenn G. Concentration fields in evaporating droplets. Int J Heat Mass Transfer 2005;48:395–402.
[193] Mukhopadhyay A, Sanyal D. A spherical cell model for multicomponent droplet combustion in a dilute spray. Int J Energy Res 2001;25:1275–94.
[194] Mukhopadhyay A, Sanyal D. A parametric study of burning of multicomponent droplets in a dilute spray. Int J Energy Res 2001;25:1295–314.
[195] Gauthier JED, Bardon MF, Rao VK. Combustion characteristics of multicomponent fuels under cold starting conditions in a gas turbine. Proceedings of the American society of mechanical engineers, Orlando, Florida; 1991. Paper 91-GT-109.
[196] Delplanque J-P, Rangel RH, Sirignano WA. Liquid-wast incineration in a parallel-stream configuration: effect of auxiliary fuel. Prog Aeronaut Astronaut 1991;132:164–84.
[197] Lage PLC, Hackenberg CM, Rangel RH. Nonideal vaporization of dilating binary droplets with radiation absorption. Combust Flame 1995;101:36–44.
[198] Continillo G, Sirignano WA. Numerical study of multicomponent fuel spray flame propagation in a spherical close volume. In: Proceedings of the twenty-second symposium (International) on combustion. Pittsburg, PA: The Combustion Institute; 1988, p. 1941–9.
[199] Continillo G, Sirignano WA. Unsteady, spherically-symmetric flame propogation through multicomponent fuel spray clouds. In: Angelino G, De Luca L, Sirignano WA, editors. Modern research topics in aerospace propulsion. New York: Springer; 1991. p. 173–98.
[200] Kazakov A, Conley J, Dryer FL. Detailed modeling of an isolated, ethanol droplet combustion under microgravity conditions. Combust Flame 2003;134:301–14.

[201] Torres DJ, O'Rourke PJ, Amsden AA. Efficient multicomponent fuel algorithm. Combust Theory Modell 2003;7:67–86.
[202] Tamim J, Hallett WLH. Continuous thermodynamics model for multicomponent vaporization. Chem Eng Sci 1995;50:2933–42.
[203] Lippert AM, Reitz RD. Modelling of multicomponent fuels using continuous distributions with application to droplet evaporation and sprays. SAE technical paper 972882; 1997.
[204] Pagel S, Stiesch G, Merker GP. Modelling of evaporation of a multicomponent fuel. In: Taine J, editor. Proceedings of the twelfth international heat transfer conference, vol. 1, Grenoble (August 18–23, 2002). Paris: Editions Scientifique et Medicale Elsevier SAS; 2002 [CD ROM].
[205] Zhu G-S, Reitz RD. A model for high-pressure vaporization of droplets of complex liquid mixture using continuous thermodynamics. Int J Heat Mass Transfer 2002;45:495–507.
[206] Arias-Zugasti M, Rosner DE. Multicomponent fuel droplet vaporization and combustion using spectral theory for a continuous mixture. Combust Flame 2003;135:271–84.
[207] Harstad K, Bellan J. Modeling evaporation of Jet A, JP-7, and RP-1 drops at 1 to 15 bars. Combust Flame 2004;137:163–77.
[208] Burger M, Schmehl R, Prommersberger K, Schäfer O, Koch R, Wittig S. Droplet evaporation modelling by the distillation curve model: accounting for kerosene fuel and elevated pressures. Int J Heat Mass Transfer 2003;46:4403–12.
[209] Harvie DJE, Fletcher DF. A simple kinetic theory treatment of volatile liquid-gas interfaces. ASME J Heat Transfer 2001;123:486–91.
[210] Kryukov AP, Levashov VYu, Sazhin SS. Evaporation of diesel fuel droplets: kinetic versus hydrodynamic models. Int J Heat Mass Transfer 2004;47:2541–9.
[211] Akhiezer AI, Akhiezer IA, Polovin RV, Sitenko AG, Stepanov KN. Plasma electrodynamics. Oxford: Pergamon Press; 1975.
[212] Elliott RJ. Plasma kinetic theory. In: Rendy R, editor. Plasma physics: an introductory course. Cambridge: Cambridge University Press; 1995. p. 29–53.
[213] Sazhin SS. Whistler-mode waves in a hot plasma. Cambridge: Cambridge University Press; 1993.
[214] Bird GA. Molecular gas dynamics. Oxford: Oxford University Press; 1976.
[215] Bird GA. Molecular gas dynamics and the direct simulation of gas flows. Oxford: Oxford University Press; 1994.
[216] Aoki K, Takata S, Kosuge S. Vapor flows caused by evaporation and condensation on two parallel plane surfaces: effect of the presence of a noncondensable gas. Phys Fluids 1998;10:1519–33.
[217] Taguchi S, Aoki K, Takata S. Vapor flows condensing at incidence onto a plane condensed phase in the presence of noncondensable gas. I. Subsonic condensation. Phys Fluids 2003;15:689–705.
[218] Taguchi S, Aoki K, Takata S. Vapor flows condensing at incidence onto a plane condensed phase in the presence of noncondensable gas. I. Supersonic condensation. Phys Fluids 2004;16:79–92.
[219] Kryukov AP, Levashov VYu, Shishkova IN. Non-equilibrium recondensation in a dusty medium. In: Zhdanok SA et al., editor. Proceedings of the fifth Minsk international heat and mass transfer forum, May 24–28, vol. 2. Minsk: Research Institute of Heat and Mass Transfer Publishing House; 2004. p. 138–9 [in Russian].
[220] Kryukov AP, Levashov VYu, Shishkova IN. Condensation in the presence of a non-condensable component. J Eng Phys Thermophys 2005;78:15–21 [in Russian].
[221] Aristov VV, Tcheremissine FG. Direct numerical solution of the Boltzmann equation. Moscow: Computer Centre of Russian Academy of Sciences; 1992.
[222] Tcheremissine FG. Conservative evaluation of Boltzmann collision integral in discrete ordinates approximation. Comput Math Appl 1998;35:215–21.
[223] Tcheremissine FG. Discrete approximation and examples of the solution of the Boltzmann equation. In: Computational dynamics of rarefied gases. Moscow: Computer Centre of Russia Academy of Sciences; 2000. p. 37–74.
[224] Chapman S, Cowling TG. The mathematical theory on non-uniform gases. Cambridge: Cambridge University Press; 1990.
[225] Bhatnagar PL, Gross EP, Krook M. A model for collision processes in gases 1. Small amplitude processes in charged and neutral one component systems. Phys Rev 1954;94:511–25.
[226] Sazhin SS. Cyclotron whistler-mode instability in a collisional plasma. In: Geomagnetic research no. 23. Moscow: Soviet Radio; 1978, p. 105–7 [in Russian].
[227] Hertz H. Über die Verdunstung der Flussigkeiten, inbesondere des Quecksilbers, im lufteeren Raume. Ann Phys Chem 1882;17:177–200.
[228] Knudsen M. Die Maximale Verdampfungsgeschwindigkeit des Quecksilbers. Ann Phys 1915;47:697–708.
[229] Kogan MN. Rarefied gas dynamics. New York: Plenum Press; 1969.
[230] Shidlovskiy VP. Introduction to the dynamics of rarefied gases. New York: American Elsevier Publishing Company; 1967.
[231] Nigmatilin RI. Dynamics of multiphase media, vol. 1. New York: Hemisphere; 1991.
[232] Hirth JP, Pound GM. Condensation and evaporation. nucleation and growth kinetics. Oxford: Pergamon Press; 1963.
[233] Neizvestny AI, Onishenko LI. Experimental determination of the condensation coefficient for distilled water. Phys Atmos Ocean 1979;15:1052–78 [in Russian].
[234] Tsuruda T, Tanaka H, Masuika T. Condensation/evaporation coefficient and velocity distribution at liquid–vapour interface. Int J Heat Mass Transfer 1999;42:4107–16.
[235] Dunikov DO, Malyshenko SP, Zhakhovskii VV. Corresponding states law and molecular–dynamics simulations of the Lennard–Jones fluid. J Chem Phys 2001;115:6623–31.
[236] Consoline L, Aggarwal SK, Murad S. A molecular dynamics simulation of droplet evaporation. Int J Heat Mass Transfer 2003;43:3179–88.
[237] Yang TH, Pan C. Molecular dynamics simulation of a thin water layer evaporation and evaporation coefficient. Int J Heat Mass Transfer 2005;48:3516–26.
[238] Marek R, Straub J. Analysis of the evaporation coefficient and the condensation coefficient of water. Int J Heat Mass Transfer 2001;44:39–53.
[239] Gumerov NA. Dynamics of vapour bubbles with non-equilibrium phase transitions in isotropic acoustic fields. Phys Fluids 2000;12:71–88.
[240] Sone Y, Sugimoto H. Strong evaporation from a plane condensed phase. In: Meier GEA, Thompson PA, editors. Adiabatic waves in liquid–vapour systems. Proceedings of the IUTAM symposium, Gottingen, Germany 1989. Berlin: Springer; 1990. p. 293–304.
[241] Lifshitz EM, Pitaevski LP. Physical kinetics. Moscow: Nauka Publishing House; 1979 [in Russian].

[242] Kucherov RYa, Rickenglaz LE. On hydrodynamics boundary conditions for modelling vaporization and condensation processes. J Exp Theor Phys 1959;37:125–6 [in Russian].
[243] Kucherov RYa, Rickenglaz RE. On the measurement of the coefficient of condensation. Reports of the Academy of Science of USSR (Doklady), vol. 133; 1960. p. 1130–1 [in Russian].
[244] Kucherov RYa, Rickenglaz RE, Tzulaya TS. Kinetic theory of additional condensation in the presence of the small temperature jump. Sov Phys Tech Phys 1963;7:1027–30.
[245] Labuntsov DA. Analysis of the evaporation and condensation processes. High Temp 1967;5:579–85.
[246] Muratova TM, Labuntsov DA. Kinetic analysis of the evaporation and condensation processes. Therm Phys High Temp 1969;7:959–67 [in Russian].
[247] Korabelnikov AV, Nakoryakov VE, Shreiber IR. Taking nonequilibrium vaporization into account in problems of vapour-bubble dynamics. High Temp 1981;19:586–90.
[248] Young-ping-Pao P. Application of kinetic theory to the problem of evaporation and condensation. Phys Fluids 1971; 14:306–11.
[249] Sone Y, Onishi Y. Kinetic theory of evaporation and condensation. J Phys Soc Jpn 1973;35:1773–6.
[250] Sone Y, Onishi Y. Kinetic theory of evaporation and condensation—hydrodynamic equation and slip boundary condition. J Phys Soc Jpn 1978;44:1981–94.
[251] Cipola JW, Lang JH, Loyalka SK. Kinetic theory of evaporation and condensation. Proceedings of the 8th international symposium rarefied gas dynamics, New York, London; 1973. p. 1773–6.
[252] Thomas JP, Chang TS, Siewert SE. Reverse temperature gradient in the kinetic theory of evaporation. Phys Rev Lett 1974;33:680–2.
[253] Shankar PN, Marble FM. Kinetic theory of transient condensation and evaporation at a plane surface. Phys Fluids 1971;14:510–6.
[254] Koffman LD, Plesset MS, Lees L. Theory of evaporation and condensation. Phys Fluids 1984;27:876–80.
[255] Ytrehus T, Aukrust T. Mott-Smith solution for weak condensation. In: Boffi V, Cercignani C, editors. Rarefied gas dynamics, vol. 2. Stuttgart: Teubner; 1986. p. 271–80.
[256] Chernyak V. The kinetic theory of droplet evaporation. J Aerosol Sci 1995;26:873–85.
[257] Anisimov SI. Evaporation of metals under the influence of laser radiation. J Exp Theor Phys 1968;54:339–42 [in Russian].
[258] Anisimov SI, Imas YaA, Romanov GS, Khodyko YuV. Effect of high intensity radiation on metals. Moscow: Nauka Publishing House; 1970 [in Russian].
[259] Kogan MN, Makashev NK. On the role of the Knudsen layer in the theory of heterogeneous reactions and flows with the surface reactions. Reports of the Academy of Sciences of USSR. Mech Liquids Gases 1971;6:3–11 [in Russian].
[260] Murakami M, Oshima K. Kinetic approach to the transient evaporation and condensation problem. In: Becker M, Fiebig M, editors. Rarefied gas dynamics. Pors-Wahn: DFVLR Press; 1974 [paper F6].
[261] Ytrehus T. Theory and experiments on gas kinetics in evaporation. In: Potter JL, editor. Rarefied gas dynamics Part 2. New York: AIAA; 1977. p. 1197–212.
[262] Labuntsov DA, Kryukov AP. Processes of intensive evaporation. Therm Power Energy (Teploenergetika) 1977;(4):8–11 [in Russian].
[263] Labuntsov DA, Kryukov AP. Analysis of intensive evaporation and condensation. Int J Heat Mass Transfer 1979;22:989–1002.
[264] Knight SJ. Theoretical modelling of rapid surface vaporization with back pressure. AIAA J 1979;17:519–23.
[265] Cercignani C. Strong evaporation of a poliatomic gas. In: Fisher SS, editor. Rarefied gas dynamics Part 1. New York: AIAA; 1981. p. 305–10.
[266] Abramov AA, Kogan MN, Makashev NK. Numerical analysis of the processes in strongly non-equilibrium Knudsen layers. Reports of the Academy of Sciences of USSR. Mech Liquid Gases 1981;(3):72-81 [in Russian].
[267] Frezzotti A. Kinetic theory study of the strong evaporation of a binary mixture. In: Boffi V, Cercignani C, editors. Rarefied gas dynamics, vol. 2. Stutgart: Teubner; 1986. p. 313–22.
[268] Sone Y, Aoki K, Sugimoto H, Yamada T. Steady evaporation and condensation on a plane condensed phase. Theor Appl Mech (Bulgaria) 1988;19:89–93.
[269] Ytrehus T, Ostmo S. Kinetic approach to interphase processes. Int J Multiphase Flow 1996;22:133–5.
[270] Takata S, Aoki K. Two-surface problems of a multi-component mixture of vapors and noncondensable gases in the continuum limit in the light of kinetic theory. Phys Fluids 1999;11: 2743–56.
[271] Sibold D, Urbassek HM. Kinetic study of evaporating flows from cylindrical jets. Phys Fluids 1991;3:870–8.
[272] Sugimoto H, Sone Y. Numerical analysis of steady flows of a gas evaporating from its cylindrical condensed phase on the basis of kinetic theory. Phys Fluids 1992;4:419–40.
[273] Sone Y, Sugimoto H. Kinetic theory analysis of steady evaporating flows from a spherical condensed phase into a vacuum. Phys Fluids 1993;5:1491–511.
[274] Sone Y, Sugimoto H. Evaporation of rarefied gas from a cylindrical condensed phase into a vacuum. Phys Fluids 1995; 7:2072–85.
[275] Sone Y, Sigimoto H, Aoki K. Cylindrical Couette flows of a rarefied gas with evaporation and condensation: reversals and bifurcation of flows. Phys Fluids 1999;11:476–90.
[276] Sone Y. Kinetic theoretical studies of the half-space problem of evaporation and condensation. Transport Theory Stat Phys 2000;29:227–60.
[277] Rose JW. Accurate approximate equations for intensive subsonic evaporation. Int J Heat Mass Transfer 2000;43:3869–75.
[278] Titarev VA, Shahov EM. Heat loss and evaporation from a flat surface after a rapid increase of its temperature. Reports of the Russian Academy of sciences. Mech liq gases 2002;(1):141–53 [in Russian].
[279] Rose J. Interphase matter transfer, the condensation coefficient and dropwise condensation. In: Lee JS, editor. Heat transfer 1998. Proceedings of 11th international heat transfer conference (August 23–28, 1998, Kyongji, Korea), vol. 1. Seoul: The Korean Society of Mechanical Engineers; 1998. p. 89–104.
[280] Kennaird EH. Kinetic theory of gases. New York: McGraw-Hill; 1938.
[281] Shen C. The concentration-jump coefficient in a rarefied binary gas mixture. J Fluid Mech 1983;137:221–31.
[282] Gombosi TI. Gaskinetic theory. Cambridge: Cambridge University Press; 1994.
[283] Sharipov F, Kalempa D. Velocity slip and temperature jump coefficients for gaseous mixtures. IV. Temperature jump coefficient. Int J Heat Mass Transfer 2005;48:1076–83.
[284] Elperin T, Krasovitov B. Radiation, thermal diffusion and

kinetic effects in evaporation and combustion of large and moderate size droplets. Int J Heat Mass Transfer 1995;38: 409–18.
[285] Sazhin SS, Serikov VV. Rarefied gas flows: hydrodynamic versus Monte Carlo modelling. Planet Space Sci 1997;45: 361–8.
[286] Peeters P, Luijten CCM, van Dongen MEH. Transitional droplet growth and diffusion coefficients. Int J Heat Mass Transfer 2001;44:181–93.
[287] Shusser M, Ytrehus T, Weihs D. Kinetic theory analysis of explosive boiling of a liquid droplet. Fluid Dyn Res 2000;27: 353–67.
[288] Flynn PF, Durrett RP, Hunter GL, zur Loye AO, Akinyemi OC, Dec JE, Westbrook CK. Diesel combustion: an integrated view combining laser diagnostics, chemical kinetics, and empirical validation. SAE report 1999-01-0509; 1999.
[289] Malyshenko SP, Dunikov DO. On the surface tension corrections in non-uniform and nonequilibrium liquid–gas systems. Int J Heat Mass Transfer 2002;45:5201–8.
[290] Xu X, Cheng C, Chowdhury IH. Molecular dynamics study of phase change mechanisms during femtosecond laser ablation. ASME J Heat Transfer 2004;126:727–34.
[291] Allen MP, Tidesley DJ. Computer simulation of liquids. Oxford: Oxford University Press; 1984.
[292] Hirschfelder JO, Curtiss CF, Bird RB. Molecular theory of gases and liquids. 4th ed. New York: Wiley; 1967.
[293] Lee LL. Molecular nonideal fluids. Boston: Butterworths; 1988.
[294] Anisimov SI, Dunikov DO, Zhakhovskii VV, Malyshenko SP. Properties of a liquid–gas interface at high-rate evaporation. J Chem Phys 1999;110:8722–9.
[295] Walther JH, Koumoutsakos P. Molecular dynamics simulation of nanodroplet evaporation. ASME J Heat Transfer 2001;123: 741–8.
[296] Dunikov DO, Malyshenko SP, Zhakhovskii VV. Liquid-gas interface during transient condensation: molecular dynamics investigation. In: Leontiev A, Klimenko A, editors. Proceedings of third Russian national heat and mass transfer conference, vol. 4. Moscow: Moscow Power Engineering Institute Publishing House; 2000. p. 257–60 [in Russian].
[297] Tsuruta T, Tanaka H, Masuoka T. Condensation/ evaporation coefficient and velocity distributions at liquid–vapor interface. Int J Heat Mass Transfer 1999;42:4107–16.
[298] Gun'ko VM, Turov VV. Structure of hydrogen bonds and ^{1}H NMR spectra of water at the interface of Oxides. Langmuir 1999;15:6405–15.
[299] Gun'ko VM, Zarko VI, Leboda R, Marciniak M, Janusz W, Chibowski S. Highly dispersed X/SiO_2 and C/X Si O_2 (X= Aluminia, Titania, Aluminia/Titania) in the gas liquid media. J Colloid Interface Sci 2000;230:396–409.
[300] Cramer CJ, Truhlar DG. Implicit solvation models: equilibria, structure, spectra, and dynamics. Chem Phys 1999;99: 2161–200.
[301] Spalding DB. Combustion and mass transfer. New York: Pergamon Press; 1979.
[302] Varshavski GA, Fedoseev DV, Frank-Kamenetskii AD. Autoignition of a fuel droplet. In: Fedoseev VA, editor. Problems of evaporation, combustion and gas dynamics in disperse systems. Proceedings of the sixths conference on evaporation, combustion and gas dynamics in disperse systems (October 1966). Odessa: Odessa University Publishing House; 1968. p. 91–5 [in Russian].
[303] Crespo A, Liñan A. Unsteady effects in droplet evaporation and combustion. Combust Sci Technol 1975;11:9–18.
[304] Brady RN. Modern diesel technology. Englewood Cliffs, NJ: Prentice-Hall; 1996.
[305] Wright YM, De Paola G, Boulouchos K, Mastorakos E. Simulation of spray autoignition and flame establishment with two dimensional CMC. Combust Flame 2005;143:402–19.
[306] Suppes GJ, Srinivasan B, Natarajan VP. Autoignition of biodiesel, methanol, and 50:50 blend in a simulated Diesel engine environment. SAE paper 952758; 1995.
[307] Minetti R, Ribaucour M, Carlier M, Sochet LR. Autoignition delays of a series of linear and branched chain alkanes in the intermediate range of temperatures. Combust Sci Technol 1996;113–114:179–92.
[308] Basevich VYa, Beliaev AA, Branshtater V, Neigauz MG, Tashl R, Frolov SM. Modelling of iso-octane and *n*-heptane autoignition with reference to IC engines. Phys Combust Explosion 1994;30:15–24 [in Russian].
[309] Minkoff GJ, Tipper CF. Chemistry of combustion reactions. London: Butterworth; 1962.
[310] Crua C, Kennaird DA, Sazhin SS, Heikal MR. Diesel autoignition at elevated in-cylinder pressures. Int J Eng Res 2004;5:365–74.
[311] Pilling MJ, Robertson SH, Seakins PW. Elementary radical reactions and autoignition. J Chem Soc Faraday Trans 1995;91: 4179–88.
[312] Chevalier C, Pitz WJ, Warnatz J, Westbrook CK, Mellenk H. Hydrocarbon ignition: automatic generation of reaction mechanisms and applications to modeling of engine knock. Twenty-fourth symposium (International) on combution. Pittsburg, PA: The Combustion Institute; 1992. p. 1405–14.
[313] Minetti R, Ribaucour M, Carlier M, Fittschen C, Sochet LR. Experimental and modelling study of oxidation and autoignition of butane at high pressure. Combust Flame 1994;96: 201–11.
[314] Kojima S. Detailed modeling of *n*-butane autoignition chemistry. Combust Flame 1994;99:87–136.
[315] Ranzi E, Faravelli T, Gaffuri P, Pennati GC, Sogaro A. A wide range modeling of propane and *n*-butane oxidation. Combust Flame 1994;100:299–330.
[316] Curran HJ, Gaffuri P, Pitz WJ, Westbrook CK. A comprehensive modeling study of *n*-heptane oxidation. Combust Flame 1998;114:149–77.
[317] Zhukov VP, Sechenov VA, Starikovskii AYu. Self-ignition of a lean mixture of n-pentane and air over a wide range of pressures. Combust Flame 2005;140:196–203.
[318] Buda F, Bounaceur R, Warth V, Glaude PA, Fournet R, Battin-Leclerc F. Progress toward a unified detailed kinetic model for the autoignition of alkanes from C_4 to C_{10} between 600 K and 1200 K. Combust Flame 2005;142:170–86.
[319] Cuoci A, Mehl M, Buzzi-Ferraris G, Faravelli T, Manca D, Ranzi E. Autoignition and burning rates of fuel droplets under microgravity. Combust Flame 2005;143:211–26.
[320] Basevich VYa. Chemical kinetics in the combustion processes. In: Cheremisinoff NP, editor. Handbook of heat and mass transfer. Advances in reactor design and combustion science, vol. 4. Houston: Gulf Publishing Company; 1990. p. 769–819.
[321] Halstead M, Prothero A, Quinn CP. Modeling the ignition and cool-flame limits of acetaldehyde oxidation. Combust Flame 1973;20:211–21.

[322] Poppe C, Schreiber M, Griffiths JF. Modelling of n-heptane autoignition and validation of the results. In: Proceedings of joint meeting of British and German Societies; 1993, p. 360–3.
[323] Blin-Simiand N, Rigny R, Viossat V, Circan S, Sahetchian K. Autoignition of hydrocarbon/air mixtures in a CFR engine: experimental and modeling study. Combust Sci Technol 1993; 88:329–48.
[324] Basevich VYa, Frolov SM. A reduced kinetic scheme for autoignition modelling of iso-octane and *n*-heptane/air mixtures during the induction period for internal combustion engines. Chem Phys 1994;13:146–56 [in Russian].
[325] Sahetchian K, Champoussin JC, Brun M, Levy N, Blin-Simiand N, Aligrot C, et al. Experimental study and modeling of dodecane ignition in a Diesel engine. Combust Flame 1995; 103:207–20.
[326] Griffiths JF, Jiao Q, Schreiber M, Meyer J, Knoche KF. Development of thermokinetic models for autoignition in a CFD code: experimental validation and application of the results to rapid compression studies. In: Twenty-fourth symposium (International) on combution. Pittsburg, PA: The Combustion Institute; 1992, p. 1809–15.
[327] Griffith JF. Kinetic fundamentals of alkane autoignition at low temperatures. Combust Flame 1993;93:202–6.
[328] Griffith JF. Reduced kinetic models and their application to practical combustion systems. Prog Energy Combust Sci 1995; 21:25–107.
[329] Pitsch H, Peters N. Investigation of the ignition process of sprays under diesel engine conditions using reduced *n*-heptane chemistry. SAE paper 2464; 1998.
[330] Tanaka S, Ayala F, Keck JC. A reduced chemical kinetic model for HCCI combustion of primary reference fuels in a rapid compression machine. Combust Flame 2003;133: 467–81.
[331] Tanabe M, Kono M, Sato J, Koenig J, Eigenbrod C, Dinkelacker F, et al. Two stage ignition of n-heptane isolated droplets. Combust Sci Technol 1995;108:103–19.
[332] Maas V, Pope SB. Implementation of simplified chemical kinetics based on intrinsic low-dimensional manifolds, In: Twenty-fourth symposium (International) on combution. Pittsburg, PA: The Combustion Institute; 1992. p. 103–12.
[333] Müller UC, Peters N, Liñan A. Global kinetics for *n*—heptane ignition at high pressures. In: Twenty-fourth symposium (International) on combution. Pittsburg, PA: The Combustion Institute; 1992. p. 777–84.
[334] Dopazo C, O'Brien EE. An approach to the autoignition of a turbulent mixture. Acta Astronaut 1974;1:1239–66.
[335] Bruel P, Rogg B, Bray KNC. On auto-ignition in laminar and turbulent non-premixed systems. In: Twenty-third symposium (International) on combution. Pittsburg, PA: The Combustion Institute; 1990. p. 759–66.
[336] Boudier P, Henriot S, Pinsot T, Baritaud T. A model for turbulent flame ignition and propagation in spark ignition engines. In: Twenty-fourth symposium (International) on combution. Pittsburg, PA: The Combustion Institute; 1992. p. 503–10.
[337] Lakshmisha KN, Zhang Y, Rogg B, Bray KNC. Modelling auto-ignition in a turbulent medium. In: Twenty-fourth symposium (International) on combution. Pittsburg, PA: The Combustion Institute; 1992. p. 421–28.
[338] Zhang Y, Rogg B, Bray KNC. Modeling of autoignition in nonpremixed turbulent systems: closure of the chemical-source terms. Prog Astronaut Aeronaut 1993;152:87–102.
[339] Zhang Y, Rogg B, Bray KNC. 2-D Simulation of turbulent autoignition with transient laminar flamelet source term closure. Combust Sci Technol 1995;105:211–27.
[340] Hilbert R, Thévenin D. Autoignition of turbulent non-premixed flames investigated using direct numerical simulations. Combust Flame 2002;128:22–37.
[341] Viggiano A, Magi V. A 2-D investigation of *n*-heptane autoignition by means of direct numerical simulation. Combust Flame 2004;137:432–43.
[342] Natarajan B, Bracco FV. On multidimensional modelling of auto-ignition in spark-ignition engines. Combust Flame 1984; 57:179–97.
[343] Cox RA, Cole JA. Chemical aspects of the autoignition of hydrocarbon–air mixtures. Combust Flame 1985;60:109–23.
[344] Halstead MP, Kirsch LJ, Quinn CP. The autoignition of hydrocarbon fuels at high temperatures and pressures—fitting of a mathematical model. Combust Flame 1977;30:45–60.
[345] Benson SW. The kinetics and thermochemistry of chemical oxidation with application to combustion and flames. Prog Energy Combust Sci 1981;7:125–34.
[346] Schäpertöns H, Lee W. Multidimensional modelling of knocking combustion in SI engines. SAE technical paper 850502; 1985.
[347] Theobald MA. Numerical simulation of Diesel autoignition. PhD Thesis, MIT; 1986.
[348] Kong S-C, Han Z, Reitz R D. The development and application of a diesel ignition and combustion model for multi-dimensional engine simulation. SAE technical paper 950278; 1996.
[349] Sazhin SS, Sazhina EM, Heikal MR, Marooney C, Mikhalovsky SV. The Shell autoignition model: a new mathematical formulation. Combust Flame 1999;117:529–40.
[350] Sazhina EM, Sazhin SS, Heikal MR, Marooney C. The Shell autoignition model: application to gasoline and diesel fuels. Fuel 1999;78:389–401.
[351] Sazhina EM, Sazhin SS, Heikal MR, Babushok VI, Johns R. A detailed modelling of the spray ignition process in diesel engines. Combust Sci Technol 2000;160:317–44.
[352] Hamosfakidis V, Reitz RD. Optimization of a hydrocarbon fuel ignition model for two single component surrogates of diesel fuel. Combust Flame 2003;132:433–50.
[353] Kuznetzov VR, Sabel'nikov VA. Turbulence and combustion. New York: Hemisphere; 1990.
[354] Durand P, Gorokhovski M, Borghi R. An application of the probability density function model to diesel engine combustion. Combust Sci Technol 1999;144:47–78.
[355] Demoulin FX, Borghi R. Modeling of turbulent spray combustion with application to diesel like experiment. Combust Flame 2003;129:281–93.
[356] Sabel'nikov V, Gorokhovski M, Baricault N. The extended IEM mixing model in the framework of the composition PDF approach; application to diesel spray combustion. Combust Theory Modell 2006; in press.
[357] Juncu Gh. Conjugate mass transfer to a spherical drop accompanied by a second-order chemical reaction inside the drop. Int J Heat Mass Transfer 2002;45:3817–29.
[358] Haywood RJ, Renksizbulut M, Raithby GB. Transient deformation and evaporation of droplets at intermediate Reynolds numbers. Int J Heat Mass Transfer 1994;37:1401–9.
[359] Mao Z-S, Li T, Chen J. Numerical simulation of steady and transient mass transfer to a single drop dominated by external resistance. Int J Heat Mass Transfer 2001;44:1235–47.

[360] Mashayek F. Dynamics of evaporating drops. Part 1: formulation and evaporation model. Int J Heat Mass Transfer 2001;44:1517–26.
[361] Waheed MA, Henschke M, Pfenning A. Mass transfer by free and forced convection from single spherical liquid drops. Int J Heat Mass Transfer 2002;45:4507–14.
[362] Shin H, Lee KW, Yoon WS, Chae JW. High pressure vaporization of burning droplet with flash vapor–liquid equilibrium calculation. Int Commun Heat Mass Transfer 2003;30:465–74.
[363] Lee KW, Chae JW, Lee JY, Yoon WS. Analysis of high-pressure drop vaporization with flash vapor–liquid equilibrium calculation. Int Commun Heat Mass Transfer 2003;30:633–41.
[364] Gogos G, Soh S, Pope DN. Effects of gravity and ambient pressure on liquid fuel droplet evaporation. Int J Heat Mass Transfer 2003;46:283–96.
[365] Gao Z, Mashayek F. Stochastic modeling of evaporating droplets polydispered in turbulent flows. Int J Heat Mass Transfer 2004;47:4339–48.
[366] Fudum O, Batsale J-C, Santander R, Bubnovich V. Analytical solution of coupled diffusion equations in semi-infinite media. ASME J Heat Transfer 2004;126:471–5.
[367] Margerit J, Sero-Guillaume O. Study of the evaporation of a droplet in its stagnant vapor by asymptotic matching. Int J Heat Mass Transfer 1996;39:3887–98.
[368] Boyadjiev Chr. On the mechanism and kinetics of the transport processes in systems with intensive interphase mass transfer. 1. Heat and mass transfer. Int J Heat Mass Transfer 2000;43: 2749–57.
[369] Boyadjiev Chr. On the mechanism and kinetics of the transport processes in systems with intensive interphase mass transfer. 2. Stability. Int J Heat Mass Transfer 2000;43:2759–66.
[370] Boyadjiev Chr. On the mechanism and kinetics of the transport processes in systems with intensive interphase mass transfer. 3. Comparative analysis of the absorption and desorption rates. Int J Heat Mass Transfer 2001;44:1119–25.
[371] Boyadjiev B, Boyadjiev Chr. On the mechanism and kinetics of the transport processes in systems with intensive interphase mass transfer. 4. Effect of the interface concentration. Int J Heat Mass Transfer 2001;44:2505–9.
[372] Boyadjiev Chr, Boyadjiev B. On the non-stationary evaporation kinetics. I. Mathematical model and experimental data. Int J Heat Mass Transfer 2003;46:1679–85.
[373] Boyadjiev B, Boyadjiev Chr. On the non-stationary evaporation kinetics. II. Stability. Int J Heat Mass Transfer 2003;46: 1687–92.
[374] Bykov V, Goldfarb I, Goldshtein V, Sazhin SS, Sazhina EM. System decomposition technique: application to spray modelling in CFD codes. 20th annual symposium of the Israeli section of the combustion institute. Book of abstracts. Beer-Sheva, Israel: Ben-Gurion University; 2004. p. 16.
[375] Sazhin SS, Wild P, Leys C, Toebaert D, Sazhina EM. The three temperature model for the fast-axial-flow CO_2 laser. J Phys D Appl Phys 1993;26:1872–83.
[376] Maas U, Pope SB. Simplifying chemical kinetics: intrinsic low-dimensional manifolds in composition space. Combust Flame 1992;117:99–116.
[377] Rhodes C, Morari M, Wiggins S. Identification of the low order manifolds: validating the algorithm of Maas and Pope. Chaos 1999;9:108–23.
[378] Kaper HG, Kaper TJ. Asymptotic analysis of two reduction methods for systems of chemical reactions. Argonne National Lab, preprint ANL/MCS-P912-1001; 2001.
[379] Lam SH, Goussis DM. The GSP method for simplifying kinetics. Int J Chem Kinet 1994;26:461–86.
[380] Hadjinicolaou M, Goussis DM. Asymptotic solutions of stiff PDEs with the CSP method: the reaction diffusion equation. SIAM J Sci Comput 1999;20:781–910.
[381] Masias A, Diamantis D, Mastorakos E, Goussis DA. An algorithm for the construction of global reduced mechanisms with CSP data. Combust Flame 1999;117:685–708.
[382] Valorani M, Goussis DM. Explicit time-scale splitting algorithm for stiff problems: auto-ignition of gaseous mixtures behind a steady shock. J Comput Phys 2001;169:44–79.
[383] Neophytou MK, Goussis DA, van Loon M, Mastorakos E. Reduced chemical mechanism for atmospheric pollution using computational singular perturbation analysis. Atmos Environ 2004;38:3661–73.
[384] Gol'dshtein V, Sobolev V. Qualitative analysis of singularly perturbed systems (in Russian). Novosibirsk: Institute of Mathematics, Siberian Branch of USSR Academy of Science; 1988 [in Russian].
[385] Gol'dshtein V, Sobolev V. Integral manifolds in chemical kinetics and combustion. Singularity theory and some problems of functional analysis. American Mathematical Society; 1992. p. 73–92.
[386] Fenichel N. Geometric singular perturbation theory for ordinary differential equations. J Differ Eqs 1979;31:53–98.
[387] Strygin BB, Sobolev VA. Decomposition of motions by the integral manifold method. Moscow: Nauka Publishing House; 1988 [in Russian].
[388] Sazhina EM, Bykov V, Goldfarb I, Goldshtein V, Sazhin SS, Heikal MR. Modelling of spray autoignition by the ODE system dynamic decomposition technique. In: Proceedings of HEFAT2005 (4th international conference on heat transfer, fluid mechanics and thermodynamics), Cairo, Egypt; 2005 [Paper number: SE2].
[389] Maxwell JB. Data book on hydrocarbons: application to process engineering. New York: van Nostrand; 1950.
[390] Poling BE, Prausnitz JM, O'Connell J. The properties of gases and liquids. New York: McGraw-Hill; 2000.
[391] Chin JS, Lefebvre AH. The role of the heat-up period in fuel drop evaporation. Int J Turbo Jet Eng 1985;2:315–25.
[392] Borman GL, Johnson JH. Unsteady vaporization histories and trajectories of fuel drops injected into swirling air. SAE technical report 620271; 1962.
[393] Durret RP, Oren DC, Ferguson CR. A multidimensional data set for Diesel combustion model validation: I. Initial conditions, pressure history and spray shapes. SAE technical report 872087; 1987.
[394] Handbook of Aviation Fuel Properties. SAE CRC technical report, No. 530; 1984.